The Electronic Structure of Photosystem II

Romero Mesa, E.

2011

document version
Publisher's PDF, also known as Version of record

THE ELECTRONIC STRUCTURE OF PHOTOSYSTEM II

CHARGE SEPARATION DYNAMICS

Elisabet Romero

The research described in this Thesis was financially supported by
Marie Curie Research Training Network **INTRO2** (MRTN-CT-505069)
of the European Union

This Thesis was reviewed by

Prof. Roberta Croce, University of Groningen, The Netherlands

Prof. Alfred R. Holzwarth, Max-Plank Institute, Mülheim a/d Ruhr, Germany

Dr. Hans J. van Gorkom, Leiden University, The Netherlands

Prof. Peter J. Nixon, Imperial College, London, UK

Dr. Raoul N. Frese, VU University Amsterdam, The Netherlands

Cover design by

Elisabet Romero and

Giuliano Pappadopoli

www.gpatelier.it

Printed by Wöhrmann Print Service, Zutphen

ISBN: 978-90-8570-729-5

VRIJE UNIVERSITEIT

The Electronic Structure of Photosystem II

Charge Separation Dynamics

ACADEMISCH PROEFSCHRIFT

ter verkrijging van de graad Doctor aan
de Vrije Universiteit Amsterdam,
op gezag van de rector magnificus
prof.dr. L.M. Bouter,
in het openbaar te verdedigen
ten overstaan van de promotiecommissie
van de faculteit der Exacte Wetenschappen
op vrijdag 25 maart 2011 om 13.45 uur
in de aula van de universiteit,
De Boelelaan 1105

door
Elisabet Romero Mesa
geboren te Barcelona, Spanje

promotor: prof.dr. R. van Grondelle

copromotor: dr. J.P. Dekker

A mis padres,

por su apoyo y comprensión

Al meu germà Daniel i

a la Mabel,

pel més bonic,

el Biel i la Iara

CONTENTS

CHAPTER 1

Introduction

Photosynthesis is a biological process whereby the Sun's energy is collected and stored by a series of events that convert the pure energy of light into the biochemical energy needed to power life. This remarkable process provides the foundation for essentially all life on Earth and provides all our food and most of our energy resources. Therefore, photosynthesis serves as the vital link between the light energy of the sun and all living organisms.

Photosynthesis takes place in photosynthetic bacteria and in oxygen evolving organisms (higher plants, algae and cyanobacteria). The oxygenic photosynthetic process requires light as energy source and two reactants: water and carbon dioxide; and produces molecular oxygen and sugars. Basically, the oxygenic photosynthetic process can be described by the following equation:

$$6\ CO_2 + 6\ H_2O \xrightarrow{\text{Light, } h\upsilon} C_6H_{12}O_6 + 6\ O_2$$

where $C_6H_{12}O_6$ represent the sugars produced.

In higher plants, the photosynthetic apparatus is located in the chloroplast, an organelle present in several copies in the plant cell. Inside the chloroplast, a membrane consisting on stacks (grana) and flat (stroma lamellae) domains holds the photosynthetic machinery which is composed by many different pigment-protein complexes with different functions.

The pigment-protein complexes are entities composed by pigment molecules (also called chromophores or cofactors) which absorb light energy and then are promoted to an excited state; and by proteins which are formed by a chain of amino acids (in some parts folded in the form of an alpha-helix) and provide a matrix for the pigments to be arranged in specific configurations. The most abundant pigments in oxygenic photosynthesis are chlorophylls and carotenoids. The function of the pigment-protein complexes depends on the type of pigments present and on the relative orientation of the pigments in the complex, since this orientation determines the interactions among pigments and their interactions with the protein. These interactions control the function of each individual pigment as well as the collective functioning of the whole complex.

The light-harvesting complexes, also called antennas, collect light and funnel it in the form of excitation energy to the reaction centers where the photochemical charge separation process takes place. Then the stabilization of energy by secondary electron transfer processes and, finally, the synthesis and export of stable products complete the solar energy storage process of photosynthesis (for further reading about the photosynthetic process see references (*1-4*)).

The focus of this Thesis is on the study of the molecular mechanisms leading to charge separation in the photosystem II reaction center (PSII RC), the unique molecular machinery capable of using light to create a charge-separated state that drives the splitting of water, one of the most stable and abundant molecules on earth.

Reaction Centers: Bacterial RC *vs*. PSII RC

Type II RCs are found in photosynthetic bacteria (bactRC) and in oxygen evolving organisms (PSII RC). They are surrounded by antenna complexes which provide the RC with the necessary excitation energy to drive photochemistry. Once the RC is excited, the energy relaxes on an ultrafast time scale (few hundred fs, 1 fs = 10^{-15} s) to the lowest energy excited state of the system. This excited state (called exciton if more than one pigment contributes), after a series of energy and electron transfer steps, eventually leads to the formation of a charge separated state. In oxygen evolving organisms, this charge separated state creates an electrochemical gradient across the membrane which drives, among other processes, water splitting and the synthesis of ATP (the molecular energetic currency used by living organisms). The electrochemical gradient created is on the order of 100 mV.

The three dimensional cofactor arrangement of Type II RC, a valuable tool when energy and electron transfer processes are investigated, has been determined by X-ray crystallography (*5-8*). The crystal structure of both bactRC and PSII RC are shown in Figure 1. A mayor difference between both RCs is their pigment content: the bactRC binds bacteriochlorophyll *a* (BChl) and bacteriopheophytin *a* (BPhe) while PSII RC binds chlorophyll *a* (Chl) and pheophytin *a* (Phe). The Q_Y absorption region reflects the excitation and electron transfer reactions in the RCs, for BChl and BPhe the Q_Y is in the 700 - 950 nm range while for Chl and Phe the Q_Y is in the 645 - 720 nm absorption range. Despite their structural similarity, the absorption spectrum of the isolated RCs is significantly different between the two systems (Figure 1). The bactRC presents three distinct and well separated bands whereas the PSII RC shows only one band with hardly any structure.

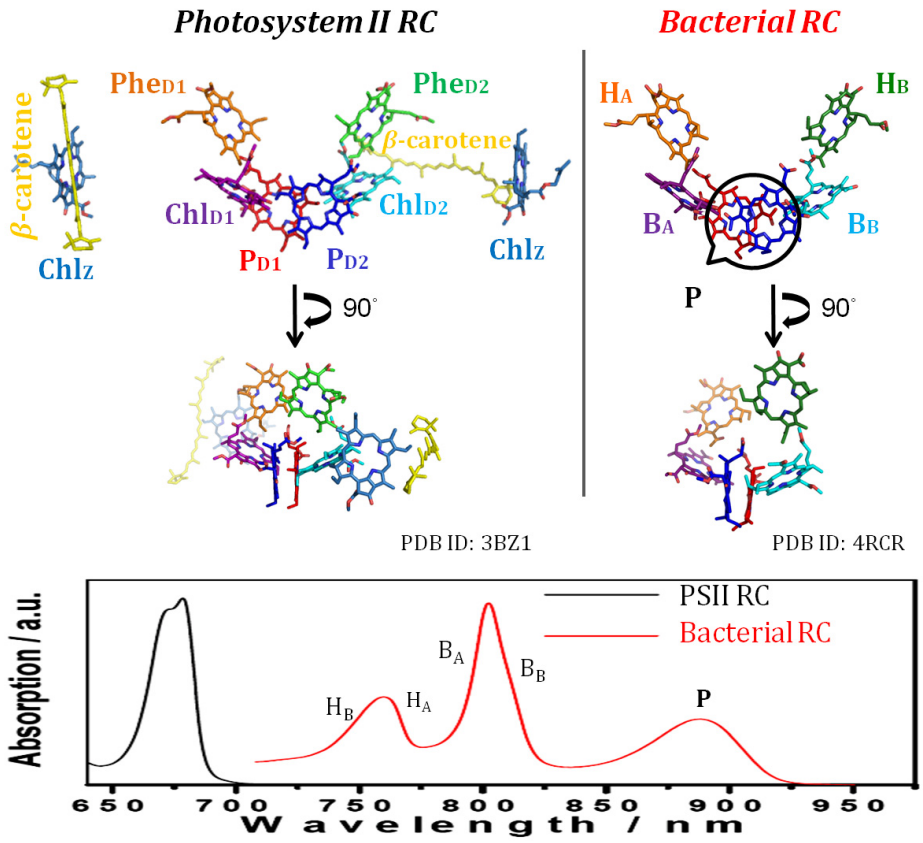

Figure 1. Three dimensional cofactor arrangement of Type II RCs. (*Left*) Photosystem II reaction center from the cyanobacteria *Thermosynechococcus elongatus* (*8*), (*right*) bacterial reaction center from *Rhodobacter sphaeroides* R-26 (*9*), (*bottom*) absorption spectra at 77 K.

The large difference in the spectroscopic properties of both systems has its origin, besides the differences between BChl and Chl, in a slight structural difference: the relative distance and mutual orientation of the two cofactors located in the center of each complex. In the bactRC this distance is a little shorter and, more important, the relative orientation permit a higher overlap between the electronic wavefunctions of the central cofactors in BactRC with respect to the overlap present in PSII RC. Therefore, in the bactRC the two central cofactors form a strongly coupled dimer, denominated P or *special pair*, which is the lowest energy state of the system. The rest of cofactors: the accessory BChls, B_A and B_B; and the BPhe, H_A and H_B; are monomeric, i.e., they operate as individual cofactors (see Figure 1 for the assignment of the absorption bands to specific cofactors). Hence, once the excitation energy reaches the bactRC, the energy is always transferred to the lowest energy state, the *special pair*. Once the *special pair* is excited, an electron is transferred to B_A in 3 ps (1 ps = 10^{-12} s) resulting in the charge separated state $P^+B_A^-$. Then, an electron is transferred from B_A to H_A in 1 ps to form $P^+H_A^-$ (only one branch is active in charge separation, the so-called active branch). However, if B_A is directly excited with ≈ 800 nm light, charge separation can occur via a different pathway, either via $B_A^+H_A^-$ or $P^+B_A^-$, without involving the excited state of the *special pair* (*10-12*). In the *in vivo* situation, this alternative route does not occur to a significant extent because B_A is too high in energy to receive excitation energy from the antennas (which provide most of the excitation energy received by the bactRC).

In the PSII RC, the overlap between the two central cofactors is weaker than in the bactRC, hence, there is no *special pair*. In the PSII RC, the similar distance of ≈ 10-11 Å between the neighbouring cofactors in the center of the complex, gives rise to a system of coupled pigments that interact, creating collective excited (or exciton) states with contributions from several pigments. The idea of the collective behaviour of the PSII RC central pigments was expressed for the first time in the "Multimer model" (*13*). This situation is reflected in the absorption spectrum of PSII RC. Conversely to what is observed in the bactRC, the PSII RC absorption spectrum displays only one band (Figure 1). This single band, which is the composite of several underlying bands, indicates that all Chls and Phes absorb at similar wavelength giving rise to a spectrally congested absorption spectrum. The spectral congestion in the PSII RC is a well-know phenomenon which greatly complicates the interpretation of the PSII RC spectroscopic data.

The photosystem II reaction center: a closer look

The PSII RC particle contains the proteins D_1, D_2, cytochrome b_{559} and PsbI. The cofactors involved in primary charge separation are bound by two protein domains, D_1 and D_2, each consisting of five alpha-helices spanning the photosynthetic membrane. The isolated PSII RC contains four Chl and two Phe molecules (Phe_{D1}, Chl_{D1}, P_{D1}, P_{D2}, Chl_{D2}, and Phe_{D2}, the RC core) in the center of the complex, two additional chlorophyll molecules ($Chls_Z$), located at opposing sites on the periphery of the complex ≈ 25 Å from the core pigments, and two *β*-carotene molecules located between $Chls_Z$ and the RC core (Figure 1) (*6-8*).

As it has been said before, the three-dimensional crystal structure is a valuable tool because it allows the researches to propose energy and electron transfer pathways among the cofactors in the structure, thus, creating a link between structure and function. However, one has to take into account that the crystal structure is a "snapshot" of the pigment-protein complex in a specific configuration. In fact, in the *in vivo* situation the system is in continuous movement, fast nuclear motions (intra- and interpigment vibrations and protein vibrations) and slow conformational motions of the protein (disorder) are decisive factors for the functionality of the complex.

The disorder induced by the slow protein motions is especially important since it creates a distribution of energetically different RC complexes. This means that for a specific protein conformation, the lowest collective exciton state in the RC is delocalized over a combination of cofactors, whereas for another protein configuration the lowest exciton state is delocatized over a different set of cofactors. Therefore, after absorption of a photon by the RC the excitation energy is distributed among the cofactors (depending on protein conformation or disorder) and converted into a charge separated state after a series of energy and electron transfer reactions.

The presence of different charge separation pathways in the BactRC was demonstrated in 1999 (*11, 12*) although, as it has been said before, *in vivo* only one pathway (starting from the *special pair* exciton state) is operative. However, in PSII the excitation energy delivered by the antenna complexes to the RC is able to reach any collective exciton state present in the RC. Therefore, in principle, in the PSII RC the final charge separated state can be reached via different charge separation pathways (*14-16*).

This Thesis

The presence of different charge separation pathways in the PSII RC from higher plants is demonstrated in the second chapter of this Thesis where we present a detailed transient absorption spectroscopy study on the isolated PSII RC from spinach. The experimental data in combination with global and target analysis (*17*) lead us to identify two different sets of cofactors (exciton states) which give rise to two different charge separation pathways (*16*). The selection of a specific pathway strongly depends on protein conformation.

In our view, the collective nature of the lowest excited state in PSII RC together with the disorder induced by the protein, represents an advantageous and flexible energetic configuration to achieve efficient charge separation

In Chapter 3, the experimental data presented in Chapter 2 is modeled using modified Redfield and generalized Förster theories. It is shown that the model describing two charge separation pathways is in better agreement with the experiment than the model consisting on a single pathway.

In Chapter 4 we present an unexpected observation: the two β-carotene molecules present in the PSII RC sense the excitation on the peripheral $Chls_Z$ manifested as an absorption blue shift. We propose that the mixing of the electronic distributions of the β-carotenes and the $Chls_Z$ may accelerate the excitation energy transfer from $Chls_Z$ to the central cofactors.

In Chapter 5 we apply Stark spectroscopy to a series of site-directed mutants in order to investigate the nature of the exciton states in PSII. We conclude that the exciton states which initiate charge separation are mixed exciton-charge transfer (CT) states and that the mixing exciton-CT promotes ultrafast and efficient charge separation.

In Chapter 6 we study the pigment-protein interactions for the sites of cation, P_{680}, and anion, Phe_{D1}, localization in the PSII RC by light-induced Fourier transform infrared (FTIR) difference spectroscopy. We examine the pigment-protein interactions for: i) P_{680} on different PSII preparations with variable antenna size and for ii) Phe_{D1} on site-directed mutants. The second part of this study shows a specific pigment-protein interaction which may control, in part, the selection of a specific charge separation pathway by each RC complex.

In Chapter 7 we study the origin of the red chlorophylls in the light-harvesting complex Lhca4, one of the peripheral antenna complexes of photosystem I, by applying Stark spectroscopy. We conclude that the mixing of the lowest exciton state with a CT state is the cause for the atypical properties of the red chlorophylls.

Spectroscopic Techniques

Transient absorption spectroscopy

The photophysical and photochemical reactions in photosynthesis, such as charge separation, are among the fastest events in biology, taking place on timescales ranging from tens of femtoseconds (fs) to a few nanoseconds (1 ns = 10^{-9} s). Therefore, ultrafast laser systems that produce pulses with femtosecond duration are necessary to follow the charge separation reactions in real time.

Transient absorption, or pump-probe, spectroscopy monitors the absorption changes produced in the sample under study by an excitation laser pulse. The pump, or excitation laser pulse, promotes the sample to an excited state which will evolve in time to reach a final state. For instance, during the charge separation process an excited state (RC*) is converted into a primary radical pair (RP1) which, in turn, evolves to a secondary radical pair (RP2), i.e., RC* → RP1 → RP2. The absorption changes associated with the sequence of energy and electron transfer events are monitored by a probe pulse (white light) as a function of a time delay (τ) between pump and probe pulses. Therefore, by probing the absorption changes induced by the pump pulse at different time delays, it is possible to follow the spectral evolution in time of the system. The interpretation of the spectral evolution of the system allows the identification of the cofactors participating at each stage of the sequence of energy and electron transfer reactions.

The absorption (*Abs*) or optical density (OD) of a sample is basically defined as:

$$Abs(\lambda) = -\log\frac{\mathrm{I}(\lambda)}{\mathrm{Io}(\lambda)}$$

where Io(λ) is the intensity of the incident light on the sample, I(λ) is the intensity of the light transmitted through the preparation and λ is the wavelength of the light.

According to the previous equation, the absorption difference spectrum in a pump-probe experiment for a given delay time, τ, between pump and probe pulses, *ΔAbs*(λ,τ), is given by:

$$\Delta Abs(\lambda,\tau) = Abs(\lambda,\tau)pump\ on\ -\ Abs(\lambda,\tau)pump\ off$$

$$= -\log\frac{\mathrm{I}(\lambda,\tau)pump\ on}{\mathrm{Io}(\lambda,\tau)pump\ off}$$

Where I(λ,τ)*pump on* and I(λ,τ)*pump off* are the transmitted light measured in the presence or absence, respectively, of the pump pulse.

In general, a *ΔAbs* spectrum contains contributions from various processes:

i) Ground-State Bleach (GSB). The action of the pump pulse promotes a fraction of the molecules to excited state, therefore, the number of molecules in the ground state decreases. As a consequence, the ground-state absorption in the excited sample (*pump on*) is lower than that in the non-excited sample (*pump off)* which generates a negative signal in the *ΔAbs* spectrum.

ii) Stimulated Emission (SE). The Einstein coefficients for absorption from the ground to the excited state and stimulated emission from the excited to the ground state are identical for a two-level system. Therefore, once the excited state is populated and the probe pulse passes through the excited volume, stimulated emission to the ground state occurs. This results in an increase of light intensity arriving to the detector and corresponds to a negative *ΔAbs* signal.

iii) Excited-State Absorption (ESA). Upon population of the excited state, optically allowed transitions from the excited state to higher excited states may exist which leads to the absorption of the probe pulse. As a consequence, a positive signal in the *ΔAbs* spectrum is observed.

iv) Product Absorption (PA). The excitation of a system may lead to reactions that result in transient or long-lived molecular states, such as triplet, charge-separated and isomerized states. The absorption of such products appears as a positive signal in the *ΔAbs* spectrum.

For a detailed overview about transient absorption spectroscopy (basic principles, instrumentation and data analysis) applied to photosynthetic complexes the reader is referred to a recent review (*18*).

This technique has been applied in Chapter 2 and 4 to investigate the energy and electron transfer processes in the isolated PSII RC.

Stark spectroscopy

The effects of an externally applied electric field on the absorption or emission spectrum of a molecule is known as the Stark effect. The experimental approach used to monitor such effects is Stark spectroscopy (the terms electrochromism and electroabsorption are also used). This technique probes the movement of charge associated with an optical transition. Therefore it is especially appropriate to study photosynthetic complexes which carry out charge separation.

The Stark absorption spectrum is a difference spectrum, the absorption in the presence of the externally applied electric field minus the absorption in the absence of the field, $Abs_{Field\ on}$ minus $Abs_{Field\ off}$. Basically, the shift in the transition energy ($h\Delta\upsilon$) experienced by a molecule in the presence of an externally applied electric field $\vec{F}$, is given by:

$$h\Delta\upsilon = -\Delta\vec{\mu}\cdot\vec{F} - \frac{1}{2}\,\vec{F}\cdot\Delta\tilde{\alpha}\cdot\vec{F} = -\Delta\vec{\mu}\cdot\vec{F} - \frac{1}{2}\,\vec{F}\cdot(\Delta\tilde{\mu})ind\cdot\vec{F}$$

where $\Delta\vec{\mu}$ represents the difference in permanent dipole moment, $\Delta\tilde{\alpha}$ is the difference polarizability tensor between the ground and excited states associated with the transition (*19, 20*) and $(\Delta\tilde{\mu})ind$ is the induced dipole moment created due to the interaction of the polarizability with the externally applied electric field .

Stark spectroscopy monitors the electronic changes directly upon photoexcitation, allowing the study of the electronic structure of the excited states. Three molecular parameters can be obtained from the Stark spectrum: the change in dipole strength, the change in dipole moment, $\Delta\mu$, and the change in polarizability, $\Delta\alpha$, between the ground and excited state for an electronic transition. The $\Delta\mu$ is a measure of the degree of charge redistribution in the excited state associated with a transition. In the case of PSII RC, $\Delta\mu$ is a measure of the charge transfer (CT) character associated to an exciton state, i.e., the degree of mixing between and exciton and a CT state. The degree of exciton-CT mixing is related to the participation of the mixed state in the charge separation process. The $\Delta\alpha$ is a measure of the deformability of the electronic structure of the states involved in the transition (*19, 20*) and it is important for understanding the electronic properties of a chromophore interacting with an organized environment.

The externally applied electric field enhances the differentiation between the states that experiment a large modification of the electronic density distribution in the excited state (with respect to the ground state), and the states that maintain the ground state electronic structure in the excited state. The Stark spectrum, for isolated absorption bands in a non-oriented, immobilized sample is described by the Liptay formalism as a linear combination of the zeroth, first, and second derivatives of the absorption spectrum (*21*). The molecular parameters $\Delta\alpha$ and $\Delta\mu$ scale with the first and second derivatives, respectively, of the absorption spectrum (classic Stark effect).

For a detailed overview about Stark spectroscopy (basic principles, instrumentation and data analysis) applied to photosynthetic complexes the reader is referred to a review (*20*) and a book chapter (*19*).

This technique has been applied in Chapter 5 and 7 of this Thesis. In Chapter 5 the nature of the excited states giving rise to charge separation in PSII RC is investigated. In Chapter 7 the origin of the spectroscopic properties of the red chlorophylls present in the light-harvesting complex Lhca4 is investigated.

Light-induced Fourier transform infrared (FTIR) difference spectroscopy

Infrared spectroscopy (IR) analyzes vibrational properties of a molecule and can thus address other properties of the PSII RC than those monitored by optical spectroscopy in the visible region (*22*). In IR spectroscopy, photons with energies which match those of vibrational sublevels of the molecule (typically in the 0.5–0.05 eV range) are directly absorbed. These low energy photons do not cause photochemistry and thus can be used at high intensities. The vibrational spectrum of the RC is composed of individual and coupled modes of the numerous bonds of the protein (polypeptide backbone and amino acid side chains), the pigments and water constituting the entire complex, and thus contains abundant information on structural details and functional properties. In the context of this Thesis, we are interested in the description of the pigment-protein interactions and the role of the protein in mediating electron transfer. However, IR spectroscopy probes all the vibrational modes present in the pigment-protein complex without any selectivity. A major problem of the non-selectivity of IR spectroscopy is the background absorption of the bulk part of the RC, water and buffer, which necessitates difference techniques. Since the size of the RC protein does not allow *classical* difference

spectroscopies where two different samples are compared, *reaction-induced* IR difference techniques on a single sample have to be used. The *trigger* inducing the reaction should provide a minimum disturbance of the sample, but specifically and quantitatively start the desired reaction. The result are highly structured difference spectra which represent the sum of all molecular changes associated with the induced reaction, and which are selective for the functionally important parts rather for the global structure. The technique used in this Thesis, light-induced Fourier transform infrared (FTIR) difference spectroscopy (or light-minus-dark FTIR difference spectroscopy) can be used for many intrinsic photoreactions of photosynthetic pigment-protein complexes. FTIR difference spectra are obtained between dark and illuminated samples, by recording many cycles consisting of *Dark-Light-Dark* (or *Dark-Light-Relaxation*). During the first *Dark* period the background absorption is recorded in the dark. During the *Light* period the sample is illuminated to start the desired reaction and the absorption is recorded under illumination. During the second *Dark* or *Relaxation* period the sample relaxes to the initial state in the dark. Special care has to be taken when setting the duration of each *Light* and *Dark* period: the illumination time has to be sufficient to initiate the reaction but not too long to induce other undesirable processes; the *Dark* or *Relaxation* period has to be long enough to allow complete sample relaxation to the initial state before starting a new cycle. An additional time delay between *Dark-Light-Relaxation* cycles is introduced to ensure complete sample relaxation. From each cycle three interferograms are recorded and two spectra are calculated: *Light* minus *Dark* (*L*-D) and *Relaxation* minus *Dark* (*R-D*). A useful test to check complete sample recovery is to calculate the double difference spectrum (*L*-D) minus (*R-D*) which should return a flat spectrum in case the sample is completely recovered after the *Relaxation* period. Light-induced FTIR difference spectroscopy combined with the use of exogeneous donors can be used to reversibly photoaccumulate a specific state of the RC.

This technique has been applied in Chapter 6 to investigate the pigment-protein interactions in different PSII preparations isolated from higher plants (spinach) and cyanobacteria (*Synechocystis* PCC. 6803).

REFERENCES

1. Blankenship, R. E. (2008) The basic principles of photosynthetic energy storage, In *Molecular mechanisms of photosynthesis* (Blankenship, R. E., Ed.), pp 1-10, Blackwell Science Ltd., Oxford.

2. Kê, B. (2001) Photosynthesis: an overview, In *Phototsynthesis: photobiochemistry and photobiophysics* (Govindjee, Ed.), pp 1-46, Kluwer Academic Publishers, Dordrecht.

3. van Grondelle, R., Dekker, J. P., Gillbro, J. P., and Sundström, V. (1994) Energy transfer and trapping in photosynthesis, *Biochim. Biophys. Acta 1187*, 1-65.

4. Wydrzynski, T. J., Satoh, K., and Freeman, J. A. (2005) Introduction to photosystem II, In *Photosystem II: the light-driven water:plastoquinone oxidoreductase* (Satoh, T. J. W. a. K., Ed.), pp 11-22, Springer, Dordrecht.

5. Deisenhofer, J., Epp, O., Miki, K., Huber, R., and Michel, H. (1985) Structure of the protein subunits in the photosynthetic reaction center of *Rhodopseudomonas viridis* at 3 Å resolution, *Nature 318*, 618-624.

6. Zouni, A., Witt, H. T., Kern, J., Fromme, P., Krauss, N., Saenger, W., and Orth, P. (2001) Crystal structure of photosystem II from *Synechococcus elongatus* at 3.8 Å resolution, *Nature 409*, 739-743.

7. Ferreira, K. N., Iverson, T. M., Maghlaoui, K., Barber, J., and Iwata, S. (2004) Architecture of the photosynthetic oxygen-evolving center, *Nature 303*, 1831-1838.

8. Guskov, A., Kern, J., Gabdulkhakov, A., Broser, M., Zouni, A., and Saenger, W. (2009) Cyanobacterial photosystem II at 2.9-Å resolution and the role of quinones, lipids, channels and chloride, *Nat. Struct. Mol. Biol. 16*, 334-342.

9. Yeates, T. O., Komiya, H., Chirino, A., Rees, D. C., Allen, J. P., and Feher, G. (1988) Structure of the reaction center from *Rhodobacter sphaeroides* R-26 and 2.4.1: protein-cofactor (bacteriochlorophyll, bacteriopheophytin, and carotenoid) interactions, *Proc. Natl. Acad. Sci. U.S.A. 85*, 7993-7997.

10. van Brederode, M. E., Jones, M. R., van Mourik, F., van Stokkum, I. H. M., and van Grondelle, R. (1997) A new pathway for transmembrane electron tranfer in photosynthetic reaction centers of *Rhodobacter sphaeroides* not involving the excited special pair, *Biochemistry 36*, 6855-6861.

11. van Brederode, M. E., and van Grondelle, R. (1999) New and unexpected routes for ultrafast electron transfer in photosynthetic reaction centers, *FEBS Lett. 455*, 1-7.

12. van Brederode, M. E., van Mourik, F., van Stokkum, I. H. M., Jones, M. R., and van Grondelle, R. (1999) Multiple pathways for ultrafast transduction of light energy in the photosynthetic reaction center of *Rhodobacter sphaeroides*, *Proc. Natl. Acad. Sci. U.S.A. 96*, 2054-2059.

13. Durrant, J. R., Klug, D. R., Kwa, S. L. S., van Grondelle, R., Porter, G., and Dekker, J. P. (1995) A multimer model for P680, the primary electron donor of photosystem II, *Proc. Natl. Acad. Sci. U.S.A. 92*, 4798-4802.

14. Novoderezhkin, V. I., Andrizhiyevskaya, E. G., Dekker, J. P., and van Grondelle, R. (2005) Pathways and timescales of primary charge separation in the Photosystem II reaction center as revealed by simultaneous fit of time-resolved fluorescence and transient absorption, *Biophys. J. 89*, 1464-1481.

15. Novoderezhkin, V. I., Dekker, J. P., and van Grondelle, R. (2007) Mixing of exciton and charge transfer states in Photosystem II reaction centers: Modeling of Stark spectra with Modified Redfield Theory, *Biophys. J. 93*.

16. Romero, E., van Stokkum, I. H. M., Novoderezhkin, V. I., Dekker, J. P., and van Grondelle, R. (2010) Two different charge separation pathways in photosystem II, *Biochemistry 49*, 4300-4307.

17. van Stokkum, I. H. M., Larsen, D. S., and van Grondelle, R. (2004) Global and target analysis of time-resolved spectra, *Biochim. Biophys. Acta 1657*, 82-104.

18. Berera, R., van Grondelle, R., and Kennis, J. T. M. (2009) Ultrafast transient absorption spectroscopy: principles and application to photosynthetic systems, *Photosynth. Res. 101*, 105-118.

19. Boxer, S. G. (1996) Stark spectroscopy of photosynthetic systems, In *Biophysical Techniques in Photosysnthesis* (Hoff, J. A. a. A. J., Ed.), pp 177-189, Kluwer Academic Publishers.

20. Bublitz, G. U., and Boxer, S. G. (1997) Stark spectroscopy: applications in chemistry, biology, and material science, *Annu. Rev. Phys. Chem. 48*, 213-242.

21. Liptay, W. (1974) In *Excited states* (Lim, E., Ed.), pp 129-229, Academic Press, New York.

22. Mäntele, W. (1996) Infrared and Fourier-transform infrared spectroscopy, In *Biophysical techniques in photosynthesis* (Hoff, J. A. a. A. J., Ed.), pp 137-160, Kluwer Academic Publishers.

CHAPTER 2

Two Different Charge Separation Pathways in Photosystem II

Elisabet Romero, Ivo H. M. van Stokkum, Vladimir I. Novoderezhkin, Jan P. Dekker and Rienk van Grondelle

Charge separation is an essential step in the conversion of solar energy into chemical energy in photosynthesis. To investigate this process, we performed transient absorption experiments at 77 K with various excitation conditions on the isolated Photosystem II reaction center preparations from spinach. The results have been analyzed by global and target analysis and demonstrate that at least two different excited states, $(Chl_{D1}Phe_{D1})^*$ and $(P_{D1}P_{D2}Chl_{D1})^*$, give rise to two different pathways for ultrafast charge separation. We propose that the disorder produced by slow protein motions causes energetic differentiation among reaction center complexes, leading to different charge separation pathways. Because of the low temperature, two excitation energy trap states are also present, generating charge-separated states on long time scales. We conclude that these slow trap states are the same as the excited states that lead to ultrafast charge separation, indicating that at 77 K charge separation can be either activation-less and fast or activated and slow.

This chapter is based on the publication:

Elisabet Romero, Ivo H. M. van Stokkum, Vladimir I. Novoderezhkin, Jan P. Dekker and Rienk van Grondelle. (2010) *Biochemistry (Accelerated Publications)*, *49*, 4300-4307

INTRODUCTION

Charge separation is one of the key processes in photosynthetic energy conversion. After absorption of a photon by the photochemically active reaction center, an electronically excited state is transformed into a short-lived charge-separated state. Subsequent electron transfer results in a stable charge-separated state which ultimately powers the photosynthetic organism.

Type II reaction centers found in purple bacteria and in oxygen evolving organisms (cyanobacteria, algae, and higher plants) are membrane proteins that contain four (bacterio)chlorophyll [(B)Chl] and two (bacterio)pheophytin [(B)Phe] molecules arranged in two symmetric branches spanning the membrane in the center of the complex. It is established that only one branch is active in charge separation (*1-4*).

The best understanding of the kinetics and energetics of charge separation has been obtained for the reaction center (RC) of photosynthetic purple bacteria (*5*). The central excitonically coupled special pair, P, of BChl molecules [P_A and P_B, ≈ 8 Å apart, center to center (*6*)], absorbing at ≈ 875 nm in *Rhodobacter sphaeroides*, are electronically excited after the energy transfer from the LH1 core antenna (absorbing at approximately equal energy). Then, an electron is transferred to the BChl molecule on the active branch (B_A) in 3 ps, and from B_A to the BPhe (H_A) in 1 ps, resulting in the final charge-separated state, $P^+H_A^-$. However, in isolated reaction centers, excitation of the accessory BChl absorbing at ≈ 800 nm (B_A) resulted in an even faster charge separation, either via $B_A^+H_A^-$ or via $P^+B_A^-$ (*7-9*). *In vivo*, this second route does not occur to a significant extent, because B_A is too high in energy to receive excitation energy from the antenna.

In the photosystem II reaction center (PSII RC) of oxygen evolving organisms, there is no special pair, and the similar distance of ≈ 10-11 Å between neighbouring pigments in the center of the complex (*10-13*) gives rise to a system of coupled pigments (*14, 15*) that interact, creating collective excited (or exciton) states with contributions from several pigments.

The PSII RC, the unique molecular machinery capable of using light to create a charge-separated state that drives water splitting, contains four chlorophyll and two pheophytin molecules (Phe_{D1}, Chl_{D1}, P_{D1}, P_{D2}, Chl_{D2}, and Phe_{D2}, the RC core), two additional chlorophyll molecules ($Chls_Z$), located at opposing sites on the periphery of the complex ≈ 25 Å from the core pigments, and two *β*-carotene molecules located between $Chls_Z$ and the RC core (*10-13*). The system is continuously moving: fast nuclear motions (intra- and interpigment vibrations and protein vibrations) and slow conformational motions of the

protein produce homogeneous and inhomogeneous broadening, respectively, of the electronic transitions. The low-energy side of the spectra, the Q_Y region, is characterized by ultrafast energy equilibration among the cofactors in the RC core, radical pair (RP) formation, and excitation energy transfer from $Chls_Z$ to the RC core. The superposition of these processes greatly complicates the interpretation of the transient absorption data and has led to a long and extensive debate in the literature regarding the mechanism and time scale of charge separation (*15, 16*). Recent work (*17, 18*) at room temperature indicates that the charge separation process follows the sequence $RC^* \rightarrow Chl_{D1}{}^{+}Phe_{D1}{}^{-} \rightarrow P_{D1}{}^{+}Phe_{D1}{}^{-} \rightarrow (P_{D1}{}^{+}Phe_{D1}{}^{-})_{relaxed}$. In ref 18, an additional Chl_Z excited state, Chl_Z^*, which feeds excitation energy into the RC core was included.

Previously, we have described all the available PSII RC spectroscopic data at room and low temperature within a physical model that takes into account the coupling of excitations to fast and slow motions of the system (*19*). In this model, the excited-state manifold includes a primary charge transfer (CT) state that is strongly mixed with the exciton states. Such a mixing connects the lowest exciton state with the CT state; i.e., it facilitates the formation of the first radical pair. The lowest exciton state is a multimeric state (*14, 20*), a coherent superposition of several PSII RC core pigments, the contribution of each pigment being not uniform and strongly dependent on protein conformation (static disorder) (*19*). Therefore, for the lowest exciton state, several combinations with different participation of different pigments are possible, which can lead to different charge separation pathways. The best description of the available data was obtained for the charge separation pathways:

Chl_{D1} path: $(Chl_{D1}Phe_{D1})^* \rightarrow Chl_{D1}{}^{+}Phe_{D1}{}^{-} \rightarrow P_{D1}{}^{+}Phe_{D1}{}^{-}$

P_{D1} path: $(P_{D1}P_{D2}Chl_{D1})^* \rightarrow P_{D2}{}^{+}P_{D1}{}^{-} \rightarrow P_{D1}{}^{+}Chl_{D1}{}^{-} \rightarrow P_{D1}{}^{+}Phe_{D1}{}^{-}$

(note that in this representation the cofactor sequence reflects the order of participation in the excitonic wave function).

In this study, we analyzed the energy transfer and charge separation reactions in the isolated PSII RC by transient absorption spectroscopy in much greater detail than was done previously. We simultaneously probed a large spectral range (from 425 to 730 nm, to investigate not only the Q_Y region of Chl and Phe but also the Phe Q_X band at 544 nm and the Phe anion band at ≈ 455 nm), monitored an extensive time range (from 10 ps before to 3 ns after the excitation pulse, to investigate all various time scales of charge separation),

recorded the data at 77 K (to enhance the spectral resolution and reduce back reactions and uphill energy transfer), and used various excitation conditions (to allow photoselection of subpopulations with different proportions of Chl_{D1} and P_{D1} pathways). Combining all results and using global and target analysis according to a kinetic scheme, we demonstrate that, in agreement with the theoretical model (*19*), at least two different charge separation pathways are operational in the isolated PSII RC. In addition, we identify two long-lived trap states that form the final radical pair on a long time scale, indicating that both initial excited states give rise to their own spectrally and kinetically distinguishable trap state at 77 K.

MATERIALS AND METHODS

Sample Preparation. The PSII RC (D_1-D_2-cyt b_{559}) complexes were isolated from spinach as described in ref (*21*). The sample was diluted in a buffer containing 60% glycerol (v/v), 20 mM BisTris (pH 6.5), 200 mM sucrose, and 0.06% β-DM. The optical density of the sample was ≈ 1 mm^{-1} at 678 nm.

Laser System. The seed pulse from a diode-pumped oscillator (Coherent Vitesse, 800 nm, 80 MHz) was amplified to 2.5 W by using a Nd:YLF high-power pump laser (Coherent Evolution-20, 527 nm). The Ti:sapphire-based amplifier (Coherent Legend-UHP) incorporates chirped pulse amplification (CPA) to deliver sub-50 fs pulses, with a center wavelength of 800 nm and 15 nm full width at half maximum (fwhm). The probe pulse, a white light continuum, was generated by focusing a small fraction of the fundamental 800 nm pulses into a laterally rotating CaF_2 plate. The duration of the white light pulses was ≈ 120 fs because of group velocity dispersion introduced by the medium. The tunable pump pulses were generated by a commercial optical paramagnetic amplifier (OPA, Coherent OperA) pumped by the Legend-UHP. The pump pulse duration was ≈ 100 fs with 10 nm fwhm. To generate the transient absorption data, we modulated the pump at 166.5 Hz. The polarization between pump and probe pulses was set to magic angle (54.7°). The pump and probe pulses were focused on the sample with spot sizes 160 and 75 μm in diameter, respectively. After the sample, the probe was spectrally dispersed by a 15 cm focal length spectrograph (Oriel) equipped with a 300 lines/mm and 500 nm blazed grating onto a home-built 256-pixel photodiode array. The temporal and spectral resolution were ≈ 140 fs and ≈ 1 nm, respectively.

Experimental Design. Femtosecond transient absorption spectra were recorded at 77 K in the visible range from 425 to 730 nm. To avoid singlet-triplet annihilation and sample degradation due to the accumulation of triplet states (lifetime of 1-2 ms), the laser system was operating at a repetition rate of 333 Hz (i.e., 6 ms between pump pulses). Six narrow (5 nm fwhm) excitation wavelengths (λ_{exc}) were used: 660, 665, 670, 675, 680, and 685 nm. In addition, three broader excitations (fwhm) were used: 662 nm (8 nm), 675 nm (12 nm), and 682 nm (8 nm). The excitation power was sufficiently low to avoid multiple excitations in a single reaction center complex (5.5-30 nJ/pulse depending on λ_{exc}). The absence of annihilation was checked by power dependence series of measurements. Typically, nine scans were recorded and averaged per data set. Each scan consisted of 275 time delays from -10 ps to 3 ns (225 time points from -10 to 100 ps), with 1000 shots taken and averaged per time delay. Statistics in real time were performed. The data was accepted only when 50% of the 1000 shots taken for time delay were within a standard deviation of 5%. Otherwise the data was discarded until it satisfied the statistical restrictions. We checked the sample integrity before and after the measurement by recording the steady-state absorption spectrum. After measurement for the usual 5 h, no sample degradation was observed.

Data Analysis. Global analysis using both parallel decaying and sequential models was applied to all data sets individually. Target analysis was performed on different groups of linked data sets as well as on individual data sets. The results were consistent.

RESULTS

Low-temperature (77 K) transient absorption spectra of the isolated PSII RC from spinach have been recorded for different sets of excitation wavelengths: six narrow excitation wavelengths at 660, 665, 670, 675, 680, and 685 nm (5 nm fwhm) (Figure 1); two broader excitation wavelengths at 662 and 682 nm (8 nm fwhm); and a nonselective excitation wavelength at 675 nm (12 nm fwhm) (Figure A1 of the Appendix). The first step in this study is the application of global analysis (*22*) using both a parallel decaying and a sequential model to follow the spectral evolution in time. The second step is to test the presence of multiple charge separation pathways by target analysis (*22*). The interpretation of the spectra obtained after global and target analysis in the spectrally congested Q_Y region is based on the known cofactor absorption: the peripheral $Chls_Z$ absorb at 670 nm (*23-25*), both Phe_{D2} and Phe_{D1} absorb at 680 nm (*26*), Chl_{D1} and Chl_{D2} also contribute to the 680 nm spectral region (*27-31*), and P_{D1} is centered at 672.5 nm (*27*).

An essential aspect of this study is the analysis of the spectrally isolated Phe Q_X band at 544 nm. The time-dependent background in this region is minimized by setting ΔA_{557} equal to 0 (*32, 33*) which facilitates the visualization of the bleach dynamics. The Phe Q_X bleach around 544 nm is present when Phe is either excited or reduced, and the Phe anion absorption band at around 455 nm occurs only when Phe is reduced, i.e., participating in a radical pair.

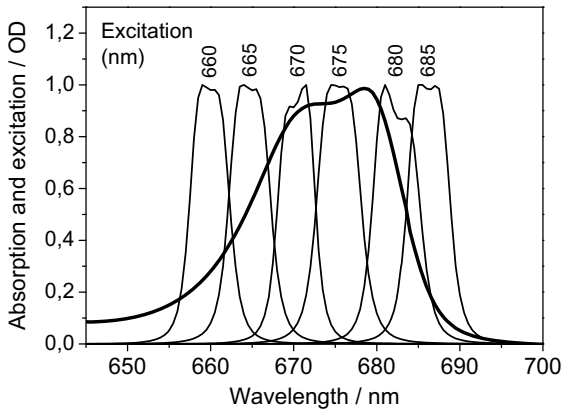

Figure 1. Photosystem II reaction center (PSII RC) absorption spectrum at 77 K *(thick line*) and narrow laser excitation profiles (*thin lines*).

Global Analysis

To identify the spectral components present in the system and estimate their lifetimes, a global analysis was performed on all the data sets using a parallel model with exponential decays. The resulting decay-associated difference spectra (DADS) and their lifetimes are given in Figure A2 and Table A1 of the Appendix. However, since it is generally accepted that the dynamics in the PSII RC follow the excited state (RC*) → RP1 → RP2 sequence, a sequential model in which one component decays into the next one is more appropriate. On the basis of the estimated lifetimes (Table A1), we chose six components with common lifetimes of 500 fs, 3 ps, 20 ps, 300 ps, 600 ps, and 20 ns to fit all the data and to facilitate comparison among the different data sets. The obtained evolution-associated difference spectra (EADS) represent a mix of species whose populations rise with the lifetime of the previous component and decay with their lifetimes. For instance, the 20 ps EADS rises in 3 ps and decays in 20 ps (*22*).

The EADS for narrow excitation are shown in Figure 2. In the Q_Y region, the initial bleach contains all initially populated exciton states and the $Chls_Z$ excited states, the proportion of which depends on the excitation wavelength.

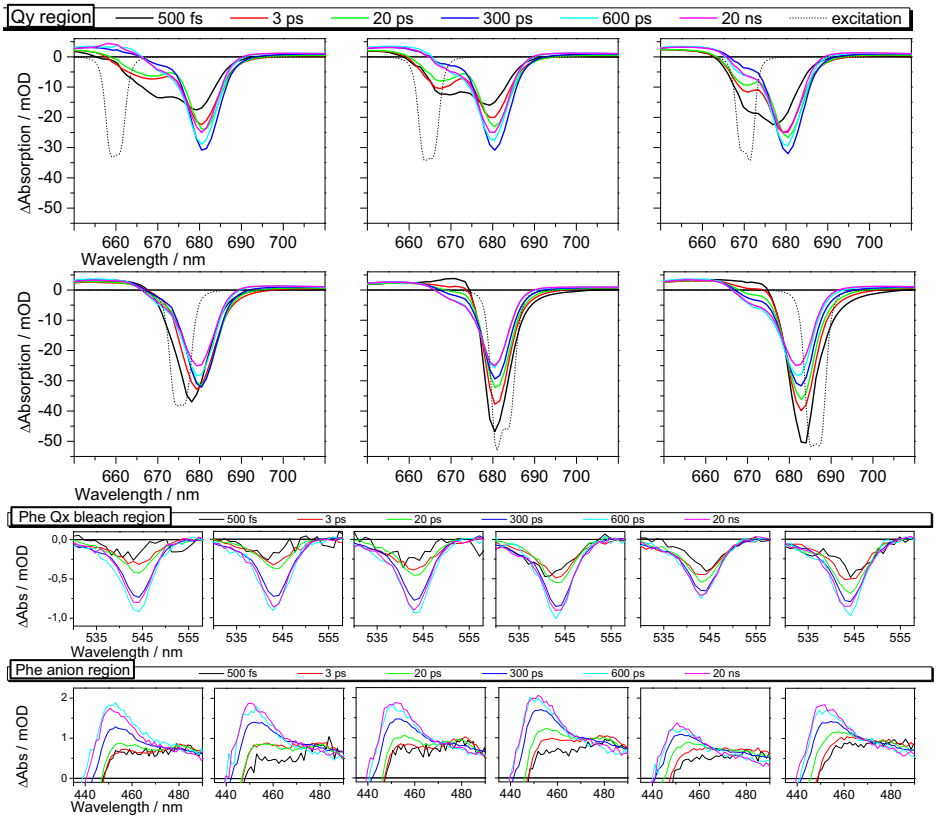

Figure 2. Evolution-associated difference spectra (EADS) for narrow excitations. The top six panels show the Q_Y absorption region (*from top to bottom and from left to right*) for 660, 665, 670, 675, 680, and 685 nm excitation. The middle panels show the Phe Q_X absorption region after background subtraction (*from left to right*) for 660-685 nm excitation. The bottom panels show the Phe anion absorption region (*from left to right*) for 660-685 nm excitation. Solid colored lines are EADS, and dotted black lines are inverted laser excitation profiles. The EADS have been normalized to the long-lived component (20 ns).

The signal after 500 fs is the combination of the absorption changes caused by the disappearance of the lowest exciton states of the RC core, $Chls_Z$ excited states that only transfer excitation energy to the RC core on the 20 ps time scale (*23, 34, 35*), and the appearance of the first radical pair(s).

At first sight, the spectral evolution in the Q_Y region can be divided into two groups with two main characteristics: blue excitation (660-670 nm) with up to 20 ps two main bleaches at around 670 and 680 nm with the amplitude of the 680 nm bleach increasing from 500 fs to 300 ps; and red excitation (680-685 nm) with one main bleach at around 680 nm decreasing in amplitude

from 500 fs to 20 ns and a shoulder around 672 nm developing from 3 to 600 ps (675 nm excitation being an intermediate case between blue and red excitation). The final evolution, from 300 to 600 ps and from 600 ps to 20 ns, is very similar for all excitations, indicating that on this long time scale the system evolves to a common species independent of the excitation wavelength. After 600 ps, the similarity between the spectra of the 600 ps and 20 ns components suggests the relaxation of the final RP, $P_{D1}^{+}Phe_{D1}^{-}$.

(i) ***Red Excitation (680-685 nm)***. The 500 fs component is dominated by a single bleach at 680.5 and 681.5 nm for 680 and 685 nm excitation, respectively (Figure 2), in agreement with the population of exciton states containing at least Chl_{D1}, Chl_{D2}, Phe_{D1}, and/or Phe_{D2} (*26-29, 31*) and the stimulated emission (SE) from these excited states at the red side of the bleach. It is worth noting that the Q_Y position for the long-lived state shifts to the red upon increasing the excitation wavelength, which implies that photoselection of subpopulations from the inhomogeneous distribution has been achieved. After 500 fs, the main 680 nm bleach decreases and a shoulder around 672 nm appears. After 3 ps, a further 680 nm bleach decrease and a 672 nm bleach increase are observed. A similar evolution is observed from 3 to 20 ps, from 20 to 300 ps, and from 300 to 600 ps. The spectral properties of this evolution are in agreement with the disappearance of an excited state/RP containing Chl_{D1} and the appearance of a RP containing P_{D1}: $Chl_{D1}^{*}/Chl_{D1} \rightarrow Chl_{D1}^{+}Phe_{D1}^{-}$ (RP1) $\rightarrow P_{D1}^{+}Phe_{D1}^{-}$ (RP2). The RP1 $\rightarrow$ RP2 evolution should give rise to a fully bleached Phe Q_X band in the 3 ps component that will remain constant in the subsequent EADS (*18*). However, the spectral evolution of the Phe Q_X band at 544 nm shows a different behaviour (Figure 2 and Table A2 of the Appendix). The amplitude of the bleach increases over a range of time scales: 500 fs (mainly due to Phe*) and 3, 20, and 300 ps (mainly due to the formation of Phe_{D1}^{-}). The evolution in the Phe_{D1} anion band at 455 nm is in agreement with the slow phases (20 and 300 ps) of RP formation containing Phe_{D1}. The slower phases of Phe_{D1}^{-} formation were previously observed (at room and low temperature) but were interpreted as charge separation limited by slow energy transfer from a red $Chls_Z$ (*18, 32, 36*). We will show (see below) that the $Chls_Z^{*}$ are not populated upon 680-685 nm excitation (Chapter 4 of this Thesis), which excludes the possibility that the slow charge separation upon red excitation is caused by the energy transfer from $Chls_Z$ to the RC core. The slow phases of Phe_{D1}^{-} formation indicate that the Chl_{D1} path as a unique charge separation mechanism (17, 18) is not able to explain the observed dynamics.

(ii) Blue Excitation (660-670 nm). The spectral shape of the 500 fs component (Figure 2) is highly dependent on excitation wavelength. However, two common bleaches at 670 and 679 nm are observed for blue excitation. The 670 nm bleach corresponds to the $Chls_Z$ excited state (*23*) and exciton states containing P_{D1} (*27*) and higher exciton states. The 679 nm bleach reflects the population of an exciton(s) with participation of at least Chl_{D1}, Chl_{D2}, Phe_{D1}, and/or Phe_{D2} (*26-29, 31*). The main changes from the 500 fs to the 3 ps component are the decrease in the 670 nm bleach and the increase and red shift of the 680 nm bleach. This evolution can be explained by exciton relaxation from the levels near 670 nm to the lowest levels peaking near 680 nm. After 3 ps (20 ps EADS), a further 670 nm bleach decrease and a 680 nm bleach increase are observed. After 20 ps, the 670 nm bleach disappears and a substantial increase in the 680 nm bleach is observed, indicating that the energy transfer from $Chls_Z$ to the RC core is completed (*23, 34, 35*). The shoulder at ≈ 672 nm reflects the formation of a RP containing P_{D1} (*27*). After 300 ps, the 600 ps component appears with a further increase in the 672 nm shoulder and a decrease in the 680 nm bleach. The spectral evolution is in agreement with the Chl_{D1} path: $Chl_{D1}^{+}Phe_{D1}^{-}$ (RP1) → $P_{D1}^{+}Phe_{D1}^{-}$ (RP2). However, on a long time scale, after 300 ps, a Phe Q_X bleach increase of 15-20% is again observed. The slow phases (20 and 300 ps) of RP formation containing Phe_{D1} are confirmed by the evolution in the Phe_{D1} anion band at 455 nm (Figure 2).

(iii) $Chls_Z$* Population and Energy Transfer to the RC Core Pigments. The evolution of the $Chls_Z$* population can be indirectly estimated by quantifying the amount of excitation energy present in the RC core at a certain time after excitation. The energy located in the RC core is measured as the amplitude of the Phe Q_X bleach for each component with respect to the final total amplitude (600 ps component). When blue and red excitations are compared on the long time scale, 300 ps, the Phe Q_X bleach amplitude is very similar. However, on the short time scale, it is clear that for blue excitation the initial amount of excitation energy in the RC core is lower: ≈ 29% for the 500 fs component versus ≈ 52% for red excitation. This significant difference indicates that for blue excitations part of the excitation energy is absorbed by cofactors not located in the RC core. Another significant difference is the Q_X bleach amplitude increase after 20 ps: ≈ 34% for blue and ≈ 13% for red excitation (last column in Table A2 of the Appendix), indicating that for blue excitation after 20 ps a significant amount of energy has been delivered to the RC core (apart from the Phe Q_X bleach increase due to RP formation). These observations are in agreement with both $Chls_Z$ absorbing around 670 nm and with the 20 ps lifetime for the energy transfer from $Chls_Z$ to the RC core (*23, 34, 35*).

Therefore, we can confidently conclude that (i) $Chls_Z$ are not populated with 680-685 nm excitation and (ii) the energy transfer from $Chls_Z$ to the RC core occurs with a lifetime of 20 ps, not on longer time scales (*18, 32, 36*) (Chapter 4 of this Thesis).

Target Analysis

The results from the global analysis strongly indicate that the generally accepted charge separation process described by the Chl_{D1} path is not unique. Therefore, additional channels of charge separation must be operational in the PSII RC. To test this hypothesis, we perform a target analysis.

The kinetic scheme that serves as the input for the target analysis consists of two parallel charge separation pathways, Chl_{D1} and P_{D1} paths, each with compartments representing the excited states and the first radical pair (RP1) converging to a common secondary radical pair (RP2) that relaxes on the long time scale, with two additional compartments, Chl_{Z667}* and Chl_{Z670}*, which transfer excitation energy to the RC core slowly (Figure 3). To gather sufficient information to resolve the spectra of eight compartments with the complication of two parallel processes occurring on the same time scale, we analyzed several data sets simultaneously. Six data sets [660, 665, 670, and 675 nm (5 nm fwhm); 662 nm (8 nm fwhm); and 675 nm (12 nm fwhm)] have been linked in the target analysis. The 680, 682, and 685 nm excitations are not included because of the strong photoselection which produces an up to 2 nm red-shifted final state with respect to blue excitation that impedes the simultaneous analysis of the whole collection of data sets (Figure 2). The target analysis results in estimated species-associated difference spectra (SADS) and microscopic decay rates. The SADS are in a first approximation the pure spectra of the species represented by the kinetic compartments (the uncertainty arises due to the spectral congestion and due to the fact that all processes occur almost simultaneously). The kinetic scheme, rate constants, and SADS are shown in Figure 3. The target analysis also estimates the initial proportion of RCs following each pathway and the contribution of $Chls_Z$ to the total absorbed energy for the different subpopulation photoselected by each excitation wavelength (Table A3 of the Appendix).

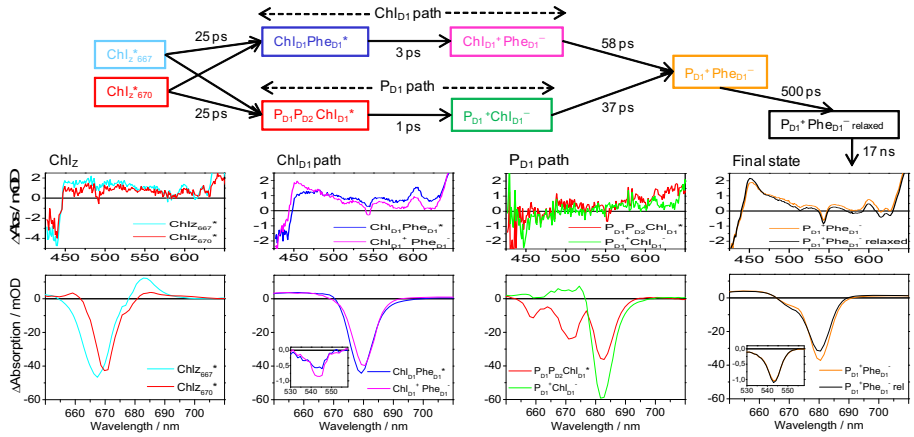

Figure 3. Kinetic scheme with two parallel charge separation pathways (*top*). SADS corresponding to the kinetic compartments (*bottom*). Insets show the Phe Q_X bleach after background subtraction. The equivalent graphs are plotted on the same scale for better comparison (except for the 425-650 nm region for $Chls_Z$).

(i) Chls$_Z$. Due to photoselection, two SADS are obtained for $Chls_Z$ with bleaches centered at 667 and 670 nm, SE around 675 and 677 nm, and a positive band at 685 nm assigned to excited state absorption. The rate of energy transfer from both $Chls_Z$* to the RC core is $(1/25\ ps)^{-1}$, in agreement with the 20 ps lifetime for $Chls_Z$* obtained from the global analysis and the literature (*23, 34, 35*).

(ii) Chl$_{D1}$ Path. In the Q_Y region, the RC* SADS $(Chl_{D1}Phe_{D1})$* consists of a bleach centered at 679 nm. This state decays in 3 ps to form a RP1 $(Chl_{D1}^{+}Phe_{D1}^{-})$ whose SADS is 1 nm red-shifted. Both SADS contain the Phe Q_X bleach at 544 nm, while RP1 shows a clear Phe anion band at 455 nm. The Phe features indicate that Phe is involved in this pathway, and the Q_Y bleach at 679 nm suggests the involvement of Chl_{D1}, in agreement with the $(Chl_{D1}Phe_{D1})^* \rightarrow Chl_{D1}^{+}Phe_{D1}^{-}$ transition. This assignment, excited state and RP, is also based on the presence of SE around 690 nm in the former and the typical RP-induced absorption in the 700-730 nm region in the latter.

(iii) P$_{D1}$ Path. In the Q_Y region, the RC* SADS $(P_{D1}P_{D2}Chl_{D1})^*$ contains bleaches at 660, 667, and 680 nm with relative amplitudes of 0.3, 0.7, and 1, respectively. The absence of the Phe features in both the RC* and RP1 $(P_{D1}^{+}Chl_{D1}^{-})$ spectra implies that Phe does not play a role in these states. Therefore, the bleaches at 660, 667, and 680 nm are consistent with contribution from high exciton states, P_{D1} and/or P_{D2}, and Chl_{D1}, respectively, in agreement with the $(P_{D1}P_{D2}Chl_{D1})^* \rightarrow P_{D1}^{+}Chl_{D1}^{-}$ process.

The RP1 spectrum has a significant bleach at 682 nm (suggesting the involvement of Chl_{D1}) but lacks the negative signal at 670 nm expected for oxidation of P_{D1}. It should be noted that the interpretation of the RP spectra is not straightforward, because oxidation or reduction will likely lead to electrochromic shifts of the absorbance spectra of nearby cofactors.

(iv) Secondary Electron Transfer. Then, both pathways converge by the transfer of an electron from Chl_{D1}^- to Phe_{D1} with a rate constant of 0.027 ps^{-1} (Chl_{D1} path) and from P_{D1} to Chl_{D1}^+ with a rate constant of 0.017 ps^{-1} (P_{D1} path). The RP2, $P_{D1}^+Phe_{D1}^-$, SADS is well-known in the literature with a main 680 nm bleach (Phe_{D1}), a shoulder around 672 nm (P_{D1}), a Phe Q_X band bleach, and a Phe anion absorption band. Compared to the final SADS, some additional excited-state absorption appears to be present between 475 and 625 nm.

(v) "Relaxation" Process. Surprisingly, in contrast with the initially hypothesized relaxation process, the spectral evolution on the 500 ps time scale shows a further increase in the population of the $P_{D1}^+Phe_{D1}^-$ final state: in the Q_Y region, there is an increase in the 672 nm shoulder and a decrease in the 680 nm bleach, and the amplitude of the Phe anion band suggests an increase in the Phe_{D1}^- population of around 20%. These findings point to the existence of a very slow channel of charge separation, which was also observed in the global analysis. It is interesting to note that from the global analysis the increase in the Phe_{D1}^- population on the long time scale was also around 20%. The fact that a 20% increase in the Phe anion band but a very small increase of less than 5% in the Phe Q_X band are observed indicates that a Phe excited state is transformed into Phe_{D1}^-.

Simplified Target Analysis

The inclusion of an extra compartment in the kinetic scheme is not possible with the available data. For this reason, we have applied a simplified target analysis in which the two parallel pathways are condensed in two compartments (RC* and RP1). This allows us to include the slow phase of charge separation observed in the data. The kinetic scheme that gives the best fit to the data consists of four excited states ($Chls_Z$*, RC*, $Trap_{65}$*, and $Trap_{585}$*) and two radical pairs [one containing a mix of RP1s and the other corresponding to the final charge-separated state, $P_{D1}^+Phe_{D1}^-$ (RP2)] (Figure 4).

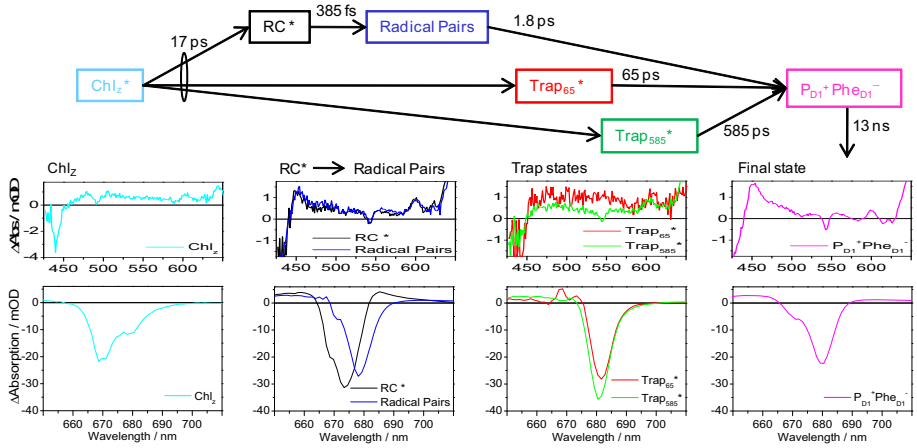

Figure 4. Simplified kinetic scheme with two trap states (*top*). SADS corresponding to the kinetic compartments for the 670 nm excitation data (*bottom*). All SADS are plotted on the same scale for better comparison (except for the 425-650 nm region for Chls$_Z$).

After 17 ps, the Chls$_Z$ excitation energy is transferred to the RC core. Trap$_{65}$* is depopulated in 65 ps to form RP2. Features of this process were already present in the DADS at 46, 39, and 36 ps (for 665, 680, and 685 nm excitation, respectively) (Figure A2 of the Appendix). As observed in the global analysis and the previous target analysis, additional RP2 is created on the 500 ps time scale, which is explained by the energy transfer from Trap$_{585}$. The SADS for the Chls$_Z$*, RC*, and mix of RP1s compartments have a spectral shape similar to that previously obtained (Figure 3). Due to photoselection, the bleach positions in the Q_Y absorption region are dependent on excitation wavelength. The Trap$_{65}$* SADS has Chl features with a bleach at 681.5 nm and SE at 690 nm but lacks features of Phe excited states. The Trap$_{585}$* SADS has a 681 nm bleach, SE at 690 nm, and a Phe Q_X bleach but no Phe anion band, which indicates that Chl and Phe contribute to this excited state. The initial distribution of excitation energy is wavelength dependent (Table A4 of the Appendix). For blue excitation (660, 662, 665, and 670 nm data sets linked), the initial excitation energy is distributed among the Chls$_Z$* (33%), RC* (43%), Trap$_{65}$* (14%), and Trap$_{585}$* (10%) states. After the transfer of energy from the Chls$_Z$ to the RC core, 59% of the final charge-separated state ($P_{D1}^+Phe_{D1}^-$) is formed via RC*, 15% via Trap$_{65}$*, and 26% via Trap$_{585}$*. For red excitation (680, 682, and 685 nm data sets linked), an expected difference with respect to the blue data is found in the initial distribution of excitation energy: 60% is absorbed by RC*, 20% is trapped by Trap$_{65}$*, and 20% is trapped by Trap$_{585}$*.

This indicates that the slow phases of RP formation arise from trap states delocalized over the central RC core pigments and not from the slow energy transfer from a red Chl_Z to the central RC pigments.

DISCUSSION

Trap States

The presence of trap states in the PSII RC from higher plants at 4 K has been reported previously [a Chl trap (*37*) and a Phe trap (*38*)]. Here, at 77 K, two slow phases of charge separation, 65 and 585 ps, have been identified as originating from trap states with Chl and ChlPhe contribution, designated $Trap_{65}$ and $Trap_{585}$, respectively. The high-resolution fluorescence line narrowing (FLN) technique showed that there is a pronounced similarity between the spectroscopic features of the emitting and charge separating states in the PSII RC (*20*); therefore, and according to the spectral features (Figure 4), we conclude that $Trap_{585}$ originates from $(Chl_{D1}Phe_{D1})^*$ and $Trap_{65}$ from $(P_{D1}P_{D2}Chl_{D1})^*$. In line with the idea of a distribution of free energy difference around zero for charge separation (*38, 39*) and taking into account the disorder, it is reasonable to consider that charge separation may be activated in part of the RC complexes at low temperatures, leading to the observed slow kinetics. It is interesting to note that the excited states $(Chl_{D1}Phe_{D1})^*$ and $(P_{D1}P_{D2}Chl_{D1})^*$ can give rise to charge separation in either an activated or activation-less manner. This has been demonstrated by the two complementary target analyses. In the first target analysis, we concentrate on resolving the two parallel activation-less charge separation pathways on the fast, picosecond time scale (Figure 3). However, in this target analysis, the SADS of the penultimate state that rises with ≈ 50 ps and decays with ≈ 500 ps still contains chlorine excited-state absorption. These slow processes could well be interpreted as activated different pathways with the simplified target analysis (Figure 4). Here we need to compromise the fast phases to resolve the slow phases of charge separation present in the data, which explains why the time scales of the RC* → RP1 → RP2 evolution in the simplified target analysis are different from the ones found with the first target analysis.

Multiple Pathways of Charge Separation

The slow phase of Phe_{D1}^- formation, present in the Q_X and anion bands, was predicted by the model (*19, 40*) via the $(P_{D1}P_{D2}Chl_{D1})^* \rightarrow P_{D2}^+P_{D1}^- \rightarrow P_{D1}^+Chl_{D1}^-$ $\rightarrow P_{D1}^+Phe_{D1}^-$ mechanism. The first step excited state → radical pair is ultrafast, and it is not resolved in our target analysis. In line with the multimer model, in which the similarity in magnitude of the exciton coupling and energetic disorder results in exciton states delocalized over several cofactors (*14, 37*), it is reasonable to consider that depending on protein conformation, distinct exciton states are present in the system. Each of these leads to a different pathway of charge separation, which has also been demonstrated for the bacterial reaction center (*7-9*). At this point a question arises: is the protein actively involved in the determination of a pathway or is this determination only dependent on random static disorder? We suggest that at room temperature both pathways are possible. In case of a deterministic pathway, a single RC could switch between different states, which has also been observed for bacterial and plant light-harvesting complexes (*41-43*) providing functional flexibility. In the case of random disorder, the presence of two different charge separation pathways may help in the maintenance of high quantum efficiency in spite of the large disorder induced by the thermal energy at physiological temperatures.

The functional role of the protein matrix has been investigated before: changes in locally flexible domains in type I and II reaction centers have been shown to provide the means for adaptation of the enzyme to the ambient temperature (*44*), in the photosystem I complex of cyanobacteria protein dynamics have been shown to induce variation in energy transfer pathways (*45*), and for the bacterial reaction center the role of the protein matrix in controlling the kinetics of initial electron transfer has been demonstrated (*46*). In the latter contribution, the authors argue that the charge separation kinetics is determined by protein conformational changes induced by the absorption of light. In our view, the protein is inhomogeneously distributed prior to light absorption, and the slow protein motions are responsible for the presence of different pathways of charge separation.

In conclusion, two different charge separation pathways have been identified in the PSII RC from higher plants. Figure 5 shows the excitation energy distribution in the excited state and the charge separation events in the core of the photosystem II reaction center.

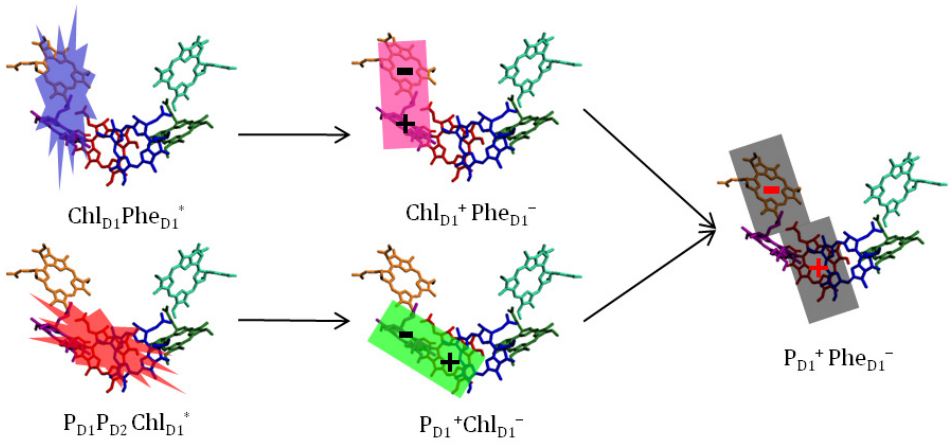

Figure 5. Excitation energy distribution in the excited state and charge separation events in the core of the PSII RC upon excitation in the Q_Y absorption band (pigment arrangement from ref (*13*)). The excited states are represented as stars, and the radical pairs are represented as rectangles

Depending on protein configuration, the charge separation events follow the Chl_{D1} path: $(Chl_{D1}Phe_{D1})^* \rightarrow Chl_{D1}^{+}Phe_{D1}^{-} \rightarrow P_{D1}^{+}Phe_{D1}^{-}$ or the P_{D1} path: $(P_{D1}P_{D2}Chl_{D1})^* \rightarrow P_{D1}^{+}Chl_{D1}^{-} \rightarrow P_{D1}^{+}Phe_{D1}^{-}$. Therefore, Phe_{D1} is an electron acceptor, P_{D1} is an electron donor, and Chl_{D1} can act both as an electron donor and as an acceptor.

The capacity of the protein to fine-tune the energy of the excited states could be an advantage under stress conditions in which a modification of the kinetics of charge separation is required. This functional flexibility may be a key aspect in the successful performance of the PSII RC.

ACKNOWLEDGMENT

We thank Jos Thieme for technical support and Henny van Roon for the expert preparation of the samples. This work was supported by Marie Curie Research Training Network INTRO2 (MRTN-CT-505069) (E.R.) of the European Union and by The Netherlands Organization for Scientific Research (NWO) and the Russian Foundation for Basic Research (V.I.N.).

APPENDIX

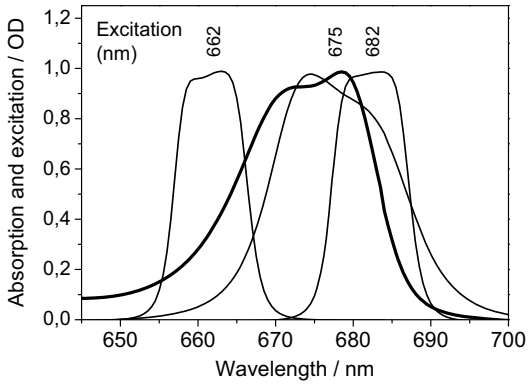

Figure A1. Photosystem II reaction center (PSII RC) absorption spectrum at 77 K (*thick line*) and broad laser excitation profiles (*thin lines*).

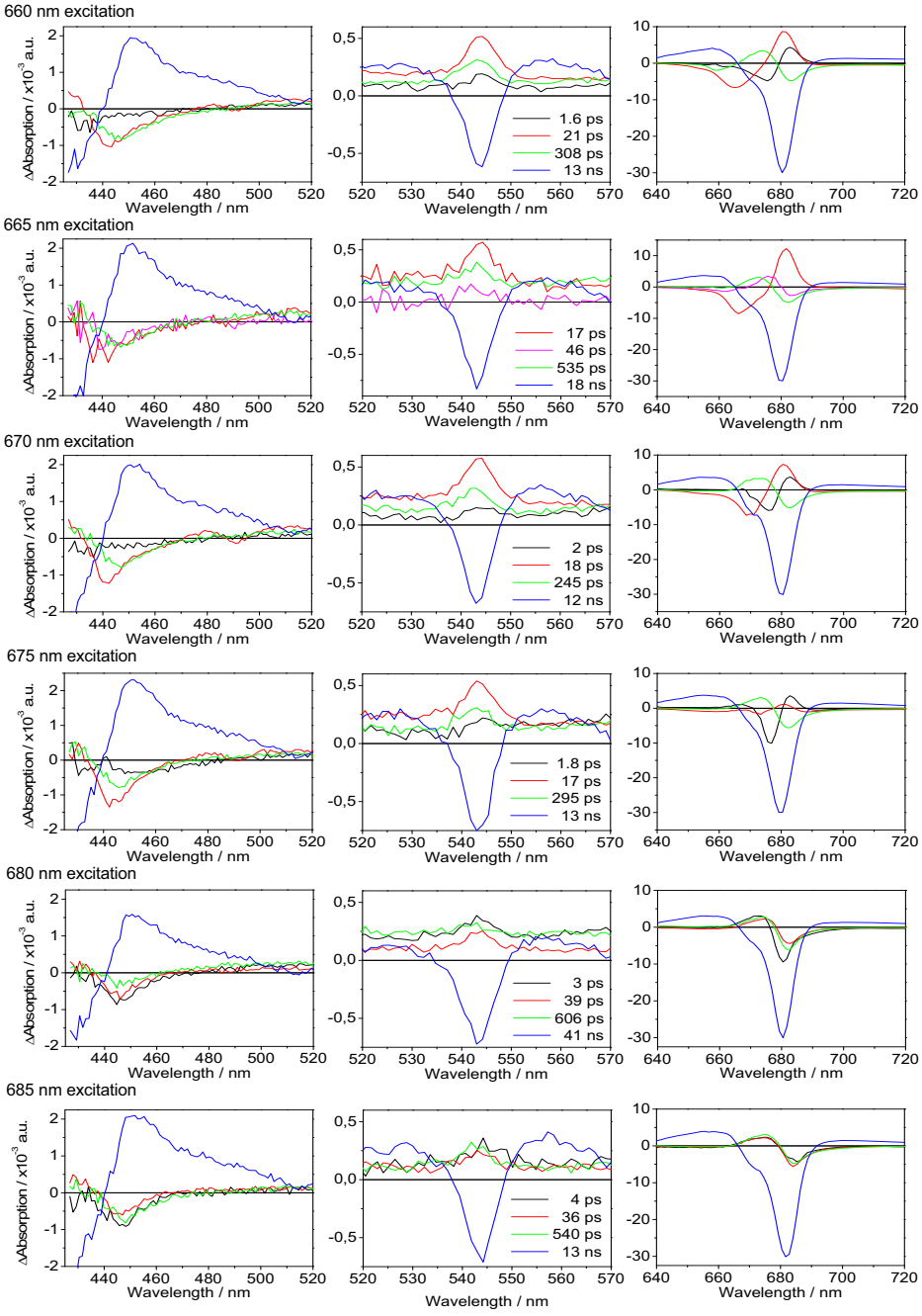

Figure A2. Decay associated difference spectra (DADS) for narrow excitations. (*From top to bottom*) 660 nm, 665 nm, 670 nm, 675 nm, 680 nm and 685 nm excitation and (*from left to right*) Phe anion, Phe Q_X and Q_Y absorption regions.

In the 440 – 460 nm region the blue DADS represents the absorption band of the non-decaying Phe anion. The other DADS indicate that two or three rise time scales are present with all excitation wavelengths. In the 535 – 555 nm region the blue DADS represents the final bleach of the Phe Q_X absorption. Likewise, in this region the bleach rises on three time scales. The area of the final bleach appears larger than the sum of the rises because of the direct Phe Q_x bleach upon excitation. In the Q_Y region the blue DADS represents the final radical pair where the changes in the position of the bleach are attributed to photoselection. The DADS with lifetimes up to 4 ps correspond to energy equilibration and early charge separation. For 660 – 670 nm excitation the ≈ 20 ps red DADS corresponds to Chl_Z decay and energy transfer to the RC core followed by fast charge separation, the small redshift of the bleach with excitation wavelength is attributed to photoselection. Two further slow time scales of ≈ 40 ps and 250 – 600 ps in which there is an additional rise of the final radical pair are present, in fact the green DADS in the Q_Y region are remarkably similar in shape for all excitations and similar also to the ≈ 40 ps red DADS for 680 – 685 nm excitation.

Table A1. Lifetimes estimated by global analysis with five parallel decays. Estimated values of all nine experiments have been collated in six columns to lump similar lifetimes.

λ_{exc}(fwhm)	**τ_1 / fs**	**τ_2 / ps**	**τ_3 / ps**	**τ_4 / ps**	**τ_5 / ps**	**τ_6 / ns**
660 nm (5)	145	1.6	21	—	308	13
665 nm (5)	680	—	17	46	535	18
670 nm (5)	199	2	18	—	245	12
675 nm (5)	138	1.8	17	—	295	13
680 nm (5)	205	3	—	39	606	41
685 nm (5)	903	4	—	36	540	13
662 nm (8)	105	1.7	20	—	331	12
675 nm (12)	62	1.3	21	—	257	12
682 nm (8)	105	1.8	—	31	576	14

The estimated relative error is 10 % for τ_2 - τ_5 and 20 % for τ_1. τ_6 is less precisely estimated because of the 3 ns time range, and can best be called *long lived*.

Table A2. Evolution of percentage of pheophytin Q_X bleach estimated by global analysis with a sequential model.

	500 fs	3 ps	20 ps	300 ps	600 ps	20 ns	Δ(300-20ps)
660 nm	29	34	47	80	100	88	33
665 nm	29	36	41	80	100	95	39
670 nm	29	42	49	83	100	96	34
675 nm	47	49	55	85	100	91	30
680 nm	54	60	73	87	100	95	14
685 nm	50	53	71	82	100	88	11

The Phe^*/Phe^- formation is calculated from the global analysis (EADS) as the amplitude of the Q_X bleach at 544 nm after background subtraction ($\Delta A_{557nm} = 0$) and expressed as a percentage with respect to the 600 ps component. The estimated relative error is 10 %.

Table A3. Distribution of excitation energy among exciton states for *blue* excitation.

λ_{exc} (fwhm)	$Chlz_{667}$*	$Chlz_{670}$*	$Chl_{D1}Phe_{D1}$*	$P_{D1}P_{D2}Chl_{D1}$*	$Chl_{D1}Phe_{D1}$*	$P_{D1}P_{D2}Chl_{D1}$*
660 nm (5)	25	0	48	27	64	36
665 nm (5)	27	5	51	17	75	25
670 nm (5)	3	27	58	12	83	17
675 nm (5)	0	8	85	7	92	8
662 nm (8)	31	0	55	14	80	20
675 nm (12)	0	12	70	18	80	20

The percentage of excitation energy in the exciton states is estimated by the target analysis of Figure 3 and expressed as a percentage with respect to the total excitation energy delivered to the system. The estimated relative error is 10%.

Table A4. Distribution of excitation energy among exciton states and their contribution to the final state.

	Blue excitation			*Red* excitation
	Initial	After $Chls_z$ ET	Final	Final
$Chls_z$*	33			
RC*	43	48% of 33 = 16	59	60
$Trap_{65}$	14	4% of 33 = 4	15	20
$Trap_{585}$	10	48% of 33 = 16	26	20

The percentage of excitation energy in the exciton states is estimated by the simplified target analysis of Figure 4 and expressed as a percentage with respect to the total excitation energy delivered to the system. The estimated relative error is 10%.

REFERENCES

1. Kirmaier, C., Holten, D., and Parson, W. W. (1985) Picosecond-photodichroism studies of the transient states in *Rhodopseudomonas sphaeroides* reaction centers at 5K. Effects of electron transfer on the six bacteriochlorin pigments, *Biochim. Biophys. Acta 810*, 49-61.
2. Lockhart, D. J., Kirmaier, C., Holten, D., and Boxer, S. G. (1990) Electric field effects on the initial electron-transfer kinetics in bacterial photosynthetic reaction centers, *J. Phys. Chem. 94*, 6987-6995.
3. Steffen, M. A., Lao, K., and Boxer, S. G. (1994) Dielectric asymmetry in the photosynthetic reaction center, *Science 264*, 810-816.
4. Diner, B. A., and Rappaport, F. (2002) Structure, dynamics, and energetics of the primary photochemistry of photosystem II of oxygenic photosynthesis, *Annu. Rev. Plant Biol. 53*, 551-580.
5. Zinth, W., and Wachtveitl, J. (2005) The first picoseconds in bacterial photosynthesis: Ultrafast electron transfer for the efficient conversion of light energy, *ChemPhysChem 6*, 871-880.
6. Yeates, T. O., Komiya, H., Chirino, A., Rees, D. C., Allen, J. P., and Feher, G. (1988) Structure of the reaction center from *Rhodobacter sphaeroides* R-26 and 2.4.1: protein-cofactor (bacteriochlorophyll, bacteriopheophytin, and carotenoid) interactions, *Proc. Natl. Acad. Sci. U.S.A. 85*, 7993-7997.
7. van Brederode, M. E., Jones, M. R., van Mourik, F., van Stokkum, I. H. M., and van Grondelle, R. (1997) A new pathway for transmembrane electron tranfer in photosynthetic reaction centers of *Rhodobacter sphaeroides* not involving the excited special pair, *Biochemistry 36*, 6855-6861.
8. van Brederode, M. E., and van Grondelle, R. (1999) New and unexpected routes for ultrafast electron transfer in photosynthetic reaction centers, *FEBS Lett. 455*, 1-7.
9. van Brederode, M. E., van Mourik, F., van Stokkum, I. H. M., Jones, M. R., and van Grondelle, R. (1999) Multiple pathways for ultrafast transduction of light energy in the photosynthetic reaction center of *Rhodobacter sphaeroides*, *Proc. Natl. Acad. Sci. U.S.A. 96*, 2054-2059.
10. Zouni, A., Witt, H. T., Kern, J., Fromme, P., Krauss, N., Saenger, W., and Orth, P. (2001) Crystal structure of photosystem II from *Synechococcus elongatus* at 3.8 Å resolution, *Nature 409*, 739-743.
11. Ferreira, K. N., Iverson, T. M., Maghlaoui, K., Barber, J., and Iwata, S. (2004) Architecture of the photosynthetic oxygen-evolving center, *Nature 303*, 1831-1838.
12. Loll, B., Kern, J., Saenger, W., Zouni, A., and Biesiadka, J. (2005) Towards complete cofactor arrangement in the 3.0 Å resolution structure of photosystem II, *Nature 438*, 1040-1044.

13. Guskov, A., Kern, J., Gabdulkhakov, A., Broser, M., Zouni, A., and Saenger, W. (2009) Cyanobacterial photosystem II at 2.9-Å resolution and the role of quinones, lipids, channels and chloride, *Nat. Struct. Mol. Biol. 16*, 334-342.

14. Durrant, J. R., Klug, D. R., Kwa, S. L. S., van Grondelle, R., Porter, G., and Dekker, J. P. (1995) A multimer model for P680, the primary electron donor of photosystem II, *Proc. Natl. Acad. Sci. U.S.A. 92*, 4798-4802.

15. Dekker, J. P., and van Grondelle, R. (2000) Primary charge separation in photosystem II, *Photosynth. Res. 63*, 195-208.

16. Rappaport, F., and Diner, B. A. (2008) Primary photochemistry and energetics leading to the oxidation of the $(Mn)_4Ca$ cluster and to the evolution of molecular oxygen in Photosystem II, *Coord. Chem. Rev. 252*, 259-272.

17. Groot, M.-L., Pawlowicz, N. P., van Wilderen, L. J. G. W., Breton, J., van Stokkum, I. H. M., and van Grondelle, R. (2005) Initial electron donor and acceptor in isolated photosystem II reaction centers identified with femtosecond mid-IR spectroscopy, *Proc. Natl. Acad. Sci. U.S.A. 102*, 13087-13092.

18. Holzwarth, A. R., Müller, M. G., Reus, M., Nowaczyk, M., Sander, J., and Rögner, M. (2006) Kinetics and mechanism of electron transfer in intact photosystem II and in the isolated reaction center: Pheophytin is the primary electron acceptor, *Proc. Natl. Acad. Sci. U.S.A. 103*, 6895-6900.

19. Novoderezhkin, V. I., Dekker, J. P., and van Grondelle, R. (2007) Mixing of exciton and charge transfer states in Photosystem II reaction centers: Modeling of Stark spectra with Modified Redfield Theory, *Biophys. J. 93*.

20. Peterman, E. J. G., van Amerongen, H., van Grondelle, R., and Dekker, J. P. (1998) The nature of the excited state of the reaction center of photosystem II of green plants: A high-resolution fluorescence spectroscopy study, *Proc. Natl. Acad. Sci. U.S.A. 95*, 6128-6133.

21. Kwa, S. L. S., Newell, W. R., van Grondelle, R., and Dekker, J. P. (1992) The reaction center of photosystem II studied with polarized fluorescence spectroscopy, *Biochim. Biophys. Acta 1099*, 193-202.

22. van Stokkum, I. H. M., Larsen, D. S., and van Grondelle, R. (2004) Global and target analysis of time-resolved spectra, *Biochim. Biophys. Acta 1657*, 82-104.

23. Vacha, F., Joseph, D. M., Durrant, J. R., Telfer, A., Klug, D. R., Porter, G., and Barber, J. (1995) Photochemistry and spectroscopy of a five-Chlorophyll reaction center of Photosystem II isolated by using a Cu affinity column, *Proc. Natl. Acad. Sci. U.S.A. 92*, 2929-2933.

24. Eijckelhoff, C., Vacha, F., van Grondelle, R., Dekker, J. P., and Barber, J. (1997) Spectroscopic characterization of a 5 Chl *a* photosystem II reaction center complex, *Biochim. Biophys. Acta 1318*, 266-274.

25. Raszewski, G., Saenger, W., and Renger, T. (2005) Theory of optical spectra of Photosystem II reaction centers: Location of the triplet state and the identity of the primary electron donor, *Biophys. J. 88*, 986-998.

26. Germano, M., Shkuropatov, A. Y., Permentier, H., Khatypov, R. A., Shuvalov, V. A., Hoff, J. A., and van Gorkom, H. J. (2000) Selective replacement of the active and inactive pheophytin in reaction centers of photosystem II by 13^1-deoxo-13^1-hydroxy-pheophytin *a* and comparision of their 6 K absorption spectra, *Photosynth. Res. 64*, 189-198.

27. Diner, B. A., Schlodder, E., Nixon, P. J., Coleman, W. J., Rappaport, F., Lavergne, J., Vermaas, W. F. J., and Chisholm, D. A. (2001) Site-directed mutations at D_1-His198 and D_2-His197 of photosystem II in *Synechocystis* PCC 6803: Sites of primary charge separation and cation triplet stabilization, *Biochemistry 40*, 9265-9281.

28. Kamlowski, A., Frankemoller, L., van der Est, A., Stehlik, D., and Holzwarth, A. R. (1996) Evidence for delocalization of the triplet state ^{3}P680 in the D_1-D_2-cyt-b_{559} reaction center complex of photosystem II, *Ber. Bunsen-Ges. 100*, 2045-2051.

29. Noguchi, T., Inoue, Y., and Satoh, K. (1993) FT-IR studies on the triplet state of P680 in the Photosystem II reaction center: Triplet equilibrium within a chlorophyll dimer, *Biochemistry 32*, 7186-7195.

30. Raszewski, G., Diner, B. A., Schlodder, E., and Renger, T. (2008) Spectroscopic properties of reaction center pigments in Photosystem II core complexes: Revision of the multimer model, *Biophys. J. 95*, 105-119.

31. van Mieghem, F. J. E., Satoh, K., and Rutherford, A. W. (1991) A chlorophyll tilted 30^o relative to the membrane in the Photosystem II reaction center, *Biochim. Biophys. Acta 1058*, 379-385.

32. Greenfield, S. R., Seibert, M., Govindjee, and Wasielewski, M. R. (1997) Direct measurement of the effective rate constant for primary charge separation in isolated photosystem II reaction centers, *J. Phys. Chem. B 101*, 2251-2255.

33. Greenfield, S. R., Seibert, M., and Wasielewski, M. R. (1999) Time-resolved absorption changes of the pheophytin Q_x band in isolated photosystem II reaction centers at 7 K: Energy transfer and charge separation, *J. Phys. Chem. B 103*, 8364-8374.

34. Schelvis, J. P. M., van Noort, P. I., Aartsma, T. J., and van Gorkom, H. J. (1994) Energy transfer, charge separation and pigment arrangement in the reaction center of photosystem II, *Biochim. Biophys. Acta 1184*, 242-250.

35. Rech, T., Durrant, J. R., Joseph, D. M., Barber, J., Porter, G., and Klug, D. R. (1994) Does slow energy transfer limit the observed time constant for radical pair formation in photosystem II reaction centers?, *Biochemistry 33*, 14768-14774.

36. Wang, J., Gosztola, D., Ruffle, S. V., Hemann, C., Seibert, M., Wasielewski, M. R., Hille, R., Gustafson, T. L., and Sayre, R. T. (2002) Functional assymetry of photosystem II D1 and D2 peripheral chlorophyll mutants of *Chlamydomonas reinhardtii*, *Proc. Natl. Acad. Sci. U.S.A. 99*, 4091-4096.

37. Kwa, S. L. S., Eijckelhoff, C., van Grondelle, R., and Dekker, J. P. (1994) Site-selection spectroscopy of the reaction center complex of Photosystem II. 1. Triplet-minus-singlet absorption difference: Search for a second exciton band of P-680, *J. Phys. Chem. 98*, 7702-7711.

38. Groot, M. L., Dekker, J. P., van Grondelle, R., den Hartog, F. T. H., and Volker, S. (1996) Energy transfer and trapping in isolated photosystem II reaction centers of green plants at low temperature. A study by spectral hole burning, *J. Phys. Chem. 100*, 11488-11495.

39. Konermann, L., Gatzen, G., and Holzwarth, A. R. (1997) Primary processes and structure of the photosystem II reaction center. 5. Modeling of the fluorescence kinetics of the D_1-D_2-cyt-b_{559} complex at 77 K, *J. Phys. Chem. B 101*, 2933-2944.

40. Novoderezhkin, V. I., Andrizhiyevskaya, E. G., Dekker, J. P., and van Grondelle, R. (2005) Pathways and timescales of primary charge separation in the Photosystem II reaction center as revealed by simultaneous fit of time-resolved fluorescence and transient absorption, *Biophys. J. 89*, 1464-1481.

41. Rutkauskas, D., Novoderezhkin, V., Cogdell, R. J., and van Grondelle, R. (2004) Fluorescence spectral fluctuations of single LH2 complexes from *Rhodopseudomonas acidophila* strain 10050, *Biochemistry 43*, 4431-4438.

42. Rutkauskas, D., Olsen, J., Gall, A., Cogdell, R. J., Neil Hunter, C., and van Grondelle, R. (2006) Comparative study of spectral flexibilities of bacterial light-harvesting complexes: Structural implications, *Biophys. J. 90*, 2463-2474.

43. Krüger, T. P. J., Novoderezhkin, V. I., Ilioaia, C., and van Grondelle, R. (2010) Fluorescence spectral dynamics of single LHCII trimers, *Biophys. J. 98*, 3093-3101.

44. Shlyk-Kerner, O., Samish, I., Kaftan, D., Holland, N., Sai, P. S. M., Kless, H., and Scherz, A. (2006) Protein flexibility acclimatizes photosynthetic energy conversion to the ambient temperature, *Nature 442*, 827-830.

45. Brecht, M., Radics, V., Nieder, J. B., and Bittl, R. (2009) Protein dynamics-induced variation of excitation energy transfer pathways, *Proc. Natl. Acad. Sci. U.S.A. 106*, 11857-11861.

46. Wang, H., Lin, S., Allen, J. P., Williams, J. C., Blankert, S., Laser, C., and Woodbury, N. W. (2007) Protein dynamics control the kinetics of initial electron transfer in photosynthesis, *Science 316*, 747-750.

CHAPTER 3

Multiple Charge Separation Pathways in Photosystem II: Modeling of Transient Absorption Kinetics

Vladimir I. Novoderezhkin, Elisabet Romero, Jan P. Dekker, and Rienk van Grondelle

We explain the transient absorption kinetics measured for isolated reaction centers of photosystem II at 77K upon excitation of the primary donor band (680 nm). The excited-state dynamics is modeled on the basis of the exciton states of 6 cofactors coupled to 4 charge-transfer (CT) states. One CT state (corresponding to charge separation within the special pair) is supposed to be strongly coupled with the excited states, whereas the other radical pairs are supposed to be localized. Relaxation within the strongly coupled manifold and transfer to localized CT's are described by the modified Redfield and generalized Förster theories, respectively. A simultaneous and quantitative fit of the 680, 545, and 460 nm kinetics (corresponding to respectively the Q_Y transitions of the red-most cofactors, Q_X transition of pheophytin, and pheophytin anion absorption) enables us to define the pathways and time scales of primary electron transfer. A consistent modeling of the data is only possible with a scheme where charge separation occurs from both the accessory chlorophyll and from the special pair, giving rise to fast and slow components of the pheophytin anion formation, respectively.

This chapter is based on the publication:

Vladimir I. Novoderezhkin, Elisabet Romero, Jan P. Dekker, and Rienk van Grondelle. (2011) *ChemPhysChem*, DOI: 10.1002/cphc.201000830

INTRODUCTION

The D1/D2/Cyt b_{559} reaction center (PSII RC) performs the initial charge separation in Photosystem II of oxygenic photosynthesis (for reviews see (*1-3*). The PSII RC contains four chlorophylls (special pair P_{D1}, P_{D2} and accessory Chl_{D1}, Chl_{D2}), two pheophytins (Phe_{D1}, Phe_{D2}), and two additional peripheral chlorophylls (Chl_{ZD1}, Chl_{ZD2}) arranged in two branches associated to the D_1 and D_2 proteins, respectively (*4-8*). Only the D_1 branch is active in charge separation (*2*).

The first successful model of the steady-state optical spectra of the isolated PSII RC was developed by Raszewski et al. (*9*), who obtained a quantitative fit of linear spectra (absorption, fluorescence, circular and linear dichroism) over a wide temperature range using the modified Redfield approach. The site energies of the 8 pigments extracted from a simultaneous evolutionary-based fit of the linear spectra were further verified by modeling of the spectra for the Phe_{D1}/Phe_{D2}-modified RCs, for the RC5 centers lacking one of the peripheral Chl_Z, triplet-minus-singlet spectra, and difference spectra associated with the formation of the reduced Phe_{D1}, and primary charge-separated state $P_{D1}^{+}Phe_{D1}^{-}$ (*9*). Later, this model was used to explain the absorption changes in intact RCs from the PSII core complexes associated with the P_{D1} and Chl_{D1} mutation and light-induced formation of primary photoproducts and triplet states (*10*). These studies suggested that the lowest exciton state is mostly localized at the accessory Chl_{D1} which may act as the primary donor, in agreement with the original suggestion of van Brederode et al. (*11*).

The approach used in (*9*) was further extended by using a realistic (experimental) exciton-phonon spectral density, including 48 high-frequency vibrational modes together with low-frequency phonons (*12*). To explain the experimentally observed Stark absorption spectrum of PSII RCs (*13*) the model was extended to include a primary charge-transfer (CT) state coupled to the excited states. This gives rise to an additional red-shifted state that is weakly allowed borrowing some dipole strength due to mixing with the pure exciton states. Its presence has a dramatic effect on the fluorescence profile determined by contributions from the two lowest states, i.e. a mixed exciton-CT state (peaking at 682 nm) and a superradiant multimeric exciton state (delocalized over the D_1 branch with predominant contribution of Chl_{D1} and peaking at 680 nm). On the other hand, the presence of the CT state with a huge static dipole significantly affects the Stark spectrum.

This Frenkel-CT exciton model allowed a quantitative explanation of the temperature-dependent fluorescence profile and the Stark spectrum together with the absorption-type spectra for normal and modified RCs (*12*). More advanced tight-binding two-band model has been developed recently for PSII RC (*14*) allowing a more realistic description of the exciton and charge separation dynamics.

Modeling of the Stark spectra of PSII RC showed that they are sensitive to the configuration of the primary CT state. The best fit of the data is obtained supposing that the CT state that is mixed with the excited states corresponds to charge separation within the special pair $P_{D1}P_{D2}$. It was proposed (*12*) that the charge separation can occur simultaneously via (i) relaxation of the excited states to the $P_{D2}^{+}P_{D1}^{-}$ state with subsequent electron transfer to Chl_{D1} and Phe_{D1} and (ii) starting from the excited state of Chl_{D1} with the formation of the $Chl_{D1}^{+}Phe_{D1}^{-}$ and $P_{D1}^{+}Phe_{D1}^{-}$ radical pairs.

In the presence of the two charge separation pathways a particular realization of the disorder can destroy one of them and create a good condition for the other. Consequently, the measured kinetics (averaged over disorder) will contain a superposition of components corresponding to different pathways. Groot et al. (*15*) suggested that possibly the *slow* phase of charge separation in PSII RCs (observed with femtosecond mid-IR spectroscopy) corresponds to realizations where Chl_{D1} could not operate as the primary electron donor due to unfavorable energetics and consequently P_{D1} took over, but with a much slower rate. Involvement of P_{D1} into first step of electron transfer in PSII RC was supposed by Shelaev et al. (*16*) based on 20-fs pump-probe studies.

It is important to note that the results obtained for the isolated PSII RC are representative for the in vivo RC. Thus, recent time-resolved absorption reports both in the visible and the infrared absorption regions support the view that the properties of the isolated PSII RC correspond with those of the PSII RC as it occurs in PSII cores. In the visible range, Holzwarth et al. (*17*) show that i) the rate constants of electron transfer in the RC are identical for PSII cores and for isolated RCs and ii) the mechanism suggested earlier for isolated RCs at cryogenic temperatures is also operative in intact PSII cores and in isolated RCs at ambient temperature.

In the infrared range Pawlowicz et al. (*18*) concluded that i) the kinetic model proposed earlier for the energy and electron transfer dynamics within the isolated PSII RC, plus two slowly energy-transferring antennas CP43 and CP47 explains the complex excited state and charge separation dynamics in the PSII core very well and ii) the time resolved IR-difference spectrum $P_{D1}^{+}Phe_{D1}^{-}$ as observed in PSII cores is virtually identical to that observed in the isolated RC complex of PSII, demonstrating that the local structure of the primary reactants has remained intact in the isolated RC complex.

In our previous paper we report the experimental studies of isolated PSII RC at 77K by measuring the transient absorption (TA) kinetics upon different excitation and probe wavelengths, including kinetics within the Chl/Phe Q_Y absorption band near 680 nm, the Phe Q_X band at 545 nm and Phe anion absorption band at 460 nm ((*19*) and Chapter 2 of this Thesis). A global and target analysis of the data revealed the main kinetic components reflecting the whole process of energy transfer and primary charge separation. But such analysis based on de-convolution of the measured kinetics cannot give direct evidence about the origins of the observed components. Tentative assignment of these components (*19*) is in agreement with the original idea of co-existence of the two different charge separation pathways (emerging from the modeling of the Stark spectra (*12*)). In the present paper we further verify this idea by modeling of the TA kinetics in the three spectral regions. Quantitative fit of the data confirm the model with two charge separation pathways and has led us to a more detailed and consistent picture of PSII RC. In particular, we can visualize the kinetics of population of the cofactors and radical pairs involved in each of the two pathways and explore how they contribute to the apparent kinetics.

The Model

In order to explore possible pathways of primary charge separation we model the kinetics upon direct excitation of the primary donor (i.e. lowest exciton level) at 680 nm. All data on which the modeling is based were obtained under strictly annihilation-free conditions. In our model the excited state manifold includes the exciton states of the 6 core pigments (special pair P_{D1}, P_{D2}; accessory chlorophylls Chl_{D1}, Chl_{D2}; and pheophytins Phe_{D1}, Phe_{D2}) and 4 radical pairs ($P_{D2}^{+}P_{D1}^{-}$, $P_{D1}^{+}Chl_{D1}^{-}$, $Chl_{D1}^{+}Phe_{D1}^{-}$, $P_{D1}^{+}Phe_{D1}^{-}$). The two peripheral chlorophylls (Chl_{ZD1}, Chl_{ZD2}) are not included because they have negligible populations upon 680 nm excitation. (The calculated $Chls_Z$ population is no more than 3 % upon 680 nm excitation according to our

exciton model. Besides, there is experimental evidence that peripheral $Chls_Z$ are not populated upon 680 nm excitation ((*20*) and Chapter 4 of this Thesis). The terminal electron acceptors Q_A and Q_B are lost during the isolation procedure of the PSII RC. Therefore, Q_A and Q_B are not included into the modeling.

The primary charge transfer within the special pair generally results in the electron and hole delocalization between the two Chls (uniformly or with predominant contribution of one molecule), thus producing two CT states each containing some superposition of $P_{D1}^-P_{D2}^+$ and $P_{D1}^+P_{D2}^-$. In principle, both of these states can be populated from the excited states of the special pair and each of them (containing some contribution of $P_{D2}^+P_{D1}^-$) can act as a donor of electron for D_1 branch. In our model we neglect population of higher states and consider only the lowest CT state (supposing that this state contains predominant or at least some sizable contribution of $P_{D2}^+P_{D1}^-$). This state is denoted as '$P_{D2}^+P_{D1}^-$'. The next radical pairs are $P_{D2}^+Chl_{D1}^-$ and $P_{D1}^+Chl_{D1}^-$. The structure-based calculations (*14*) suggest that these states are strongly coupled and that $P_{D1}^+Chl_{D1}^-$ is significantly lower in energy. In our scheme we consider only the lowest state with predominant contribution of $P_{D1}^+Chl_{D1}^-$ (denoted as '$P_{D1}^+Chl_{D1}^-$'). Connection between the '$P_{D2}^+P_{D1}^-$' and '$P_{D1}^+Chl_{D1}^-$' states (via concerted two-electron transfer) is accounted for by introducing a single effective coupling describing the efficiency of the two-step transfer.

According to our earlier suggestion (Novoderezhkin et al., 2007) we suppose that the primary $P_{D2}^+P_{D1}^-$ state is strongly mixed with the excited states, whereas the intermediate states ($P_{D1}^+Chl_{D1}^-$, $Chl_{D1}^+Phe_{D1}^-$) and the final radical pair ($P_{D1}^+Phe_{D1}^-$) are supposed to be localized. Thus, the equilibration among the 6 core pigments and $P_{D2}^+P_{D1}^-$ is modeled by modified Redfield theory.

The transfer from the excited states (mixed with $P_{D2}^+P_{D1}^-$) to the intermediate states ($P_{D1}^+Chl_{D1}^-$, $Chl_{D1}^+Phe_{D1}^-$) is calculated by generalized Förster theory. We mean generalization of the standard Förster formula (valid for energy transfer between two localized states) to the case of energy transfer between weakly connected clusters, or between a cluster and a localized state (pigment or radical pair). For instance, the rate of energy transfer from the k-th exciton state to the localized intermediate state is proportional to the square of the effective matrix element $\sum_n c_n^k M_{nm}$, where c_n^k is the wavefunction amplitude showing a participation of the n-th elementary excitation (n=1-6 for the cofactors and n=7 for primary CT) in the k-th exciton state, m designates the intermediate radical pair, and M_{nm} is the coupling between the n-th site and m-th radical pair (see Table 2).

In this generalized Förster formula, the donor state k can have an arbitrary degree of delocalization, but the couplings M_{nm} are supposed to be small compared with the energy gap between the donor and acceptor states.

The transfer from the intermediate to the final state $P_{D1}^{+}Phe_{D1}^{-}$ is given by the standard Förster/Marcus formula. This scheme is illustrated in Figure 1. The Förster, generalized Förster, and modified Redfield formulas are given in (*21*) together with the detailed quantitative comparison between the three theories. Notice that in our formulation the Förster and Redfield rates are expressed in terms of donor–acceptor couplings and phonon functions (*21*), that is, they are not related to the transition dipoles and spectral overlaps as in the popular form of the Förster equation. This way we can apply them for the dark states too. In particular, these expressions can be used both for the energy and electron transfers.

Parameters of the excited states of 6 cofactors (in the site representation) and radical pairs are listed in Table 1. Couplings between of the 6 sites and 4 radical pairs are given in Table 2. The one-exciton Hamiltonian of the 6 core pigments coupled to $P_{D2}^{+}P_{D1}^{-}$ is essentially the same as in our previous work (*12*), where we used the dipole-dipole interaction energies and the structural data of Kamiya and Shen (*8*). Now we use couplings calculated by the *ab-initio* TrEsp method (data taken from (*10*)) and more recent structural data (Protein Data Bank, file 2AXT (*6*)). The site energies adjusted after these updates from simultaneous fit of 8 low-temperature 4-10K spectra (see Table 1) are not much different from the values extracted from the same fitting procedure before (*12*). Energies and couplings for the intermediate and final radical pairs have been extracted from the fit of the TA kinetics.

The site inhomogeneity value is supposed to be the same for all 6 cofactors. Its value has been determined from the fit of the steady-state spectra in (*12*). Herein this value has been further adjusted (slightly increased) from the fit of the TA kinetics. Coupling to low-frequency phonons is described by overdamped Brownian oscillator model with a coupling strength of λ_0= 35 cm^{-1} and damping constant of γ_0= 40 cm^{-1}. Couplings to 48 underdamped high-frequency modes are the same as in previous modeling (see Table 1 in (*22*)). It is widely accepted that the inhomogeneity value as well as couplings to nuclear modes are significantly bigger for radical pairs (compared to the excited states). The corresponding scaling factors determined from the fit of the kinetics at different wavelengths are listed in Table 1.

Table 1. Parameters of the excited states of 6 cofactors (in the site representation) and radical pairs, including the energies of electronic transitions E and reorganization energies λ (cm^{-1}), positions of the zero-phonon transitions E_{ZPL} (nm), disorder values (FWHM) σ (cm^{-1}), static dipoles d_{st} and the effective transition dipoles d_{tr} (debye). The static disorder and coupling to phonons for radical pairs are supposed to be bigger than for the excited states. The corresponding scaling factors are $scal_{\sigma}$ and $scal_{\lambda}$.

	E, [cm^{-1}] (-λ,[cm^{-1}])	$scal_{\lambda}$	E_{ZPL} [nm]	σ [cm^{-1}]	$scal_{\sigma}$	d_{st} [debye]	d_{tr} [debye]
P_{D1}	15260 (-540)	1	679.3	95	1	1.41	4.0
P_{D2}	15190 (-540)	1	682.6	95	1	1.41	4.0
Chl_{D2}	15100 (-540)	1	686.8	95	1	1.41	4.0
Phe_{D1}	15030 (-540)	1	690.1	95	1	1.22	3.16
Phe_{D2}	15020 (-540)	1	690.6	95	1	1.22	3.16
Chl_{D1}	15000 (-540)	1	691.6	95	1	1.41	4.0
$P_{D2}{}^{+}P_{D1}{}^{-}$	15182 (-810)	1.5	695.8	190	2	38*	0
$Chl_{D1}{}^{+}Phe_{D1}{}^{-}$	15992 (-1620)	3	695.8	380	4	49*	0
$P_{D1}{}^{+}Chl_{D1}{}^{-}$	15842 (-1620)	3	703.1	380	4	51*	0
$P_{D1}{}^{+}Phe_{D1}{}^{-}$	16132 (-2160)	4	715.7	570	6	74*	0

*) static dipole of radical pairs corresponding to a charge distribution approximated by point charges at the centers of the two pigments

The two-exciton Hamiltonian needed to calculate the TA spectra is constructed by taking into account the electrochromic shift (i.e. shift of the site energies upon population of the CT states), as suggested by Raszewski et al. (*9*). The value of this shift depends on dielectric constant and the static dipoles for the excited states. Variation of the dielectric constant has led us to the value of 2.8 which allows the best fit of the absorption changes at large delays associated with the radical pairs formation.

It should be noticed that in our Frenkel-CT exciton model the CT states are treated as additional two-level sites with the zeros transition dipoles. Therefore, constructing the two-exciton states we miss some features (like electron-hole interactions, fermionic properties of electrons and holes, etc.).

In principle, these issues can be accounted for within the more general approach developed recently by Abramavicius and Mukamel (*14*).

Table 2. Couplings between the 6 cofactors (data taken from Raszewski et al. (2008)), couplings between the excited and CT states, and CT-CT couplings (cm^{-1}). Couplings with and between the CTs have been adjusted from the fit of kinetics.

	P_{D2}	Chl_{D2}	Phe_{D1}	Phe_{D2}	Chl_{D1}	$P_{D2}^{+}P_{D1}^{-}$	$Chl_{D1}^{+}Phe_{D1}^{-}$	$P_{D1}^{+}Chl_{D1}^{-}$	$P_{D1}^{+}Phe_{D1}^{-}$
P_{D1}	150	-55	-6	17	-42	45	0	0	0
P_{D2}		-36	20	-2	-56	45	0	0	0
Chl_{D2}			-5	37	7	0	0	0	0
Phe_{D1}				-3	46	0	70	0	0
Phe_{D2}					-4	0	0	0	0
Chl_{D1}						0	70	0	0
$P_{D2}^{+}P_{D1}^{-}$							0	70	0
$Chl_{D1}^{+}Phe_{D1}^{-}$								0	40
$P_{D1}^{+}Chl_{D1}^{-}$									40
$P_{D1}^{+}Phe_{D1}^{-}$									

RESULTS

Figure 1 shows the fit of the 460 and 545 nm kinetics and the time constants corresponding to a formation of the CT states extracted from this fitting. The instantaneous bleach at 545 nm is about 55-60% of the final bleach. This instantaneous bleach reflects the population of Phe_{D1} and Phe_{D2} during the pump pulse tuned to 680 nm (5 nm FWHM), i.e. to the red-most absorption band, determined by contributions from mainly Chl_{D1}, Phe_{D1}, and Phe_{D2} (*9, 12*). The amplitude of the 545 nm signal at nonzero delays is equal to the total population of the Phe_{D1} and Phe_{D2} excited states plus population of the radical pairs containing Phe, i.e. $Chl_{D1}^{+}Phe_{D1}^{-}$ and $P_{D1}^{+}Phe_{D1}^{-}$ states. Absorption changes at 460 nm show a population of the $Chl_{D1}^{+}Phe_{D1}^{-}$ and $P_{D1}^{+}Phe_{D1}^{-}$ only.

There is no instantaneous response at 460 nm implying that there is no instantaneous charge separation and that the $Chl_{D1}^{+}Phe_{D1}^{-}$ radical pair is not strongly mixed with the excited states (thus confirming the suggestion based on the Stark spectroscopy (*12*)). So, the difference between the 460 and 545 nm kinetics corresponds to the pure Phe_{D1} and Phe_{D2} excited states.

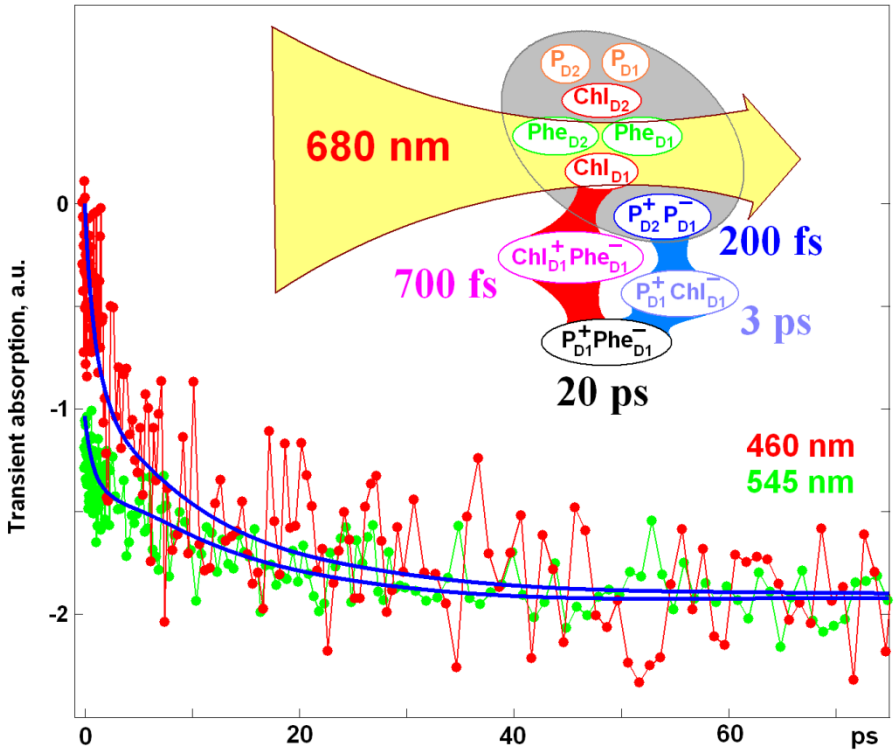

Figure 1. Modeling of 77K TA kinetics of PSII RC upon 680 nm excitation. ***Red points:*** TA kinetics measured at 460 nm (*19*) extracted from the background (485-490 nm) and inverted. ***Green points:*** TA kinetics measured at 545 nm (*19*) extracted from the background (average of the 525 nm and 560 nm kinetics). Measured 545 nm and inverted 460 nm kinetics (green and red) are scaled in order to have the same level at large delays (>50 ps). ***Blue lines:*** calculated dynamics of populations (Phe_{D1} + Phe_{D2} + $Chl_{D1}^{+}Phe_{D1}^{-}$ + $P_{D1}^{+}Phe_{D1}^{-}$) and ($Chl_{D1}^{+}Phe_{D1}^{-}$ + $P_{D1}^{+}Phe_{D1}^{-}$), responsible for the bleaching of Pheo Q_X band at 545 nm and Pheo anion absorption at 460 nm, respectively. ***Inset:*** a schematic representation of the model. The excited states (mixed with primary CT state) are encircled by gray, the two pathways of charge transfer to the localized CT states are shown by blue and red. The numbers indicate the apparent time constants corresponding to population of the primary, intermediate, and final CT states upon 680 nm excitation at 77K.

Figure 2 shows the same kinetics (together with the 680 nm TA kinetics) for delays from 0 to 16 ps calculated with taking into account the two pathways of charge separation (left), as well as just one pathway (right, i.e. using the 'traditional' scheme, where the charge separation is initiated from Chl_{D1}).

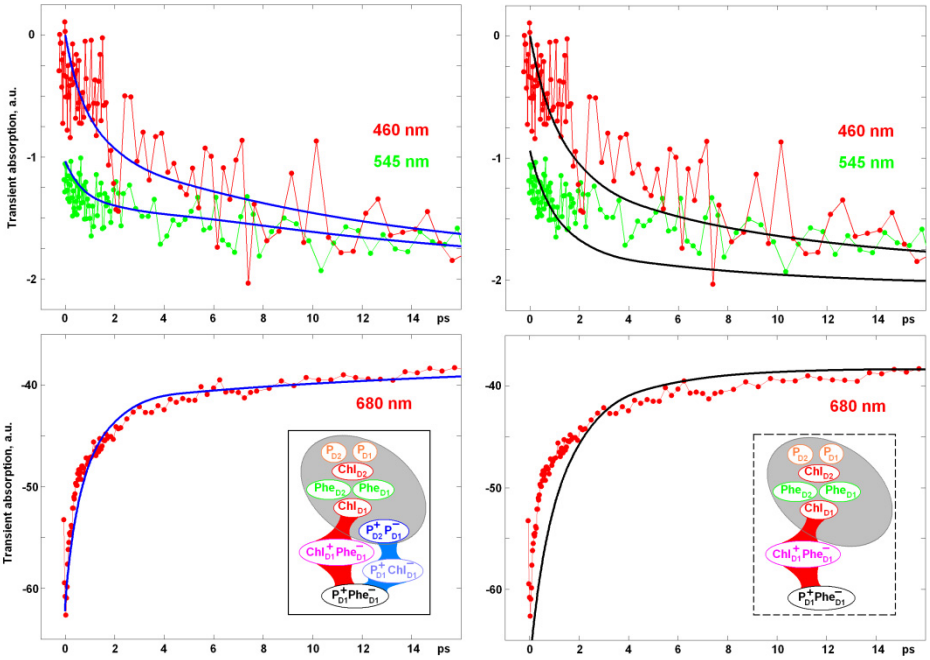

Figure 2. Modeling of the 460, 545, and 680 nm kinetics upon 680 nm excitation. Points show experimental data (Romero et al., 2010), lines correspond to the model (the 460 nm kinetics are inverted). ***Right:*** modeling with one pathway (starting from the accessory Chl_{D1}); the second pathway (with charge separation within the special pair) is excluded as shown in the inset. ***Left***: modeling of the kinetics with the two pathways (shown in the inset).

In the single-pathway scheme (Figure 2, right) the calculated 680 and 460 nm kinetics in the first 10 ps (corresponding to depopulation of the excited states and population of Phe_{D1}^- containing radical pairs, respectively) have approximately the same time constants. This symmetry reflects a conservation of the number of excitations: every quantum leaving the excited states goes to $Chl_{D1}^+Phe_{D1}^-$ or $P_{D1}^+Phe_{D1}^-$ containing the Phe_{D1}^- state. Thus, the decay of the excited states bleaching at 680 nm should always be accompanied by a proportional increase of the Phe anion absorption at 460 nm.

In contrast, the experimental 680 nm decay is significantly faster than the measured 460 and 545 nm dynamics. As a result the single-pathway kinetics are always slower than measured at 680 nm and faster than measured at 460 and 545 nm.

In order to speed-up the 680 nm decay and slow-down the 460 and 545 nm kinetics we include the second charge separation channel. In the two-pathways scheme (Figure 2, left) a quick exciton relaxation of the excited states to $P_{D2}^{+}P_{D1}^{-}$ produces faster decay of the 680 nm kinetics. On the other hand, this ultrafast depopulation of the excited states and following charge separation step ($P_{D2}^{+}P_{D1}^{-} \rightarrow P_{D1}^{+}Chl_{D1}^{-}$) do not contribute to the Phe_{D1}^{-} formation. Increase of the Phe_{D1}^{-} population (contributing to the 460 nm signal) occurs only at the next charge separation step ($P_{D1}^{+}Chl_{D1}^{-} \rightarrow P_{D1}^{+}Phe_{D1}^{-}$). Thus, the presence of the second channel ($P_{D2}^{+}P_{D1}^{-} \rightarrow P_{D1}^{+}Chl_{D1}^{-} \rightarrow P_{D1}^{+}Phe_{D1}^{-}$) produces slower 460 nm kinetics together with faster 680 nm decay in better agreement with the experiment.

Dynamics of the site populations extracted from the TA fit is shown in Figure 3. Initially, the 680 nm excitation populates the accessory Chl_{D1} and two pheophytins (that contribute to the red-most 680 nm band). Due to the broad spectrum of the pump there is some initial population of Chl_{D2} together with some population of the special pair. Peripheral $Chls_{Z}$ have an even lower population that is neglected in our analysis. Population of the $P_{D2}^{+}P_{D1}^{-}$ state is very small initially, but quickly increases (with the time constant of about 200 fs) due to exciton-type relaxation from the pure exciton states that are higher in energy. A following transfer $P_{D2}^{+}P_{D1}^{-} \rightarrow P_{D1}^{+}Chl_{D1}^{-}$ limits the further growth of the $P_{D2}^{+}P_{D1}^{-}$ population and results in the $P_{D1}^{+}Chl_{D1}^{-}$ formation with the apparent time constant of about 3 ps.

Another channel of the excited-state depopulation is connected with the $Chl_{D1}^{*} \rightarrow Chl_{D1}^{+}Phe_{D1}^{-}$ transfer (here Chl_{D1}^{*} denotes any collective excited state with contribution from Chl_{D1}). The apparent time constant of the $Chl_{D1}^{+}Phe_{D1}^{-}$ formation is about 700 fs.

The transfers $P_{D1}^{+}Chl_{D1}^{-} \rightarrow P_{D1}^{+}Phe_{D1}^{-}$ and $Chl_{D1}^{+}Phe_{D1}^{-} \rightarrow P_{D1}^{+}Phe_{D1}^{-}$ result in populating the final radical pair with an apparent time constant of 20 ps. Notice that all the time constants we are talking about reflect a combined action of the forward (downhill) and back (uphill) transfers and are averaged over disorder. It should be pointed out that only thermally-activated up-hill back transfers from radical pairs to the excited states are included. The charge recombination reactions due to other mechanisms (involving triplets etc.) that occur in longer time scales are not taken into account.

We remind the reader that the TA signal at 460 nm is given by the sum of the $Chl_{D1}^{+}Phe_{D1}^{-}$ and $P_{D1}^{+}Phe_{D1}^{-}$ kinetics. Their relative amplitudes determine the ratio of fast and slow components in the 460 nm dynamics. In the single-pathway scheme the $Chl_{D1}^{+}Phe_{D1}^{-}$ amplitude is bigger (see dashed magenta kinetics in Figure 3), thus increasing the amplitude of the fast component both in 460 and 545 nm kinetics (as shown in Figure 2). On the other hand in the single-pathway scheme the decay of the excited states is slower due to the absence of the relaxation pathway to $P_{D2}^{+}P_{D1}^{-}$ (see dashed red and green curves in Figure 3) which would give rise to a slower 680 nm decay.

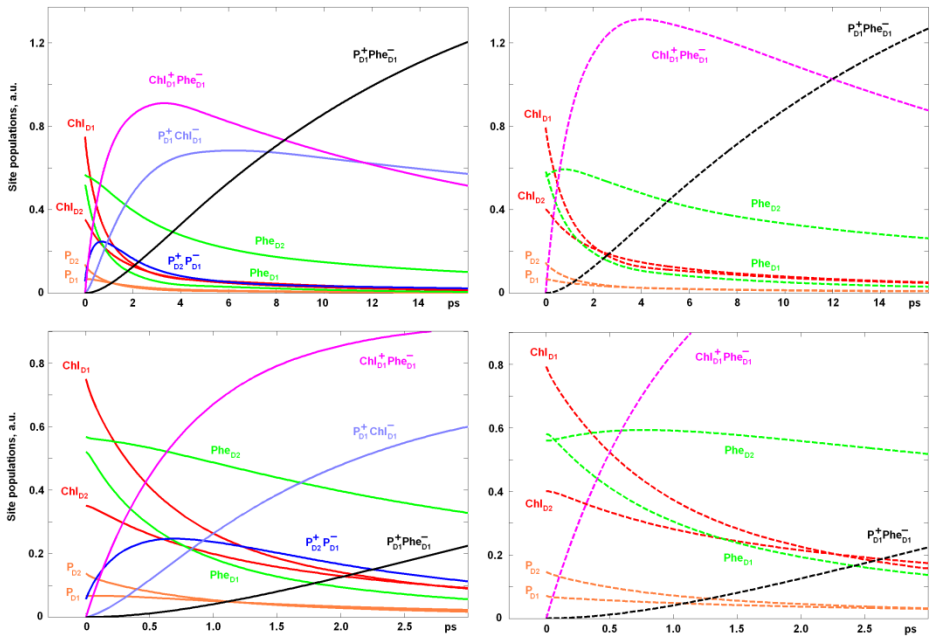

Figure 3. Dynamics of the site populations upon 680 nm excitation including the 6 core pigments and 4 radical pairs. Delays of 0-16 ps (top) and 0-3.0 ps (bottom) are shown. Solid lines (in the left frames) correspond to the kinetics obtained with the two-pathways scheme, the dashed curves (in the right frames) correspond to the single-pathway scheme (shown in the right frame of Figure 2).

Difference between the 460 and 545 nm kinetics is determined by the excited states of the two pheophytins. Long-lived difference between the 460 and 545 nm kinetics (in the time scale of 50-70 ps as shown in Figure 1) is determined in this model mostly by Phe_{D2} (see the kinetics shown by green in Figure 3). This site is red-shifted and therefore acts as a trap (in the time scale of less than 50 ps) being effectively decoupled from the excited states of the active D_1 branch.

DISCUSSION

Assignment of the time constants. The apparent time constants of the radical pair formation (extracted from our fit) should be the same as the time constants visible in the dynamics of spectral responses. Notice that global analysis of the TA data (*19*) gave components of 0.5 ps, 3 ps and 20 ps. The 0.5 ps dynamics is close to the fast dynamics of the present model with the major and minor components of 0.7 and 0.2 ps, respectively. The 3 and 20 ps components of the model are the same as in the global analysis.

Target analysis gave two intermediate charge-separation species formed with 3 ps and 1 ps and assigned to $Chl_{D1}^{+}Phe_{D1}^{-}$ and $P_{D1}^{+}Chl_{D1}^{-}$, respectively. According to the target analysis the final radical pair $P_{D1}^{+}Phe_{D1}^{-}$ is formed in 58 ps via Chl_{D1} path and in 37 ps via P_{D1} path (with a total rate corresponding to 22 ps in the case of equal contribution of the two channels). The present model suggests 3 ps and 0.7 ps for intermediate states and 20 ps for the final state in agreement with the target analysis. But the assignment of the 3 ps and 0.7 ps components is different: in the modeling the fastest (0.7 ps) channel corresponds to the $Chl_{D1}^{+}Phe_{D1}^{-}$ intermediate (in contrast to the scheme suggested previously (*19*), where the $P_{D1}^{+}Chl_{D1}^{-}$ formation is faster).

Long-lived trap states. Herein we restrict ourselves to modeling of the kinetics in the time window of 0-75 ps (Figure 1). In the 0-16 ps time scale (Figure 2) the most populated among the excited states is pheophytin Phe_{D2} that acts like a trap of excitations. Its population (mirrored by the difference between the 460 and 545 nm kinetics) disappear after 50 ps (as shown in Figure 1). At longer time there exist even more long-lived trap states that contribute to the observed slow kinetics (*19*).

An analysis of the vibronic fine structure of the PSII RC emission at 5K (*23*) demonstrated pronounced similarity between the spectroscopic features of the emitting and charge separating states. It was concluded that the contribution of pheophytin to the total (time-intergrated) emission was at 5K not more than 10%. Based on this, we believe that also at 77K the pheophytin of the inactive branch will have a minor contribution at longer time delays. Thus, the two long-lived trap states obtained by target analysis (65 and 585 ps) have been assigned to the same excited states giving rise to ultrafast charge separation (*19*). The energy can be trapped by these excited states when they are lower than $P_{D2}^{+}P_{D1}^{-}$ or $Chl_{D1}^{+}Phe_{D1}^{-}$, respectively, due to energetic disorder. In the present model, for instance, the disorder values for the Chl_{D1}* and $Chl_{D1}^{+}Phe_{D1}^{-}$ states are 95 and 380 cm^{-1} (FWHM), respectively. Even for the unperturbed energy gap between them of 250 cm^{-1}, one can easily imagine a situation where Chl_{D1}* is significantly lower in energy, giving rise to slow (activated) charge separation (see also discussion in (*19*)).

Comparing PSII RC and bacterial RC. Our scheme of charge separation in PSII RC has some common features with the bacterial RCs. First, in both types of RC the special pair is mixed with a CT state (in purple bacteria this coupling is stronger, producing pronounced temperature dependence of the special pair lowest absorption band (*24*). Secondly, in both types of RC an electron transfer from the special pair to accessory (B)Chl occurs with an effective time of about 3 ps. Finally, there is an alternative, faster (few hundred fs) channel of charge separation from the excited accessory (B)Chl (originally found in bacterial RC (*25*)).

In the bacterial RC the special pair is much lower in energy than the accessory BChl, and the electron transfer starts from special pair at all temperatures. In PSII RC all the cofactors are more strongly mixed, so that a co-existence of different charge-transfer channels is possible. Because the accessory Chl_{D1} is lower in energy than the special pair an alternative channel becomes dominant at lower temperatures.

The 77K vs room temperature dynamics. Our model is based on the data obtained at 77K, and one could wonder how the results are related to a functioning of the complex at physiological temperatures. The co-existence of the two channels of charge separation (that is the principal feature of our model) is dependent on conformational disorder. This phenomenon is more convenient to study at lower temperatures, because at room temperature the mixing of the two channels will be more pronounced, so that it will be more difficult to distinguish/assign them. In addition, performing the experiments at

77K enables us to (i) enhance the spectral resolution (due to narrower line shapes of the exciton components); (ii) reduce back reactions and uphill energy transfer; and (iii) to allow photoselection of subpopulations with different proportions of the Chl_{D1} and P_{D1} pathways (in combination with various excitation conditions).

On the other hand the freezing slows down protein motions responsible for switching between different conformational changes. In principle one could imagine that tuning to room temperature will make available conformational states that are not activated at 77K. Moreover, at higher temperatures some conformations can be fast enough to influence the kinetics in the ns or even sub-ns time scale. But we still believe that the mechanisms of energy transfer and charge separation will not change dramatically at different temperatures. A proof for this statement is presented in a recent time-resolved absorption studies in the visible range. Holzwarth et al. (*17*) showed that the mechanism suggested earlier for isolated RCs at cryogenic temperatures is also operative in intact PSII cores and in isolated RCs at ambient temperature.

CONCLUSIONS

We explain the transient absorption kinetics measured for isolated reaction centers of photosystem II at 77K upon excitation of the primary donor band (680 nm). Simultaneous quantitative fit of the 680, 545, and 460 nm kinetics (corresponding to the Q_Y transitions of the red-most cofactors, Q_X transition of pheophytin, and pheophytin anion absorption) enables us to define the pathways and time scales of primary electron transfer. A consistent modeling of the data is only possible with the scheme where charge separation occurs both from the accessory chlorophyll and from the special pair. An exciton-type relaxation to the special pair CT state (with an effective time constant of 200 fs) determines fast depopulation of the excited states. Long-lived components of the excited states decay are determined mostly by the inactive branch pheophytin, acting as a trap of excitations. Fast and slow components of the pheophytin anion formation are determined by the Förster-type electron transfer from the excited state of the accessory chlorophyll (with fastest components of about 700 fs) and slower electron transfer from the special pair to the accessory chlorophyll (3 ps) and further on to the pheophytin (20 ps).

ACKNOWLEDGMENT

V.N. was supported by the visitor's grant from the Netherlands Organisation for Scientific Research (NWO) and by the Russian Foundation for Basic Research, Grant No. 09-04-00605a. E.R. was supported by Marie Curie Research Training Network INTRO2 (MRTN-CT-505069) of the European Union.

REFERENCES

1. Dekker, J. P., and van Grondelle, R. (2000) Primary charge separation in photosystem II, *Photosynth. Res. 63*, 195-208.
2. Diner, B. A., and Rappaport, F. (2002) Structure, dynamics, and energetics of the primary photochemistry of photosystem II of oxygenic photosynthesis, *Annu. Rev. Plant Biol. 53*, 551-580.
3. Renger, T., and Schlodder, E. (2010) Primary photophysical processes in photosystem II: Bridging the gap between crystal structure and optical spectra, *Chem. Phys. Chem. 11*, 1141-1153.
4. Ferreira, K. N., Iverson, T. M., Maghlaoui, K., Barber, J., and Iwata, S. (2004) Architecture of the photosynthetic oxygen-evolving center, *Nature 303*, 1831-1838.
5. Guskov, A., Kern, J., Gabdulkhakov, A., Broser, M., Zouni, A., and Saenger, W. (2009) Cyanobacterial photosystem II at 2.9-Å resolution and the role of quinones, lipids, channels and chloride, *Nat. Struct. Mol. Biol. 16*, 334-342.
6. Loll, B., Kern, J., Saenger, W., Zouni, A., and Biesiadka, J. (2005) Towards complete cofactor arrangement in the 3.0 Å resolution structure of photosystem II, *Nature 438*, 1040-1044.
7. Zouni, A., Witt, H. T., Kern, J., Fromme, P., Krauss, N., Saenger, W., and Orth, P. (2001) Crystal structure of photosystem II from *Synechococcus elongatus* at 3.8 Å resolution, *Nature 409*, 739-743.
8. Kamiya, N., and Shen, J.-R. (2003) Crystal structure of oxygen-evolving photosystem II from *Thermosynechococcus vulcanus* at 3.7 Å resolution, *Proc. Natl. Acad. Sci. U.S.A. 100*, 98-103.
9. Raszewski, G., Saenger, W., and Renger, T. (2005) Theory of optical spectra of Photosystem II reaction centers: Location of the triplet state and the identity of the primary electron donor, *Biophys. J. 88*, 986-998.
10. Raszewski, G., Diner, B. A., Schlodder, E., and Renger, T. (2008) Spectroscopic properties of reaction center pigments in Photosystem II core complexes: Revision of the multimer model, *Biophys. J. 95*, 105-119.

11. van Brederode, M. E., van Mourik, F., van Stokkum, I. H. M., Jones, M. R., and van Grondelle, R. (1999) Multiple pathways for ultrafast transduction of light energy in the photosynthetic reaction center of *Rhodobacter sphaeroides*, *Proc. Natl. Acad. Sci. U.S.A. 96*, 2054-2059.

12. Novoderezhkin, V. I., Dekker, J. P., and van Grondelle, R. (2007) Mixing of exciton and charge transfer states in Photosystem II reaction centers: Modeling of Stark spectra with Modified Redfield Theory, *Biophys. J. 93*.

13. Frese, R. N., Germano, M., de Weerd, F. L., van Stokkum, I. H. M., Shkuropatov, A. Y., Shuvalov, V. A., van Gorkom, H. J., van Grondelle, R., and Dekker, J. P. (2003) Electric field effects on the chlorophylls, pheophytins, and β-carotenes in the reaction center of photosystem II, *Biochemistry 42*, 9205-9213.

14. Abramavicius, D., and Mukamel, S. (2010) Energy-transfer and charge-separation pathways in the reaction center of photosystem II revealed by coherent two-dimensional optical spectroscopy, *J. Chem. Phys. 133*.

15. Groot, M.-L., Pawlowicz, N. P., van Wilderen, L. J. G. W., Breton, J., van Stokkum, I. H. M., and van Grondelle, R. (2005) Initial electron donor and acceptor in isolated photosystem II reaction centers identified with femtosecond mid-IR spectroscopy, *Proc. Natl. Acad. Sci. U.S.A. 102*, 13087-13092.

16. Shelaev, I. V., Gostev, F. E., Nadtochenko, V. A., Shkuropatov, A. Y., Zabelin, A. A., Mamedov, M. D., Yu., S. A., M., S. O., and A, S. V. (2008) Primary light-energy conversion in tetrameric chlorophyll structure of photosystem II and bacterial reaction centers: II. Femto- and picosecond charge separation in PSII D1/D2/Cyt b559 complex, *Photosynth. Res. 98*, 95-103.

17. Holzwarth, A. R., Müller, M. G., Reus, M., Nowaczyk, M., Sander, J., and Rögner, M. (2006) Kinetics and mechanism of electron transfer in intact photosystem II and in the isolated reaction center: Pheophytin is the primary electron acceptor, *Proc. Natl. Acad. Sci. U.S.A. 103*, 6895-6900.

18. Pawlowicz, N. P., Groot, M. L., van Stokkum, I. H. M., Breton, J., and van Grondelle, R. (2007) Charge separation and energy transfer in the photosystem II core complex studied by femtosecond midinfrared spectroscopy *Biophys. J. 93*, 2732-2742.

19. Romero, E., van Stokkum, I. H. M., Novoderezhkin, V. I., Dekker, J. P., and van Grondelle, R. (2010) Two different charge separation pathways in photosystem II, *Biochemistry 49*, 4300-4307.

20. Romero, E., van Stokkum, I. H. M., Dekker, J. P., and van Grondelle, R. Ultrafast carotenoid band shifts correlated with Chl_Z excited states in the photosystem II reaction center: are the carotenoids involved in energy transfer?, *Phys. Chem. Chem. Phys.*

21. Novoderezhkin, V. I., and van Grondelle, R. (2010) Physical origins and models of energy transfer in photosynthetic light harvesting, *Phys. Chem. Chem. Phys. 12*, 7352-7365.

22. Novoderezhkin, V. I., Andrizhiyevskaya, E. G., Dekker, J. P., and van Grondelle, R. (2005) Pathways and timescales of primary charge separation in the Photosystem II reaction center as revealed by simultaneous fit of time-resolved fluorescence and transient absorption, *Biophys. J. 89*, 1464-1481.

23. Peterman, E. J. G., van Amerongen, H., van Grondelle, R., and Dekker, J. P. (1998) The nature of the excited state of the reaction center of photosystem II of green plants: A high-resolution fluorescence spectroscopy study, *Proc. Natl. Acad. Sci. U.S.A. 95*, 6128-6133.

24. Renger, T. (2004) Theory of optical spectra Involving charge transfer states: dynamic localization predicts a temperature dependent optical band shift, *Phys. Rev. Lett. 93*, 188101.

25. van Brederode, M. E., Jones, M. R., van Mourik, F., van Stokkum, I. H. M., and van Grondelle, R. (1997) A new pathway for transmembrane electron tranfer in photosynthetic reaction centers of *Rhodobacter sphaeroides* not involving the excited special pair, *Biochemistry 36*, 6855-6861.

CHAPTER 4

Ultrafast Carotenoid Band Shifts Correlated with Chl_Z Excited States in the Photosystem II Reaction Center: Are the Carotenoids Involved in Energy Transfer?

Elisabet Romero, Ivo H. M. van Stokkum, Jan P. Dekker and Rienk van Grondelle

We show a correlation between the electronic excitation of the peripheral chlorophylls ($Chls_Z$) of the photosystem II reaction center and a shift of the S_2 absorption bands of β-carotene, and suggest that the carotenoids may enhance the excitation energy transfer rate from these chlorophylls to the central cofactors.

This chapter is based on the publication:

Elisabet Romero, Ivo H. M. van Stokkum, Jan P. Dekker and Rienk van Grondelle. (2011) *Phys. Chem. Chem. Phys. (Communication)* DOI: 10.1039/C0CP02896G.

The conversion of solar energy into chemical energy has been mastered in photosynthesis. The understanding of the molecular mechanisms underlying photosynthesis is crucial for achieving the efficient utilization of our largest energy source: the Sun.

In higher plants, algae and cyanobacteria a key step in photosynthetic energy conversion takes place in the photosystem II reaction center (PSII RC) where a series of energy and electron transfer reactions give rise to a charge separated state which ultimately powers the photosynthetic organism. The PSII RC contains six chlorophylls (Chls), two pheophytins (Phes) and two *β*-carotenes (Car). The X-ray crystal structure of PSII from cyanobacteria (*1, 2*) shows that four Chls and two Phes arranged in two branches, D_1 and D_2, are situated in the center of the reaction center complex and two additional Chls ($Chls_Z$) are located at opposing sides at the periphery of the complex (Figure 1).

Each of the two *β*-carotenes is located between $Chls_Z$ and the center of the complex with different orientation with respect to the thylakoid membrane, Car_{D1} is oriented perpendicularly to the membrane plane while the Car_{D2} orientation is parallel (Figure 1).

For charge separation in the PSII RC, it has been demonstrated that: i) the central cofactors absorbing around 680 nm are excitonically coupled (*3*) which ii leads to charge separation via two different ultrafast charge separation pathways (*4*) and that iii) the peripheral $Chls_Z$ absorbing at 670 nm transfer excitation energy to the central cofactors in about 20 ps (*5-7*).

The absorption spectrum of plant PSII RC in the Car S_2 absorption region is shown in Figure 2(A, B). Linear dichroism (LD) experiments on PSII RC and larger PSII particles from spinach showed that the Car $S_0 - S_2$ vibrational transitions at 442, 474 and 506 nm are oriented parallel to the membrane plane while the 458 and 490 nm transitions are approximately perpendicular to it (*8-10*). Therefore, the broad band around 465 nm contains both 458 nm (Car_{D1}) and 474 nm (Car_{D2}) transitions and the 489 nm and 506 nm transitions correspond to Car_{D1} and Car_{D2}, respectively (Figure 2A).

It is known that Car perform a wide range of functions in photosynthetic organisms: they protect the photosynthetic machinery, absorb blue-green light not captured by the Chls, stabilize the pigment-protein structures and are involved in regulation of energy flow from and to Chl (for reviews see (*11*) and (*12*)). However, transient absorption studies show that the quantum efficiency of *β*-carotene-to-chlorophyll singlet energy transfer upon direct Car excitation is poor in spinach PSII RC and it involves mainly the S_2 state. The "hot" and relaxed S_1 states do not participate in excitation energy transfer (EET)(*13*) (it should be noted that in this study only Car_{D2} was excited).

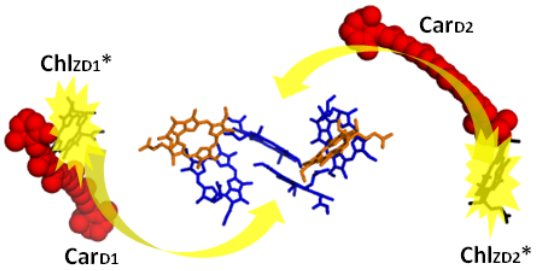

Figure 1. Cofactor arrangement in the PSII RC (adapted from (*2*)): Chls$_Z$ (*black*), Car (*red*), central Chls (*blue*) and central Phes (*orange*). The yellow stars on Chls$_Z$ represent the excitation energy, the yellow arrows represent the possible involvement of Car in the excitation energy transfer process from Chls$_Z$ to the central cofactors.

In this study, transient absorption spectra of isolated PSII RC at 77K have been recorded for: six narrow excitation wavelengths covering the Chl and Phe Q_Y region from 660 to 685 nm (5 nm fwhm), two broader excitation wavelengths at 662 and 682 nm (8 nm fwhm), and a non-selective excitation at 675 nm (12 nm fwhm). The aim of these experiments is to investigate the EET among the cofactors in the PSII RC.

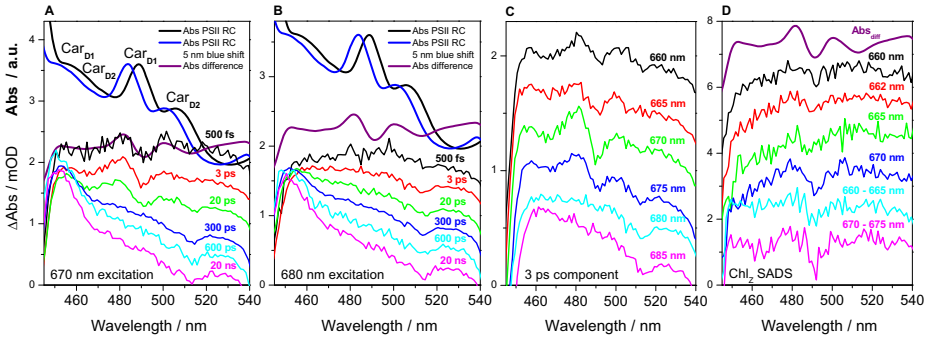

Figure 2. PSII RC ground state and transient absorption spectra at 77 K in the carotenoid region. All the spectra have been vertically translated arbitrarily for better comparison. (A and B) PSII RC ground state, 5 nm blue shifted absorption and their difference spectra (*thick lines*); Evolution Associated Difference Spectra (EADS) for (A) 670 nm and (B) 680 nm excitation. (C) EADS for the 3 ps component upon different excitation wavelength. (D) Species Associated Difference Spectra (SADS) for Chls$_Z$ from the target analysis of six linked data sets (660, 665, 670 and 675 nm (5 nm fwhm); 662 nm (8 nm fwhm); and 675 nm (12 nm fwhm) excitation wavelength) (660-665 nm and 670-675 nm SADS), and from a simplified target analysis of four linked data sets (660, 662, 665 and 670 nm) together with the absorption difference spectra (*thick line*).

The data sets have been globally analyzed with a sequential model in order to follow the spectral evolution in time. The evolution associated difference spectra (EADS) obtained represent a mix of species which population rises with the lifetime of the previous component and decays with its lifetime, i.e. the third EADS rises with the second lifetime and decays with the third lifetime (*14*). An excellent description of the multi-exponential spectral evolution following those various excitations was obtained using the following set of lifetimes: 500 fs, 3 ps, 20 ps, 300 ps, 600 ps and 20 ns. Additionally, we have performed a target analysis according to a kinetic scheme. The target analysis generates the species associated difference spectra (SADS) which represent the spectra of the pure species described in the kinetic scheme (for details about the experimental conditions and dynamics related to Chl and Phe see (*4*) and Chapter 2 of this Thesis).

The long wavelength laser light used to excite the chlorins in the PSII RC is too low in energy to excite the Car to the S_2 state; therefore no changes in the absorption due to Car are expected. However, the EADS display two negative features around 465 and 492 nm (Fig. 2A, C and D). Interestingly, these features are only present in the 500 fs, 3 ps and 20 ps EADS.

The small differences in the shape of the negative features are due to the band overlap with contributions from other signals: the Phe anion band at 455 nm, the Phe vibrational Q_X(0-1) band at 512 nm and the featureless excited state absorption from Chl and Phe in the 500 fs and 3 ps components. We note that the same negative Car features are also observed in the Chl_Z SADS obtained by target analysis (*4*) which represent the spectra of the pure Chl_Z excited states plus their effect on the Car S_2 states. The Chl_Z SADS decays in about 20 ps.

In addition, the amplitude of the negative features around 465 and 492 nm are highly dependent on the excitation wavelength (Figure 2C): it increases from 660 nm to a maximum at 670 nm, decreases at 675 nm and are completely absent at 680 and 685 nm excitation. This effect is also observed in the SADS obtained by target analysis (Figure 2D).

These facts and the proximity of the Car to the $Chls_Z$ strongly indicate that the negative features are related to the population of Chl_Z excited states ($Chls_Z$*). A similar effect was reported for the LH2 antenna complex from photosynthetic bacteria (*15*) in which ultrafast Car band shifts were observed which correlated with energy transfer between the B800 and B850 bacteriochlorophyll rings. The ultrafast carotenoid response was interpreted as an electrochromic shift due to the changes in the local electric field near carotenoid molecules upon photoexcitation of the bacteriochlorophyll molecules.

This interpretation was further supported by quantum chemical calculations (*16*). Time dependent density functional theory (TDDFT) strongly suggests that the mutual pigment orientation determines the extent of electrochromic shift (*17*).

Along the same line, in the PSII RC the shape of the negative features can be reproduced by a five nanometers blue shift of the absorption spectrum (Figure 2A, B and D). Surprisingly, both negative features, at 465 and 492 nm, are reproduced in the absorption difference spectra ($Abs_{5nm\ blueshifed} - Abs_{ground\ state}$) despite the fact that the two Car have a completely different orientation with respect to the tetrapyrrol ring and the Q_Y transitions of $Chls_Z$.

Then the question arises: is this Car absorption blue shift a simple effect of the local electric field generated by the Chl_Z excited states or, in addition, does it have physiological significance? The data clearly shows that both Car sense the excitation on $Chls_Z$, manifested as an electrochromic shift of their $S_0 - S_2$ transition. This shift could just be a result of the close proximity of the Car and $Chls_Z$ with no influence in the EET dynamics among the cofactors in the PSII RC.

However, at this point, we would like to move a step further and hypothesize an additional energetic implication for this phenomenon: the shift of the Car $S_0 - S_2$ transition could imply the presence of mixing between the electronic states of $Chls_Z$ and the Car. Due to the location of the Car (between $Chls_Z$ and the central cofactors) this mixing may increase the coupling between $Chls_Z$ and the exciton states of the central cofactors and thereby enhance the EET rate between $Chls_Z$ and the central cofactors.

This proposition is based on several evidences. On one hand, the discrepancy between experiment and theory on the energy transfer rate from $Chls_Z$ to RC central cofactors (also found in LH2 (*18*)). From the experiment, the energy transfer rate is $(20\ ps)^{-1}$ (*5-7*), while from modeling of spectroscopic data using modified Redfield/modified Förster theory, both approaches treat the electronic states of the central cofactors as excitonic, energy transfer rates of up to $(100\ ps)^{-1}$ (*19, 20*) were found (note that these theoretical studies do not take into account the presence of Car). On the other hand, quantum mechanical calculations on LH2 from purple bacteria showed that interaction of the B800 and B850 bacteriochlorophylls transition densities with the Car molecules had an effect on B800 and B850 electronic couplings, increasing them up to ≈ 30%. As a consequence, the Car appear to be capable of enhancing the energy transfer rate (by ca. 50 – 70%) from B800 to B850 (*21*).

Accordingly, in our view the Car in the PSII RC could act as electronic coupling bridges between the peripheral $Chls_Z$ and the RC central cofactors increasing the rate of energy transfer from $Chls_Z$ to the central cofactors estimated from modified Redfield/modified Förster theory. Nevertheless, further experiments combined with quantum mechanical calculations including the coupling between Car and $Chls_Z$ are necessary to verify this hypothesis.

CONCLUSIONS

We have demonstrated that the two β-carotene molecules present in the PSII RC from higher plants feel the excitation on $Chls_Z$ manifested as a five nanometers blue shift of their $S_0 - S_2$ transition. We propose that the Car may increase the electronic coupling between $Chls_Z$ and the central Chls. To our knowledge, this is the first time that experimental evidence pointing to a possible role of the carotenoid molecules in enhancing the excitation energy transfer rate between Chls in the PSII RC has been reported.

ACKNOWLEDGMENT

We thank Jos Thieme for technical support and Henny van Roon for the expert preparation of the samples. This work was supported by Marie Curie Research Training Network INTRO2 (MRTN-CT-505069) (E.R.) of the European Union and by The Netherlands Organization for Scientific Research (NWO).

REFERENCES

1. Loll, B., Kern, J., Saenger, W., Zouni, A., and Biesiadka, J. (2005) Towards complete cofactor arrangement in the 3.0 Å resolution structure of photosystem II, *Nature 438*, 1040-1044.
2. Guskov, A., Kern, J., Gabdulkhakov, A., Broser, M., Zouni, A., and Saenger, W. (2009) Cyanobacterial photosystem II at 2.9-Å resolution and the role of quinones, lipids, channels and chloride, *Nat. Struct. Mol. Biol. 16*, 334-342.
3. Durrant, J. R., Klug, D. R., Kwa, S. L. S., van Grondelle, R., Porter, G., and Dekker, J. P. (1995) A multimer model for P680, the primary electron donor of photosystem II, *Proc. Natl. Acad. Sci. U.S.A. 92*, 4798-4802.
4. Romero, E., van Stokkum, I. H. M., Novoderezhkin, V. I., Dekker, J. P., and van Grondelle, R. (2010) Two different charge separation pathways in photosystem II, *Biochemistry 49*, 4300-4307.
5. Rech, T., Durrant, J. R., Joseph, D. M., Barber, J., Porter, G., and Klug, D. R. (1994) Does slow energy transfer limit the observed time constant for radical pair formation in photosystem II reaction centers?, *Biochemistry 33*, 14768-14774.
6. Schelvis, J. P. M., van Noort, P. I., Aartsma, T. J., and van Gorkom, H. J. (1994) Energy transfer, charge separation and pigment arrangement in the reaction center of photosystem II, *Biochim. Biophys. Acta 1184*, 242-250.
7. Vacha, F., Joseph, D. M., Durrant, J. R., Telfer, A., Klug, D. R., Porter, G., and Barber, J. (1995) Photochemistry and spectroscopy of a five-Chlorophyll reaction center of Photosystem II isolated by using a Cu affinity column, *Proc. Natl. Acad. Sci. U.S.A. 92*, 2929-2933.
8. van Dorssen, R. J., Breton, J., Plijter, J. J., Satoh, K., van Gorkom, H. J., and Amesz, J. (1987) Spectroscopic properties of the reaction center and of the 47 kDa chlorophyll protein of Photosystem II, *Biochim. Biophys. Acta 893*, 267-274.
9. Breton, J. (1990) In *Perspectives in photosynthesis* (Jortner, J., and Pullman, B., Eds.), pp 23-28, Kluwer, Dordrecht.
10. Kwa, S. L. S., Newell, W. R., van Grondelle, R., and Dekker, J. P. (1992) The reaction center of photosystem II studied with polarized fluorescence spectroscopy, *Biochim. Biophys. Acta 1099*, 193-202.
11. Frank, H. A., and Brudvig, G. W. (2004) Redox functions of carotenoids in photosynthesis, *Biochemistry 43*, 8607-8615.
12. Telfer, A. (2005) Too much light? How β-carotene protects the photosysten II reaction center, *Photochem. Photobiol. Sci. 4*, 950-956.

13. de Weerd, F. L., Dekker, J. P., and van Grondelle, R. (2003) Dynamics of β-carotene-to-chlorophyll singlet energy transfer in the core of photosystem II, *J. Phys. Chem. B 107*, 6214-6220.

14. van Stokkum, I. H. M., Larsen, D. S., and van Grondelle, R. (2004) Global and target analysis of time-resolved spectra, *Biochim. Biophys. Acta 1657*, 82-104.

15. Herek, J. L., Polívka, T., Pullerits, T., Fowler, G. J. S., Hunter, C. N., and Sundström, V. (1998) Ultrafast carotenoid band shifts prove structure and dynamics in photosynthetic antenna complexes, *Biochemistry 37*, 7057-7061.

16. He, Z., Sundström, V., and Pullerits, T. (2001) Excited states of carotenoid in LH2: an ab initio study, *Chem. Phys. Lett. 334*, 159-167.

17. Herek, J. L., Wendling, M., He, Z., Polívka, T., Garcia-Asua, G., Cogdell, R. J., Hunter, C. N., van Grondelle, R., Sundström, V., and Pullerits, T. (2004) Ultrafast carotenoid band shifts: experiment and theory, *J. Phys. Chem. B 108*, 10398-10403.

18. Pullerits, T., Hess, S., Herek, J. L., and Sundström, V. (1997) Temperature dependence of excitation transfer in LH2 of *Rhodobacter sphaeroides*, *J. Phys. Chem. B 101*, 10560-10567.

19. Raszewski, G., Saenger, W., and Renger, T. (2005) Theory of optical spectra of Photosystem II reaction centers: Location of the triplet state and the identity of the primary electron donor, *Biophys. J. 88*, 986-998.

20. Novoderezhkin, V. I., Andrizhiyevskaya, E. G., Dekker, J. P., and van Grondelle, R. (2005) Pathways and timescales of primary charge separation in the Photosystem II reaction center as revealed by simultaneous fit of time-resolved fluorescence and transient absorption, *Biophys. J. 89*, 1464-1481.

21. Scholes, G. D., and Fleming, G. R. (2000) On the mechanism of light harvesting in photosynthetic purple bacteria: B800 to B850 energy transfer, *J. Phys. Chem. B 104*, 1854-1868.

CHAPTER 5

The Electronic Structure of Photosystem II: Stark Spectroscopy on Site–directed Mutants

Elisabet Romero, Bruce A. Diner, Peter J. Nixon, Jan P. Dekker and Rienk van Grondelle

The light-induced charge separation is the primary photochemical event in photosynthesis. In order to investigate this process we have applied absorption and Stark spectroscopy at low temperature to a series of photosystem II reaction center (PSII RC) site-directed mutants from the cyanobacterium *Synechocystis* sp. PCC 6803. The site-directed mutations modify the protein environment of the cofactors involved in the charge separation process: P_{D1}, P_{D2}, Chl_{D1} and Phe_{D1}. The results demonstrate that at least two different exciton states are mixed with charge transfer (CT) states yielding exciton states with CT character: $(P_{D1}^{\delta-}P_{D2}^{\delta+}Chl_{D1})^*_{673nm}$ and $(Chl_{D1}^{\delta+}Phe_{D1}^{\delta-})^*_{681nm}$. Moreover, the CT state $P_{D2}^{+}P_{D1}^{-}$ acquires excited state character due to its mixing with and exciton producing $(P_{D2}^{+}P_{D1}^{-})^{\delta*}_{684nm}$ (the subscript indicates the approximate center wavelength of the electronic transition for each mixed state). It is concluded that the states which initiate charge separation are mixed states, not pure exciton states and that the degree of mixing between exciton and CT states determines the quantum yield of radical pair formation and, therefore, the efficiency of charge separation (the higher the mixing, the higher the efficiency of charge separation). The results also show that the pigment-protein interactions fine-tune the energy of the exciton and CT states and hence the mixing between these states which ultimately control the selection and efficiency of a specific charge separation pathway. Therefore, Stark spectroscopy applied to site-directed mutants demonstrates that the protein has the capacity to control the functionality of the PSII RC complex.

Manuscript in preparation

INTRODUCTION

The primary photochemical event in photosynthesis is the light-induced charge separation. This process takes place in the membrane-bound photochemically active reaction center (RC), a pigment-protein complex found in purple bacteria and oxygen evolving organisms (cyanobacteria, algae, and higher plants). The charge separated state created in the RC of photosystem II (PSII) drives water splitting and generates an electrochemical gradient across the membrane which is used to generate ATP. The understanding of the molecular mechanisms leading to charge separation is crucial since the success of photosynthesis depends on the efficiency of charge separation.

According to the X-ray structure of cyanobacterial PSII (*1-4*) the RC contains eight chlorins, two quinones and two carotenes. Four chlorophyll (Chl), two pheophytin (Phe) and two quinone (Q) molecules are arranged in two symmetrical branches spanning the membrane in the center of the complex; two additional Chl molecules, $Chls_Z$, are located at opposing sites on the periphery of the complex and two β-carotene molecules are situated between the peripheral $Chls_Z$ and the center of the complex. The spatial distribution of the central cofactors (Phe_{D1}, Chl_{D1}, P_{D1}, P_{D2}, Chl_{D2}, and Phe_{D2}) gives rise to a system of coupled pigments which interact, creating collective excited (exciton) states with contributions from various cofactors. In addition, the system is not static, fast nuclear motions (intra- and interpigment vibrations and protein vibrations) and slow conformational motions of the protein produce homogeneous and inhomogeneous broadening, respectively, of the electronic transitions. Therefore, after absorption of a photon by the RC the excitation energy is distributed among the cofactors (depending on protein conformation or disorder) and converted into a charge separated state after a series of energy and electron transfer reactions. This means that charge separation can be initiated from different combinations of cofactors (*5, 6*) giving rise to different charge separation pathways (*7-11*).

Recently, we have presented theoretical (*10, 12*) and experimental (*11*) evidence which demonstrate that, at least, two different low-energy exciton states, ($Chl_{D1}Phe_{D1}$) and ($P_{D1}P_{D2}Chl_{D1}$), are present in the PSII RC of higher plants leading to two different charge separation pathways (note that the cofactors sequence corresponds with their order of participation in the excitonic wavefunction). Depending on protein conformation, the low-energy exciton state is delocalized over a certain set of excitonically coupled cofactors. The slow protein motions create disorder which produces a distribution of energetically different RC complex within the ensemble.

The theoretical modelling and the experimental data showed that the selection of a certain pathway by a single RC complex in the ensemble is strongly dependent on disorder (protein conformation). The sequence of states for the two charge separation pathways, the so-called Chl_{D1} and P_{D1} paths, are:

Chl_{D1} path: $(Chl_{D1}Phe_{D1})^* \rightarrow Chl_{D1}^{+}Phe_{D1}^{-} \rightarrow P_{D1}^{+}Phe_{D1}^{-}$

P_{D1} path: $(P_{D1}P_{D2}Chl_{D1})^* \rightarrow P_{D2}^{+}P_{D1}^{-} \rightarrow P_{D1}^{+}Chl_{D1}^{-} \rightarrow P_{D1}^{+}Phe_{D1}^{-}$

The participation of an exciton in the primary charge separation reaction (exciton* → radical pair, RP), depends on its degree of mixing with a charge transfer (CT) state. As a consequence of the mixing, the CT state becomes dipole-allowed as it borrows some dipole strength from the exciton state. In the same way, the static dipole moment of the exciton state increases considerably which will manifest itself as a significant dipole moment increase in the excited state with respect to the ground state. An extremely sensitive technique to measure dipole moment changes ($\Delta\mu$) is Stark spectroscopy (*10, 13, 14*) which monitors the changes in absorption or emission spectra in the presence of an externally applied electric field. Three molecular parameters can be obtained from the Stark spectra: the change in dipole strength, the change in dipole moment, $\Delta\mu$, and the change in polarizability, $\Delta\alpha$, between the ground and excited state for an electronic transition. The $\Delta\mu$ is a measure of the degree of charge redistribution in the excited state associated with a transition. The $\Delta\alpha$ is a measure of the deformability of the electronic structure of the states involved in the transition (*13, 14*). The Stark effect on the absorption spectrum monitors the electronic changes directly upon photoexcitation, allowing the study of the electronic structure of the excited states. The externally applied electric field enhances differentiation between the states that experiment a large modification of the electronic density distribution in the excited state (with respect to the ground state), and the states that maintain the ground state electronic structure in the excited state.

The Stark spectrum, $Abs_{Field\ on}$ minus $Abs_{Field\ off}$, for isolated absorption bands in a non-oriented, immobilized sample is described by the Liptay formalism as a linear combination of the zeroth, first, and second derivatives of the absorption spectrum (*15*). The molecular parameters $\Delta\alpha$ and $\Delta\mu$ scale with the first and second derivatives, respectively, of the absorption spectrum (classic Stark effect). The shape of the Stark spectrum of PSII RC from higher plants has been shown to be dominated by the second derivative of the absorption spectrum (2DAbs) (*16*) and, therefore, by $\Delta\mu$.

However, in that work deviations from the classic Stark effect were found at wavelengths longer than 675 nm where the Stark spectrum was red shifted with respect to the 2DAbs (non-classic Stark effect which is not included in the Liptay formalism). The fitting of the Stark PSII RC spectrum according to our model, where excitonic interactions and exciton-CT mixing are explicitly included, shows that: i) excitonic interactions produce band shifts in the Stark spectrum and ii) exciton-CT mixing produce increased Stark band amplitudes when compared with the 2DAbs (*10*). Therefore, the comparison of the 2DAbs with the Stark spectrum is a useful tool for a qualitative interpretation of the Stark spectrum. That work also showed that the Stark spectrum line shape depends on the energy and configuration of the CT states.

The information contained in the Stark spectra of PSII is difficult to extract due to the spectral congestion in the Q_Y absorption region. In order to overcome this problem, we have chosen a combined approach: Stark spectroscopy applied to site-directed mutants. A specific amino acid mutation alters the electrostatic environment of a cofactor, i.e. the energy of the exciton and primary radical pairs states in which the cofactor participates, as well as the exciton-CT mixing. As a result, the line shape and amplitude of the Stark spectra of the mutants changes with respect to the wild-type (WT). These changes can be directly correlated with the energetic changes induced by the mutation as observed in the absorption spectrum allowing a band assignment which finally leads to a description of the charge separation mechanisms.

The effect of site-directed mutagenesis in the primary photochemistry of PSII has been studied by several groups: i) It was shown that mutations affecting radical cations and anions modulate the quantum yield of primary radical pair formation (*17, 18*); ii) Low temperature optical spectroscopy on mutants was employed to assign the Q_Y absorption bands of the cofactors in the PSII RC (*19*); iii) The characterization of a series of P_{D1} and P_{D2} mutants showed that the reduction potential of the redox couple P^+/P and, therefore, the charge distribution between P_{D1} and P_{D2}, could be modulated by ligand replacement at position D_1-His198 and, to a minor extent, at position D_2-His197 (*20*); iv) The mutants were crucial to determine the sites of primary charge separation and cation and triplet stabilization (*20*) and; v) The Stark spectra of a series of bacterial RC mutants was investigated in order to develop a systematic description of the electronic structure of the excited state of the special pair in the bacterial RC (*21*).

In this study we intend to test the validity of our model in a different organism, the cyanobacterium *Synechocystis* sp. PCC 6803 (*Syn*.) for which site-directed mutants are available. The mutations studied modify the protein environment and hence the site energy of the cofactors involved in the charge separation process (Phe_{D1}, P_{D1}, P_{D2} and Chl_{D1}). Due to the excitonic couplings among the cofactors in the PSII RC the mutations induce changes in the energy of the exciton states in which the cofactors participate. On the one hand, we analyze the effect of the modification of the hydrogen-bond interaction between the residue in position D_1-130 and the 13^1-keto carbonyl of Phe_{D1} in the electronic structure of the PSII RC complex. On the other hand, a series of site-directed mutants which modify the protein environment of P_{D1}, P_{D2} and Chl_{D1} is analyzed. In the latter case, the system of study is the more intact PSII core complex consisting of the RC, the antenna complexes CP43 and CP47 and several smaller protein subunits. This system is the smallest PSII particle able to split water due to the high oxidation potential species created as a result of charge separation.

The hydrogen-bond interaction between the protein residue in position D_1-130 and the 13^1-keto carbonyl of Phe_{D1} (Figure 1) has important implications regarding the quantum yield of charge separation in PSII. The modification of this hydrogen-bond interaction has been shown to exert a significant effect in the quantum yield of primary radical pair formation (Φ_{RP}) in the PSII RC isolated from *Syn*. In *Syn*. the residue in position D_1-130 is a glutamine (Gln) while in higher plants it is a glutamate (Glu). Nanosecond and picosecond transient absorption measurements indicate that $\Phi_{RP\ higher\ plant} > \Phi_{RP\ D1\text{-}Gln130Glu\ mutant} > \Phi_{RP\ \textit{Syn.}\ WT}$ (*17*). The authors, by considering the $\Phi_{RP\ higher\ plant}$ equal to unity, show that $\Phi_{RP\ D1\text{-}Gln130Glu\ mutant} \approx 0.75$ and $\Phi_{RP\ \textit{Syn.}\ WT} \approx 0.55$. The complete removal of the hydrogen-bond interaction in the D_1-Gln130Leu results in an even lower Φ_{RP} (≈ 0.35). Due to the chemical structure of these residues, Gln contains an amide and Glu contains a carboxylic acid, the hydrogen-bond strength to the 13^1-keto carbonyl of Phe_{D1} is stronger in higher plants than in cyanobacteria as has been shown by light-induced Fourier transform infrared (FTIR) difference spectroscopy (*22*). The authors of this FTIR study also showed by density functional theory (DFT) calculations that the redox potential (E_{red}) of Phe with the 13^1-keto carbonyl hydrogen bonded with Glu is higher than with Gln by 84 mV (*22*). This means that the strengthening of the hydrogen-bond interaction facilitates the reduction of Phe. In the present study, the absorption and Stark spectra of the cyanobacterium *Syn*. PSII RC isolated from the WT and D_1-Gln130Glu mutant strains is compared with the PSII RC isolated from a higher plant (spinach).

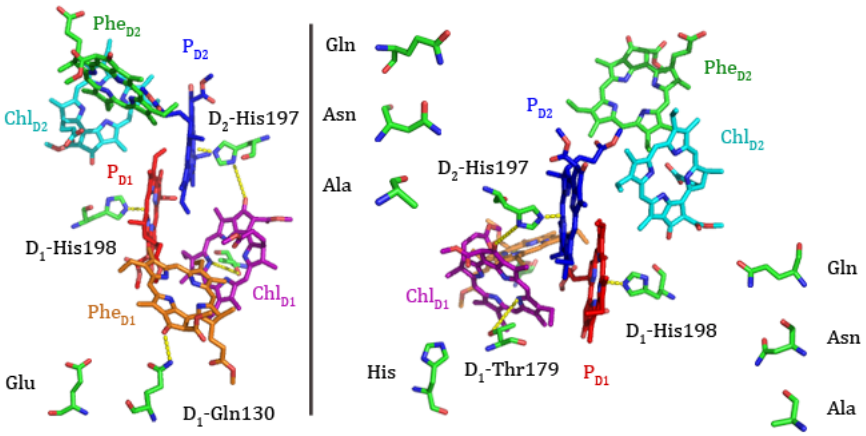

Figure 1. Relative positions of the central cofactors in the PSII RC complex together with the positions of the mutated residues (D_1-Gln130, D_1-His198, D_2-His197 and D_1-Thr179) and the chemical structures of the introduced residues (Glu, Gln, Asn, Ala and His) (adapted from (*4*)).

The role of the chlorophylls involved in the charge separation process (P_{D1}, P_{D2} and Chl_{D1}) is investigated. We use seven site-directed mutants which modify the protein environment of: P_{D1} (D_1-His198Gln, D_1-His198Asn and D_1-His198Ala); P_{D2} (D_2-His197Gln, D_2-His197Asn and D_2-His197Ala); and Chl_{D1} (D_1-Thr179His) (see Figure 1). All the introduced mutations allow RC assembly and complete chromophore binding (*17, 20, 23*). For the P_{D1} and P_{D2} mutants the histidine (His) which axially coordinates P_{D1} and P_{D2} is exchanged by glutamine (Gln), asparagine (Asn) or alanine (Ala). The electronic polarizability of the π-system of the imidazole moiety of His stabilizes the excited states of nearby cofactors by dispersive interactions. Therefore, in these mutants the site energy of P_{D1} or P_{D2} and consequently the exciton states in which P_{D1} and/or P_{D2} participate are expected to shift to the blue (*20*). In addition, the D_2-His197 mutation is also likely to perturb the energy of the exciton states containing Chl_{D1} because the His residue removed is proposed to be, by analogy to purple bacterial reaction centers (*24*), indirectly hydrogen bonded to the 13^1-keto carbonyl of Chl_{D1} through a water molecule. Indeed, the comparison of two site-directed mutants at the position D_2-His197 with the WT in an infrared transient absorption study allowed the assignment of the characteristic vibrations of Chl_{D1} (*25*).

The introduced residues, Gln and Asn, contain an amide moiety which could, directly or indirectly though a water molecule, coordinate the central magnesium of P_{D1} and P_{D2}, or create hydrogen-bond interactions with nearby carbonyls while this is not possible for the alkyl side-chain of the Ala residue. For the D_1-Thr179His mutant, the replacement of threonine (Thr), which overlies Chl_{D1}, with His is expected to stabilize the Chl_{D1} site energy and consequently the exciton states in which Chl_{D1} participates producing a red shift in the absorption spectrum of the mutant (*23*). Previous spectroscopic analyses of these mutants (*20, 23*) lead to the assignment of i) the 683 nm transition to the lowest exciton state in the RC localized mainly on Chl_{D1} and ii) the 673 nm transition to the low energy exciton state formed mostly by P_{D1} and P_{D2}.

The aim of this work is to investigate the participation of the cofactors: Phe_{D1} (one of the primary electron acceptors (*11, 26, 27*)); P_{D1} and P_{D2} (the counterpart of the bacterial special pair and an electron donor (P_{D1}) (*11, 26, 27*)); and Chl_{D1} (considered the lowest energy Chl (*20, 28*) and a primary electron donor and acceptor (*11*)) in the exciton states which are the precursors of the primary radical pairs involved in the charge separation process. This participation is measured by the presence of a non-classical contribution to the Stark spectrum. We report the comparison of the low temperature (77 K) absorption and Stark spectra of WT and eight site-directed mutants: D_1-Gln130Glu, D_1-His198Gln, D_1-His198Asn, D_1-His198Ala, D_1-Thr179His, D_2-His197Gln, D_2-His197Asn and D_2-His197Ala. The results show that at least two different exciton states are mixed with CT states yielding exciton states with CT character: $(P_{D1}^{\delta-}P_{D2}^{\delta+}Chl_{D1})^*_{673nm}$ and $(Chl_{D1}^{\delta+}Phe_{D1}^{\delta-})^*_{681nm}$. Moreover, the CT state $P_{D2}^{+}P_{D1}^{-}$ acquires excited state character due to its mixing with and exciton producing $(P_{D2}^{+}P_{D1}^{-})^{\delta*}_{684nm}$ (the subscript indicates the approximate center wavelength of the electronic transition for each mixed state). Therefore, the mixed states $(P_{D1}^{\delta-}P_{D2}^{\delta+}Chl_{D1})^*_{673nm}$, $(Chl_{D1}^{\delta+}Phe_{D1}^{\delta-})^*_{681nm}$ and $(P_{D2}^{+}P_{D1}^{-})^{\delta*}_{684nm}$ give rise to two different charge separation pathways in photosystem II.

MATERIALS AND METHODS

Sample preparation. PSII RC samples from *Synechocystis* sp. PCC 6803 were prepared as described previously (*17*). PSII core samples from *Synechocystis* sp. PCC 6803 were prepared as described previously (*20, 29*). The PSII RC isolated from spinach was prepared as described previously (*30*). The monomeric PSII core samples were analyzed and purified by fast-phase liquid chromatography (FPLC) using a size-exclusion column in order to eliminate possible PSI contamination and contributions of free chlorophylls (Chls) and carotenoids to the spectra. The samples were PSI free but some of them contained a significant amount of carotenoids aggregates. The purified samples were diluted in a buffer containing 50 mM MES pH 6.5, 20 mM $CaCl_2$, 5 mM $MgCl_2$, 100 μM $K_3Fe(CN)_6$, 0.03% β-DM and 57% glycerol (v/v). The $K_3Fe(CN)_6$ was added in order to oxidaize Q_A^- to the neutral state hence maintaining the reaction centers open for charge separation. The PSII RC samples were diluted in a buffer containing 20 mM BisTris pH 6.5, 20 mM NaCl, 5 mM $MgCl_2$, 0.09% β-DM and 57% glycerol (v/v). The addition of $K_3Fe(CN)_6$ is not necessary for the RC samples because Q_A is lost during the isolation procedure.

Spectroscopy. Absorption and Stark spectra were simultaneously recorded at 77 K in a home-built setup as described previously (*31, 32*). The OD of the samples in the Stark cell (thickness 80 μm) was around 0.7 cm^{-1}. The Stark cell was immersed in liquid nitrogen, in an Oxford liquid nitrogen cryostat. The Stark cell was rotated 45° with respect to the propagation direction of the horizontally polarized measuring light in order to set the angle between the electric field component of the light and the externally applied electric field, χ, to magic angle. The Stark spectra were recorded at an externally applied electric field strength of 2.25×10^5 V cm^{-1}.

RESULTS AND DISCUSSION

Phe_{D1} mutant

The simultaneously recorded 77 K absorption and Stark spectra of *Synechocystis* sp. PCC 6803 (*Syn.*) PSII RC WT and D_1-Gln130Glu mutant; and of spinach PSII RC WT (D_1-Glu130) are shown in Figure 2. The replacement of Gln by Glu in the *Syn*. D_1-Gln130Glu mutant converts this mutant into a spinach-like RC complex.

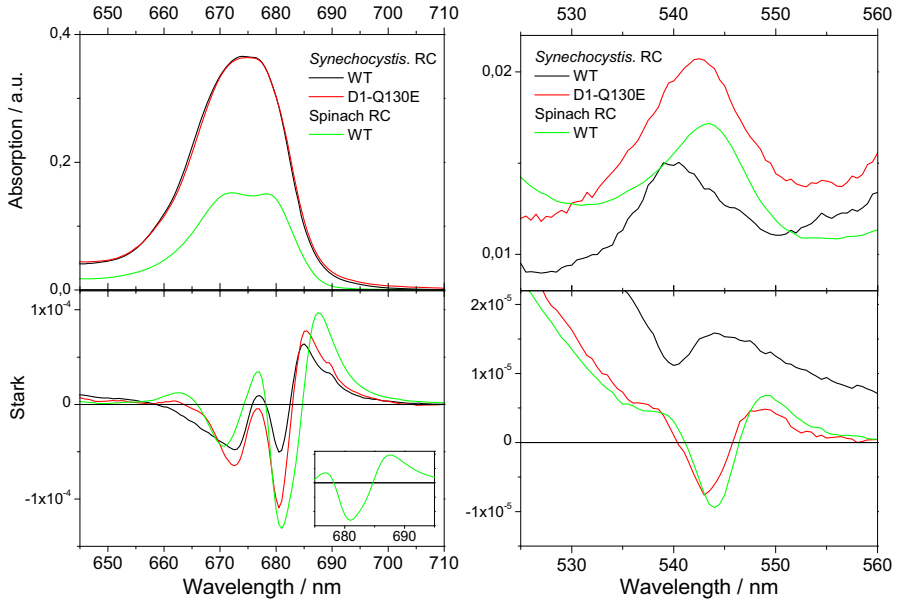

Figure 2. Simultaneously recorded 77 K absorption and Stark spectra for *Synechocystis* RC complex WT and D_1-Gln130Glu mutant; and for spinach RC complex WT. (*Left panel*) Chl-Phe Q_Y absorption region, (*inset*) spinach RC WT 681 nm Stark minimum expanded; and (*right panel*) Phe Q_X absorption region. The absorption and Stark spectra are normalized to the integrated area of the absorption spectra in the 645-710 nm range according to the Chl content. The Stark spectra were recorded at $\chi = 54.7°$ and at an external electric field strength of 2.25 x 10^5 V cm^{-1}.

Absorption. Figure 2 shows the absorption spectra of *Syn*. WT, D_1-Gln130Glu mutant RC and spinach RC complex WT in the Chl-Phe Q_Y absorption region and in the Phe Q_X absorption region normalized to the Chl content. The amplitude of the *Syn*. RC samples absorption is higher with respect to the spinach RC. This is explained by the fact that the *Syn*. RC samples are not completely pure, they contain approximately one CP47 antenna complex per two RC complexes, i.e., they are RC-enriched preparations (in the following called RC complexes). Therefore the absorption and Stark spectra have been normalized according to the Chl content of each sample: 17 Chl and 2 Phe per *Syn*. RC and 6 Chl and 2 Phe per spinach RC. Therefore, the total transition dipole moment strength of the *Syn*. and spinach RC is 18.5 and 7.5 Chl units, respectively (considering the transition dipole moment strength of Chl equal to one and that of Phe equal to 0.75 Chl units). The small differences in the antenna content of the *Syn*. RC complexes hinder the comparison of the WT and mutant absorption line shape. However, the difference in composition between the *Syn*. RC complexes and between *Syn*. and spinach RC have a minor effect in the Stark spectra due to the small contribution to the Stark spectra of the CP47 antenna complex in the absorption regions of interest (with respect to the contribution to the Stark spectra of the RC, Figure A1 in the Appendix). In the Phe Q_X absorption region, the replacement of Gln in WT for Glu in the D_1-Gln130Glu mutant produces a 2.5 nm red shift of the Phe Q_X band at 540 nm in WT to 542.5 nm in the mutant as observed before (*17*). In fact, this shift can be used as a confirmation of the presence of the mutation. For the spinach RC which contains a Glu at position D_1-130 (as the D_1-Gln130Glu mutant), the maximum of the Phe Q_X band peaks at 543.5 nm. The amplitude of the Phe Q_X band is very similar in the three RC preparations (which indicates that the normalization procedure is correct).

Stark. Figure 2 shows the Stark spectra of the *Syn*. RC WT and D_1-Gln130Glu mutant, and of the spinach RC complex WT in the Chl-Phe Q_Y absorption region and in the Phe Q_X absorption region. The Stark spectra of the three RC samples resemble the second derivative of the absorption spectra (2DAbs) (Figure 3) indicating that, in first approximation, these Stark spectra are dominated by a change in dipole moment, $\Delta\mu$, between the ground and excited states associated to the electronic transitions. A similar Stark effect was observed in the bacterial RC (*33-35*) and in the previously reported Stark spectrum of higher plant PSII RC (spinach) (*16*). In the PSII RC the Stark spectra is dominated by the excitonically coupled (and coupled to CT states) cofactors located in the active branch (P_{D1}, Chl_{D1}, Phe_{D1}) and in the inactive branch (P_{D2}).

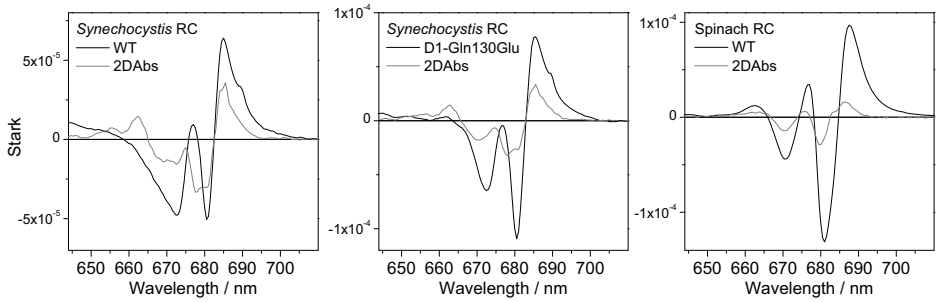

Figure 3. Comparison of the Stark and second derivative of the absorption (2DAbs) spectra of (*from left to right*) *Synechocystis* RC complex WT and D_1-Gln130Glu mutant; and for spinach RC complex WT. The Stark spectra were recorded at $\chi = 54.7°$ and an external electric field strength of 2.25×10^5 V cm^{-1}.

The monomeric $Chls_Z$, Chl_{D2} and Phe_{D2} cofactors are not expected to give a significant Stark response (*16*) because they do not contribute to the collective excitonic states (*10*). It has been shown that the Stark spectrum of the Phe_{D2} modified RC did not differ in the 660-750 nm range from the standard RC, meaning that Phe_{D2} is neither contributing to the exciton states coupled to charge transfer states nor to the charge separated states (*16*).

By comparing the Stark spectra of the *Syn*. RC WT and D_1-Gln130Glu mutant, and of the spinach RC complex WT, we analyze the effect of the Glu residue in position D_1-130, i.e., the effect of strengthen the hydrogen-bond interaction between the residue at position D_1-130 and the 13^1-keto carbonyl of Phe_{D1}. The Stark spectra of the *Syn*. RC WT in the Q_Y absorption region is composed of two negative bands at 672.5 and 680.5 nm; and three maxima at 677, 685 and 689.5 nm (shoulder). For the D_1-Gln130Glu mutant, the position of the Stark bands is virtually identical to WT. The main difference between WT and mutant is the two-fold amplitude increase of the negative band at 680.5 nm in the mutant. The Stark spectra of the spinach RC WT in the Q_Y absorption region is composed of two negative bands at 670.5 and 681 nm; and three maxima at 663, 676.5 and 687.5 nm as reported before (*16*). The Stark band shifts in the spinach RC with respect to the *Syn*. samples may be due to small differences in the energy of the exciton states between the two organisms. The amplitude of the 670.5 nm Stark minimum in the spinach RC is similar to its *Syn*. counterparts while the amplitude of the 681 nm minimum is similar to the 680.5 nm minimum in the D_1-Gln130Glu mutant.

It is interesting to note that upon Gln exchange by Glu in the D_1-Gln130Glu mutant the amplitude of the 680.5 nm Stark minimum resembles the amplitude of the spinach RC which also contains a Glu in position D_1-130. In the Phe Q_X absorption region, an amplitude increase of the Phe_{D1} Stark minima is also clearly observed for the D_1-Glu130 samples (*Syn*. mutant and spinach RC WT) with respect to the D_1-Gln130 sample (*Syn*. RC WT). For the *Syn*. RC WT the Phe_{D1} Q_X Stark minimum is at 540 nm (no shift in position between Stark and absorption bands) and its amplitude is $5x10^{-6}$ (ΔOD/a.u.); while for the D_1-Gln130Glu mutant and the spinach RC WT the Phe_{D1} Q_X Stark minima are at 542.5 and 543.5 nm (0.5 nm red shift of the Stark with respect to the absorption band) and their amplitude are $13x10^{-6}$ and $15x10^{-6}$ (ΔOD/a.u.), respectively.

These observations indicate that i) Phe_{D1} contributes to the 680.5-681 nm exciton state in the three RC samples analyzed and; ii) the strengthening of the hydrogen-bond interaction between the residue at position D_1-130 and the 13^1-keto carbonyl of Phe_{D1} (in the mutant and spinach RC) enhances the mixing exciton-CT for the 680.5-681 nm state (with respect to *Syn*. WT).

According to the experimental evidence presented here (see also P_{D1}, P_{D2} and Chl_{D1} mutants section) and to our model (*10-12*) the mixing between the exciton $(Chl_{D1}Phe_{D1})^*$ and the CT state $Chl_{D1}^{+}Phe_{D1}^{-}$ generates an exciton with CT character $(Chl_{D1}^{\delta+}Phe_{D1}^{\delta-})^*$ which gives rise to the Stark minimum at 680.5-681 nm in the *Syn*. and spinach RC samples (where δ+ and δ- indicate the fraction of CT acquired by the exciton state).

It is important to remember that the replacement of Gln at position D_1-130 by Glu in the D_1-Gln130Glu mutant increases the quantum yield of radical pair formation (Φ_{RP}) from 0.55 in *Syn*. RC WT to 0.75 in the *Syn*. RC mutant (considering the Φ_{RP} of a higher plant RC equal to one). Remarkably, the increase of Φ_{RP} correlates with the increase of the Stark minimum amplitude at 680.5-681 nm. In addition, a similar trend is observed when comparing the Stark with the 2DAbs spectra (Figure 3), the larger the Stark amplitude with respect to the 2DAbs spectra, the higher the quantum yield of radical pair formation. These observations indicate that the Stark spectrum and its comparison with the 2DAbs spectrum are a direct measure of the quantum yield of radical pair formation in PSII.

Interestingly, in the red tail of the Stark spectra of the *Syn*. RC samples, a positive shoulder at 689.5 nm is also observed (Figure 2). The higher amplitude of the shoulder in the *Syn*. RC mutant is most likely due to the overlap with the more intense 680.5 nm Stark band in the mutant with respect to WT which suggests that the red shoulder is not affected by the mutation.

Therefore, the presence of the shoulder indicates that another state without participation of Phe_{D1} contributes to the intense negative Stark signal at 680.5 nm in the *Syn*. RC samples. In spinach this shoulder is not resolved in the red positive tail of the Stark spectra (most likely due to spectral overlap with the maxima at 687.5 nm). However, the negative 681 nm Stark band is asymmetric with a shoulder around 684 nm (inset in the left panel of Figure 2). This spectral shape suggests that also in spinach more than one state may contribute to the intense negative Stark signal at 681 nm. The presence of two states contributing to the 680.5-681 nm Stark minimum is predicted in the 2DAbs spectra in which two separated minima compose the red-most Stark minimum (Figure 3). According to our model (*10-12*), the CT state $P_{D2}^{+}P_{D1}^{-}$ is strongly mixed with the $(P_{D1}P_{D2})^*$ exciton state. In this case, the CT state borrows dipole strength from the exciton producing a red-most state $(P_{D2}^{+}P_{D1}^{-})^{\delta*}$ with an absorption centered around 684 nm (where δ^* indicates the fraction of dipole strength acquired by the CT state). Due to its CT character, this state is expected to contribute to the Stark spectra which will be dominated by $\Delta\mu$ and, therefore, will resemble the second derivative of the absorption spectra. Thus, we suggest that the $(P_{D2}^{+}P_{D1}^{-})^{\delta*}$ state contributes to the red edge of the 680.5-681 nm Stark minimum; it appears as a positive shoulder at 689.5 nm in the *Syn*. RCs, while it appears as a negative shoulder around 684 nm in the spinach RC.

P_{D1}, P_{D2} and Chl_{D1} mutants

The simultaneously recorded 77 K absorption and Stark spectra of *Synechocystis* sp. PCC 6803 core complex for WT, D_1-His198Gln and D_2-His197GlnAla mutants; WT, D_1-His198Asn and D_2-His197Asn mutants; WT, D_1-His198Ala and D_2-His197Ala mutants; and WT and D_1-Thr179His mutant are shown in Figures 4-6.

Q_Y absorption region

Absorption. Figure 4 shows the absorption spectra of WT and mutants in the Q_Y region. The site-directed mutations are expected to induce perturbations in the electronic properties of the cofactors within the RC, not in the CP43 and CP47 antenna complexes present in the core samples. As first approximation we assume that the mutations influence the energy of the electronic transition of a certain exciton state (in which the mutated cofactor participates), not the transition dipole moment strength or direction. Within this approximation, in order to examine the energy shifts, the absorption spectra of WT and mutants have been normalized to the integrated area in the 645-710 nm range.

The best way to visualize the effects of the mutations is to calculate the absorption difference spectra (Abs_{dif} equals Abs_{mutant} minus Abs_{WT}) (Figure 4) in which the negative bands (or minima) correspond to absorption bands that disappear in the WT upon mutation and the positive bands (or maxima) correspond to new absorption bands that appear upon mutation. However, it is important to keep in mind that the reaction center cofactors represent 1/5 of the total number of cofactors (35 Chl and 2 Phe) present in the core complex (RC: 6 Chl and 2 Phe, CP43: 13 Chl, CP47 16 Chl, taking into account only the cofactors absorbing in the Q_Y region). Therefore, the amplitude of the changes observed in the Abs_{dif} spectra should be compared with and absorption which is 20% of the total amplitude of the core complex. In order to facilitate the comparison between the changes induced by the mutations and the total amplitude of the RC absorption, we multiply the Abs_{dif} spectra by five. In this way, the amplitude of the changes observed in the Abs_{dif} spectra (multiplied by five as shown in Figure 4) can be directly compared with the total absorption amplitude of the core complex (considering that the total absorption amplitude corresponds only to the RC). Three different mutations are constructed at positions D_1-His198 and D_2-His197 which axially coordinate P_{D1} and P_{D2}, respectively.

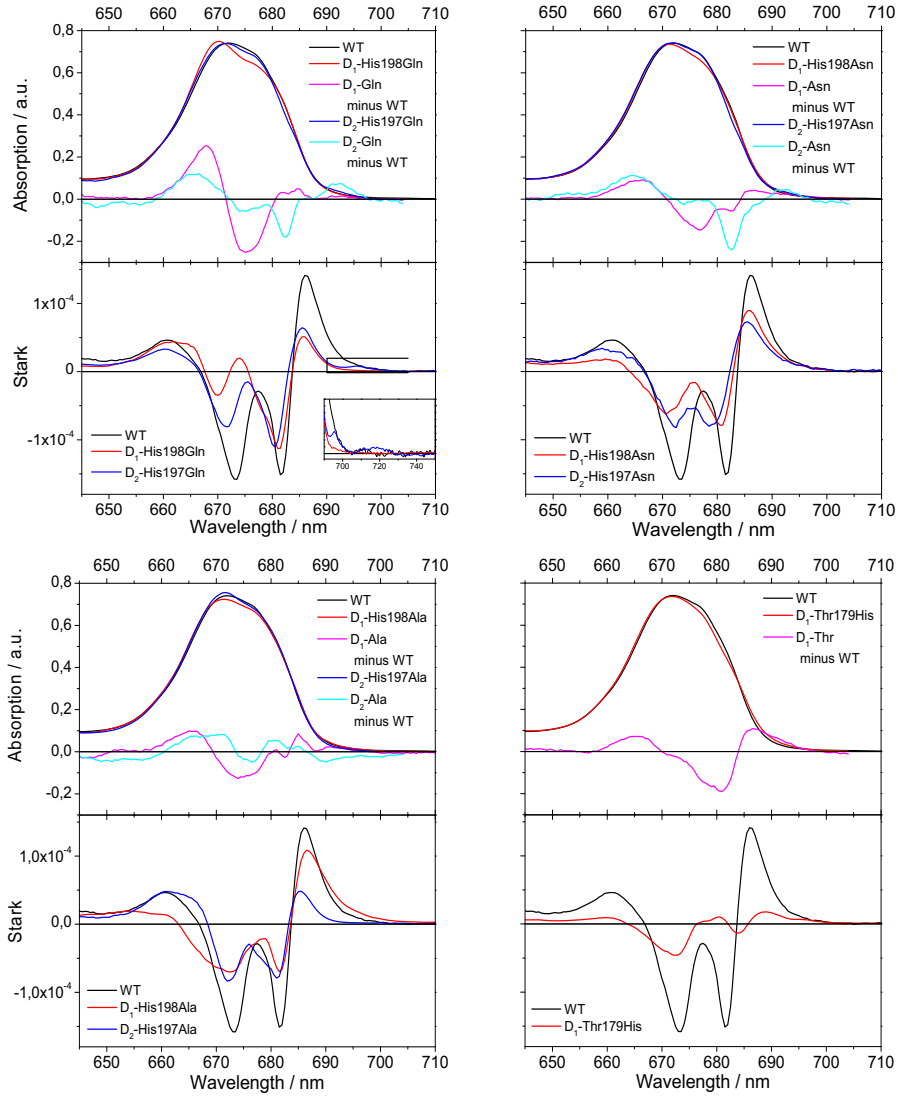

Figure 4. Simultaneously recorded 77 K absorption and Stark spectra of *Synechocystis* core complex in the Q_Y absorption region for (*from left to right*): WT, D_1-His198Gln and D_2-His197Gln mutants; WT, D_1-His198Asn and D_2-His197Asn mutants; WT, D_1-His198Ala and D_2-His197Ala mutants; and WT and D_1-Thr179His mutant. The absorption and Stark spectra are normalized to the integrated area of the absorption spectra in the 645-710 nm range. The absorption difference spectra have been multiplied by five. The Stark spectra were recorded at $\chi = 54.7^{\circ}$ and an external electric field strength of 2.25 x 10^5 V cm^{-1}.

The absorption changes induced by the exchange of His for the amide residues, Gln and Asn, are similar for the D_1 branch mutants, as well as for the D_2 branch mutants (Figure 4), as expected considering the similarity between the Gln and Asn chemical structures (Figure 1). In the four mutants (D_1-His198Gln, D_1-His198Asn, D_2-His197Gln and D_2-His197Asn) two minima at around 675 and 683 nm and one maximum at around 666 nm with different relative amplitude and width are observed in the absorption difference spectra (Figure 4). For the two D_1-His198 mutants the main change upon mutation is an apparent blue shift of the 675 nm band to 666 nm, in agreement with the assignment of a band at 673 nm to the low energy exciton state formed predominantly by P_{D1} and P_{D2} ($P_{D1}P_{D2}$ exciton) (see below) (*20, 23, 36*) which shifts to the blue upon His replacement. For the D_2-His197 mutants the amplitude of the 675 nm minimum is significantly smaller indicating that the participation of P_{D2} in the $P_{D1}P_{D2}$ exciton is lower than for P_{D1}. The observed absorption loss at 683 nm is similar for both D_2-His197 mutants. We assign the absorption loss at 683 nm to a secondary effect on Chl_{D1} related to D_2-His197 exchange.

This secondary effect on Chl_{D1} might have several origins: the loss of the hydrogen-bond to the 13^1-keto carbonyl which makes the Chl_{D1} π-conjugated system less asymmetric and/or the disappearance of the dispersive interactions provided by His which also stabilizes the exciton states in which Chl_{D1} participates. Both explanations are expected to induce a blue shift in the absorption. Alternatively, the mutation may increase the disorder in the system. In this case, a narrow localized state may become more delocalized in order to compensate for the higher disorder of the system, i.e., the narrow band broadens. The second explanation is more in line with the second derivative line shape of the Abs_{dif} spectra. When comparing the effect of the Gln and Asn mutations in the active and inactive branches, it is interesting to note that the main absorption loss has its counterpart, with smaller amplitude, in the other branch mutant, highlighting the presence of excitonic coupling between P_{D1} and P_{D2}.

For both the Ala mutants, D_1 and D_2, the absorption difference spectrum has similar spectral shape. The minimum at 683 nm is similar in both mutants, the main difference is found in the 675 nm band which is broader and has higher amplitude in the D_1 mutant. In the Ala mutants the complete removal of the polar environment (Figure 1) affects both sides in a similar way, with the D_1 side the most affected. These observations support that P_{D1} and P_{D2} are energetically coupled, i.e., they contribute to the same exciton state which low-energy state is located around 675 nm (with higher participation from P_{D1}) (*23, 28*).

The high-energy state located around 660 nm (*28*) has lower transition dipole moment strength, therefore is not observed in the Abs_{dif} spectra.

The mutation constructed at position D_1-Thr179, which overlies Chl_{D1}, gives rise to a different absorption difference spectral shape with respect to the P_{D1} and P_{D2} mutants. In this case an asymmetric minimum with contributions from 681, 677 and 671 nm components (in decreasing order of amplitude) and two maxima at 666 and 687 nm are observed. This spectral shape could be understood as a band broadening (the asymmetric minimum broadens to a band extending from 660 to 700 nm with around 25 nm fwhm) or as a band shift (taking into account the amplitude of the maxima and minima, the 681 nm band red shifts to 687 nm and the 677 and 671 nm bands blue shift to 666 nm). Recent experimental (*23*) and theoretical (*36*) work on this mutant which shows the red shift of the Chl_{D1} exciton upon Thr exchange by His, supports the second interpretation. For this mutant, the red shift of the main 681 nm band and the blue shift of the minor 671 and 677 nm bands indicate that Chl_{D1} participates in two excitons, in the Chl_{D1} exciton and, to a lesser extent, in the $P_{D1}P_{D2}$ exciton. In summary, the results are consistent with the presence of two different low-energy exciton states in the reaction center (*10, 11, 20, 23, 37*): the $P_{D1}P_{D2}Chl_{D1}$ exciton which low-energy exciton state absorbs around 675 nm, and the $Chl_{D1}Phe_{D1}$ exciton state (see above RC Stark and below Phe Q_X sections) with absorption around 681 nm, in agreement with the literature (note that the order of the cofactors in the exciton nomenclature reflects their order of participation in the exciton state).

Stark. The Stark spectra of PSII cores, WT and mutants, resemble the second derivative of the absorption spectra (2DAbs) (Figure 5) indicating that, in first approximation, these Stark spectra are dominated by a change in dipole moment, $\Delta\mu$, between the ground and excited states associated to the electronic transitions. A similar Stark effect was observed in the bacterial RC (*33, 34*) and in the higher plant PSII RC (*16*) (see above RC Stark section). Our system of study, the core complex, contains the photochemically active reaction center as well as the core antenna proteins CP43 and CP47. In higher plants (spinach) for which the RC, CP43 and CP47 isolation procedures are well established (*30, 38-41*) the amplitude of the antenna Stark spectra with respect to that of the RC is approximately equal around 670 nm and presents about a four-fold decrease around 680 nm (Figure A1 in the Appendix). Taking this into account and the fact that the mutations only affect the cofactors in the reaction center, the core complex absorption and Stark spectra will be discussed in terms of changes within the reaction center.

The interpretation of the Stark spectra will be based on: i) the comparison of the absorption and Stark spectra between WT and mutants (Figure 4) in terms of band shifts and differences in band amplitudes, and ii) on the comparison of the Stark spectra with the second derivative of the absorption spectra (2DAbs) (Figure 5).

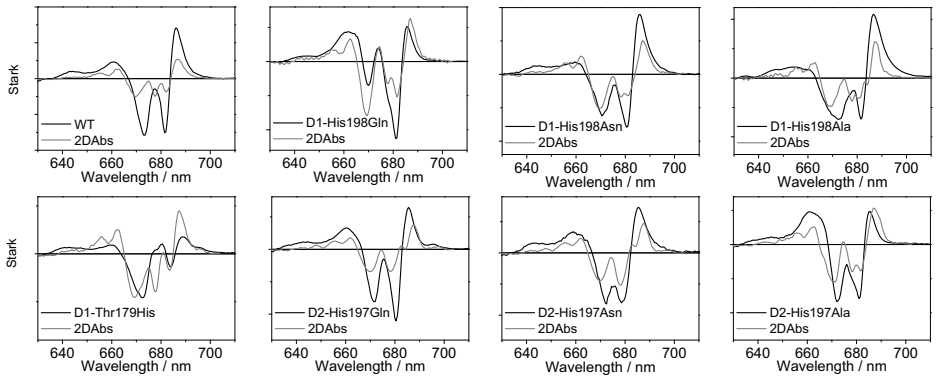

Figure 5. Comparison of the Stark and second derivative of the absorption (2DAbs) spectra of *Synechocystis* core complex for WT and mutants (*from left to right and from top to bottom*): WT, D_1-His198Gln, D_1-His198Asn, D_1-His198Ala, D_1-Thr179His, D_2-His197Gln, D_2-His197Asn and D_2-His197Ala mutants. The Stark spectra were recorded at χ = 54.7° and an external electric field strength of 2.25 x 10^5 V cm^{-1}. Each division in the vertical axis corresponds to 5x10^{-5} (ΔOD/a.u.).

The Stark spectrum of the WT is composed of two main minima at 673.25 and 681.75 nm and three maxima located at 644, 661 and 686.25 nm. In the second derivative of the absorption spectrum (Figure 5) three minima are present at 670, 677.5 and 682.5 nm; and two maxima at 661 and 687 nm. The Stark spectrum presents shifts of 1-3 nm (non-classic Stark effect) and a three-fold amplitude increase with respect to the 2DAbs which indicates that exciton couplings among the cofactors and exciton-CT mixing, respectively, are present in the WT core complex. For all mutants, band shifts in the Stark spectra with respect to the 2DAbs are observed indicating that the exciton couplings are also present. However, for all mutants with the exception of D_2-His197Gln, the amplitude of the 2DAbs is on the order of the Stark amplitude indicating that the mixing with CT states is reduced or absent (Figure 5). The most significant Stark band position and amplitude in the Q_Y region are collected in Table 1.

Table 1. Stark maxima and minima parameters in the Q_Y absorption band.

	Minima blue		Minima red		Maxima red	
	λ_{min} (nm)	amplitude	λ_{min} (nm)	amplitude	λ_{max} (nm)	amplitude
WT	673.25	1.00	681.75	1.00	686.25	1.00
D_1-His198Gln	670.00	0.22	681.25	0.75	685.75	0.36
D_2-His197Gln	671.50	0.51	680.50	0.73	685.50	0.45
D_1-His198Asn	670.50	0.39	680.50	0.51	685.75	0.65
D_2-His197Asn	672.50	0.56	678.75	0.53	685.75	0.51
D_1-His198Ala	671.00	0.44	681.50	0.46	686.75	0.77
D_2-His197Ala	672.25	0.53	681.00	0.52	685.25	0.34
D_1-Thr179His	672.50	0.29	684.00	0.09	689.00	0.22

The amplitude of the Stark maxima and minima are calculated relative to WT.

D_1-His198Gln and D_2-His197Gln mutants. The red-most maxima and minima in the Stark spectra of the mutants are blue shifted with respect to WT (Figure 4). For the D_1 mutant the maxima and minima are 0.5 nm blue shifted and their amplitudes are $^1/_3$ and ¾, respectively, with respect to WT. For the D_2 mutant the maximum and minimum are 0.75 and 1.25 nm blue shifted and their amplitudes are ½ and ¾, respectively, with respect to WT. The minimum at 673.25 nm in WT is blue shifted to 670 and 671.5 nm with amplitudes ¼ and ½ with respect to WT for the D_1 and D_2 mutants, respectively. In the red tail of the Stark spectrum a narrow band at 695.5 nm (4.5 nm fwhm) and a broad band at 718 nm (16.5 nm fwhm) are observed for the D_2-His197Gln mutant. This effect is explained as Type II contributions to the Stark signal. The physical model presented in (*10*) predicts the creation of additional Stark bands in spectral regions far from the main absorption bands when the energy of the CT states is shifted from the optimal value obtained by the model.

D_1-His198Asn and D_2-His197Asn mutants. The red-most maxima and minima in the Stark spectra of the mutants are blue shifted with respect to WT (Figure 4). For the D_1 mutant the maxima and minima are 0.5 and 1.25 nm blue shifted, respectively, and their amplitudes are ½ with respect to WT. For the D_2 mutant the maximum and minimum are 0.5 and 3 nm blue shifted and their amplitudes are ½ with respect to WT. The minimum at 673.25 nm in WT is blue shifted to 670.5 and 672.5 nm with amplitudes $^1/_3$ and ½ with respect to WT for the D_1 and D_2 mutants, respectively.

D_1-His198Ala and D_2-His197Ala mutants. For the D_1 mutant, the red-most maxima and minima are 0.5 nm red shifted and 0.25 nm blue shifted with amplitudes ¾ and ½, respectively, with respect to WT (Figure 4). For the D_2 mutant the maxima and minima are 1 and 0.75 nm blue shifted and their amplitudes are $^1/_3$ and ½, respectively, with respect to WT. The minimum at 673.25 nm in WT is blue shifted to 671.0 and 672.25 nm with amplitudes 0.44 and 0.53 with respect to WT for the D_1 and D_2 mutants, respectively.

D_1-Thr179His mutant. The Chl_{D1} mutant presents the most significant differences with respect to WT (Figure 4): the maxima at 686.23 nm in WT is 2.75 nm red shifted with ¼ of the amplitude in the WT, the minimum at 681.75 nm in WT is 2.25 nm red shifted with only 1/10 of the amplitude in the WT while the minimum at 673.25 nm is 0.75 nm blue shifted with $^1/_3$ of the amplitude in the WT.

The blue minimum, at 673.25 nm in WT, is blue shifted 0.75 – 3.25 nm and displays a two to four fold amplitude decrease upon mutation (Table 1). For all mutants the blue shift is in agreement with the analysis of the absorption: an exciton band with participation from $P_{D1}P_{D2}Chl_{D1}$ absorbing around 675 nm shifts to the blue upon mutation. According to the order of participation in the exciton state, the shift (for a specific mutation) is more pronounced for the P_{D1} than for the P_{D2} mutants and even less significant for the Chl_{D1} mutant. Thus far the Stark spectrum has confirmed the assignments from the absorption and the literature (*20, 23*). At this point, we will examine the potential of the $P_{D1}P_{D2}Chl_{D1}$ exciton state to initiate charge separation. This potential depends on the degree of mixing between the exciton and CT states; the stronger the mixing, the larger the Stark amplitude and the higher the potential to initiate charge separation (*10*). The changes in band position and amplitude for the P_{D1} and P_{D2} mutants show a correlation between the blue shift and the amplitude decrease of the 673.25 nm minimum: the stronger the shift, the larger the Stark amplitude decrease (Figure A2 in the Appendix). This correlation indicates that the absorption band shift induced by the mutations decreases the exciton-CT mixing present in the WT, i.e., in the WT the $(P_{D1}P_{D2}Chl_{D1})^*$ exciton absorbing at 673.25 nm is mixed with the $P_{D2}^+P_{D1}^-$ CT state (due to the strong overlap between the electronic wavefunctions of these states) (*10*) yielding the $(P_{D1}^{\delta-}P_{D2}^{\delta+}Chl_{D1})^*$ state.

Thus, we conclude that the mixed $(P_{D1}^{\delta-}P_{D2}^{\delta+}Chl_{D1})^*$ state initiates charge separation following the P_{D1} path, $(P_{D1}^{\delta-}P_{D2}^{\delta+}Chl_{D1})^* \rightarrow P_{D2}^+P_{D1}^- \rightarrow P_{D1}^+Chl_{D1}^- \rightarrow P_{D1}^+Phe_{D1}^-$ (*11*), in a fraction of reaction centers in which this mixed exciton-CT state is the lowest energy state.

Concerning the red minimum, at 681.75 nm in WT, the mutants can be divided in two groups: the P_{D1} and P_{D2} mutants with blue shift (more significant for the P_{D2} mutations) and decrease in amplitude (similar for P_{D1} and P_{D2} mutants) depending on the specific mutation; and the Chl_{D1} mutant with a red shift and a significant amplitude decrease. Considering the contribution of two exciton-CT states to the red Stark minimum observed in the RC samples, the blue shift present in the P_{D1} and P_{D2} mutants can be understood as a loss of a red component in the red Stark minimum. As discussed above, the P_{D1} and P_{D2} mutations induce a decrease in the $(P_{D1}P_{D2}Chl_{D1})^* \leftrightarrow P_{D2}^{+}P_{D1}^{-}$ mixing which reduces the Stark amplitude of the 673.25 nm Stark minima (the $(P_{D1}P_{D2}Chl_{D1})^*$ exciton has less CT character). In turn, the decrease of the mixing reduces the transition dipole moment of the red-most $P_{D2}^{+}P_{D1}^{-}$ CT state. Therefore, the decrease of the (red) contribution of $P_{D2}^{+}P_{D1}^{-}$ CT state to the Stark spectra appears as a blue shift of the red Stark minimum. The fact that the decrease in Stark amplitude is the same in both P_{D1} and P_{D2} mutants is explained by considering that the P_{D1} and P_{D2} cofactors contribute equally to the $P_{D2}^{+}P_{D1}^{-}$ CT state. In the case of the 673.25 nm minimum the mutation effect is more pronounced for the P_{D1} mutants because the contribution of the P_{D1} cofactor is larger than the contribution of P_{D2}. In the D_1-Thr179His mutant, the absorption red shift of the exciton with participation of Chl_{D1} produces a substantial amplitude decrease (1/10 of the value for WT) and red shift (3.25 nm with respect to WT) of the red Stark minimum. These observations could be interpreted as a decrease of the Chl_{D1} exciton-CT mixing due to the red shift of the Chl_{D1} exciton absorption. However, the fact that two exciton-CT states contribute to the red Stark minimum and the comparison of the D_1-Thr179His Stark spectra with the 2DAbs indicate that the situation is more complex. This comparison shows that the 677.75 nm minimum in the 2DAbs is almost completely absent in the Stark spectrum and that the 684 nm minimum in the 2DAbs overlaps with the Stark minimum (Figure 5). These observations indicate that i) the red shift of the Chl_{D1} exciton absorption in the mutant disrupts the mixing with a CT state present in WT (as suggested by the absence of the 677.75 nm Stark minimum) and ii) the 684 nm minimum corresponds to the Stark contribution of the $(P_{D2}^{+}P_{D1}^{-})^{\delta *}$ CT state (in agreement with the interpretation of the RCs Stark spectra). The fact that the 684 nm Stark minimum has the same amplitude as the 2DAbs (and not higher as expected for a CT state) suggests that the mutation in the environment of Chl_{D1} also affects the electronic properties of the $(P_{D2}^{+}P_{D1}^{-})^{\delta *}$ CT state.

Therefore, combining all results we propose that the Stark minimum at 681.75 nm in WT arises from the combination of two different states. On the one hand, the $(Chl_{D1}^{\delta+}Phe_{D1}^{\delta-})^*$ state (produced by the mixing of the $(Chl_{D1}Phe_{D1})^*$ exciton with the $Chl_{D1}^{+}Phe_{D1}^{-}$ CT state) contributes to the blue edge of the 681.75 nm Stark minimum (≈ 681 nm). On the other hand, the $(P_{D2}^{+}P_{D1}^{-})^{\delta*}$ state (formed by the mixing of the $P_{D2}^{+}P_{D1}^{-}$ CT state with the $(P_{D1}P_{D2}Chl_{D1})^*$ exciton) contributes to the red edge of the 681.75 nm Stark minimum (≈ 684 nm). Thus, we conclude that the $(Chl_{D1}^{\delta+}Phe_{D1}^{\delta-})^*$ state leads to charge separation via the Chl_{D1} path (*11*), whenever this exciton is the lowest energy state of the reaction center. In addition, direct excitation of the $(P_{D2}^{+}P_{D1}^{-})^{\delta*}$ state leads to charge separation via the P_{D1} path (*10*).

In summary, we conclude that the electronic states initiating charge separation are mixed exciton-CT states, not pure exciton states. This finding leads to the refined charge separation schemes:

P_{D1} path: $(P_{D1}^{\delta-}P_{D2}^{\delta+}Chl_{D1})^*_{673nm} \rightarrow P_{D2}^{+}P_{D1}^{-} \rightarrow P_{D1}^{+}Chl_{D1}^{-} \rightarrow P_{D1}^{+}Phe_{D1}^{-}$

Chl_{D1} path: $(Chl_{D1}^{\delta+}Phe_{D1}^{\delta-})^*_{681nm} \rightarrow Chl_{D1}^{+}Phe_{D1}^{-} \rightarrow P_{D1}^{+}Phe_{D1}^{-}$

P_{D1} path: $(P_{D2}^{+}P_{D1}^{-})^{\delta*}_{684nm} \rightarrow P_{D2}^{+}P_{D1}^{-} \rightarrow P_{D1}^{+}Chl_{D1}^{-} \rightarrow P_{D1}^{+}Phe_{D1}^{-}$

where the subscripts indicate the approximate center wavelength of the electronic transition for each mixed state.

This conclusion is in excellent agreement with the results from a high resolution fluorescence spectroscopy (fluorescence line-narrowing, FLN) study (*42*). The authors of that paper studied the electronically excited state of PSII RC with FLN spectroscopy at 5 K and compared the obtained spectral features with those obtained earlier for the primary electron donor (*43*). Their results show that there is a striking resemblance between the emitting and charge separating states, such as a very similar shape of the phonon wing, almost identical frequencies of a number of vibrational modes, a very similar double-Gaussian shape of the inhomogeneous distribution function, and relatively strong electron-phonon coupling for both states. All these observations are explained by the fact that the excited states which give rise to charge separation in the PSII RC are mixed exciton-CT states, for instance, strong electron-phonon coupling is expected for states with CT character.

It is also interesting to note that the best numerical simulation of the absorption, nonselectively and selectively excited emission spectra was obtained with an inhomogeneous distribution function consisting of two Gaussians, one peaking at 680.6 nm (width 80 cm^{-1}, relative area 0.91) and the other at 683.6 nm (width 70 cm^{-1}, fwhm) (*42*).

These values are in agreement with the properties and center wavelengths for the $(Chl_{D1}{}^{\delta+}Phe_{D1}{}^{\delta-})^*_{681nm}$ and $(P_{D2}{}^{+}P_{D1}{}^{-})^{\delta*}_{684nm}$ states, respectively, found in the present study. The state simulated by a Gaussian band centered at 680.6 nm corresponds to the mixed exciton-CT $(Chl_{D1}{}^{\delta+}Phe_{D1}{}^{\delta-})^*_{681nm}$ state which carries most of the oscillator strength due to its major exciton character. The state simulated by a Gaussian band centered at 683.6 nm corresponds to the mixed CT-exciton $(P_{D2}{}^{+}P_{D1}{}^{-})^{\delta*}_{684nm}$ state with lower oscillator strength due to its minor exciton character (acquired by borrowing oscillator strength from the $(P_{D1}P_{D2}Chl_{D1})^*$ exciton state).

The Pheophytin Q_X absorption band

Absorption and Stark. The Phe Q_X absorption band (Figure 6) at 540.4 nm in WT is an excellent reporter of the energetic changes induced upon mutation because, despite its low amplitude, it is spectrally isolated from contributions from other cofactors in the reaction center.

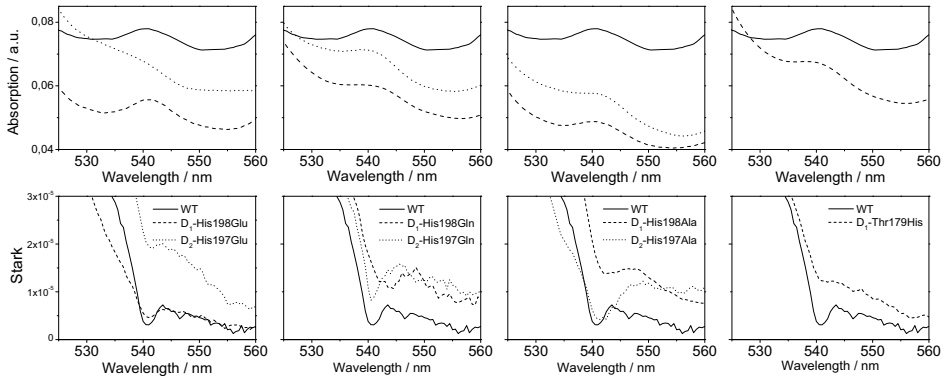

Figure 6. Simultaneously recorded 77 K absorption (*upper panels*) and Stark spectra (*lower panels*) of *Synechocystis* core complex in the Pheophytin Q_X absorption region for (*from left to right*): WT, D_1-His198Gln and D_2-His197Gln mutants; WT, D_1-His198Asn and D_2-His197Asn mutants; WT, D_1-His198Ala and D_2-His197Ala mutants; and WT and D_1-Thr179His mutant. The absorption and Stark spectra are normalized to the integrated area of the absorption spectra in the 645 – 710 nm range. The Stark spectra were recorded at $\chi = 54.7^\circ$ and an external electric field strength of 2.25 x 10^5 V cm^{-1}.

The Stark effect for the Phe Q_X absorption band in the higher plant PSII RC preparation was shown to: i) arise from the Phe in the active branch, Phe_{D1}; ii) to be strong and dominated by the change in dipole moment, $\Delta\mu$ = 2 D; and iii) to display a classic Stark response (*16*).

In this work, for the *Syn*. core complexes, WT and mutants, the Stark effect on the Phe Q_X band (Figure 6) is also dominated by the $\Delta\mu$, i.e., the Stark spectrum resembles the second derivative of the absorption spectrum and, by analogy with the spinach reaction center, can be considered to arise from Phe_{D1}. However, in the *Syn*. core complex the amplitude of the Phe Stark signal is significantly reduced with respect to spinach. The mutations produce changes in the position, width and amplitude of the absorption maxima and Stark minima of the Phe_{D1} Q_X absorption band (Table 2). Only two mutants, D_1-His198Gln and D_2-His197Ala, display a classic Stark effect (no shift between Abs_{max} and $Stark_{min}$). Non-classic Stark effects are observed for WT and the rest of the mutants which can be divided in three groups: 0.4 nm red shift (WT), 1 nm red shift (D_2-His197Asn and D_1-Thr179His) and 1.6-1.7 nm red shift (D_1-His198Asn and D_1-His198Ala). For the D_2-His197Gln mutant the red shift is 0.6 nm although in this case the position of the absorption band is difficult to estimate due to spectral overlap with the absorption of carotenoid aggregates which, despite the purification procedure (see materials and methods), are present as a contamination.

Table 2. Pheophytin Q_X absorption band.

	λ / nm			fwhm / nm		amplitude / OD[a]	
	Abs_{max}	$Stark_{min}$	Shift	Abs	Stark	Abs	Stark
WT	540.4	540.8	+ 0.4	9.2	3.0	5	6.5
D_1-His198Gln	541.0	541.0	0.0	8.6	2.4	7	4.1
D_2-His197Gln	541.0	541.6	+ 0.6	—	1.6	—	2.3
D_1-His198Asn	541.8	543.5	+ 1.7	9.6	5.9	4	7.8
D_2-His197Asn	540.5	541.5	+ 1.0	8.8	3.7	5	11.7
D_1-His198Ala	540.9	542.5	+ 1.6	7.8	4.0	4	4.9
D_2-His197Ala	541.8	541.8	0.0	7.0	6.5	5	11.6
D_1-Thr179His	540.0	541.0	+ 1.0	8.2	2.8	4	2.0

[a]The amplitude units are: x 10^{-3} and x 10^{-6} for Abs and Stark, respectively.

The changes in position, width and amplitude of the Phe_{D1} Q_X band in the absorption and Stark spectra of all the mutants with respect to WT shows that the modification of the P_{D1}, P_{D2} and Chl_{D1} protein environment affects the electronic properties of Phe_{D1}.

This effect could be explained by i) excitonic interactions among these four cofactors and ii) secondary effects (the mutations, although being specific to a single residue, influence the energetics of the whole system, not only the energy of the exciton in which the mutated Chl participates). Although it is not straightforward to distinguish between the two explanations, results from previous work (*11, 23, 36*) and the proximity factor among the cofactors indicate that i) the effect on D_1-Thr179His is due to the strong excitonic coupling between Phe_{D1} and Chl_{D1} which gives rise to the $Chl_{D1}Phe_{D1}$ exciton state and ii) the mutations close to P_{D1} and P_{D2} produce secondary effects on the electronic properties of Phe_{D1}. Therefore, part of the 681.75 nm minimum in WT is due to the mixing of an exciton containing Chl_{D1} and Phe_{D1}, the $(Chl_{D1}Phe_{D1})^*$ exciton state, with the radical pair $Chl_{D1}^{+}Phe_{D1}^{-}$, i.e., the $(Chl_{D1}^{\delta+}Phe_{D1}^{\delta-})^*_{681nm}$ state.

CONCLUSIONS

The results demonstrate that the states which initiate charge separation are mixed exciton-CT or CT-exciton states, not pure exciton states as previously believed. The degree of mixing between exciton and CT states determines the quantum yield of radical pair formation and, therefore, the efficiency of charge separation (the higher the mixing, the higher the efficiency of charge separation). The identity of the exciton-CT states which initiate charge separation are $(P_{D1}^{\delta-}P_{D2}^{\delta+}Chl_{D1})^*_{673nm}$ and $(Chl_{D1}^{\delta+}Phe_{D1}^{\delta-})^*_{681nm}$ (the subscript indicates the approximate center wavelength of the electronic transition for each mixed state). Moreover, the CT state $P_{D2}^{+}P_{D1}^{-}$ acquires excited state character due to its mixing with and exciton producing the $(P_{D2}^{+}P_{D1}^{-})^{\delta*}_{684nm}$ CT-exciton state which is also able to initiate charge separation.

The results also show that the pigment-protein interactions fine-tune the energy of the exciton and CT states and hence the mixing between these states which ultimately controls the selection and efficiency of a specific charge separation pathway.

APPENDIX

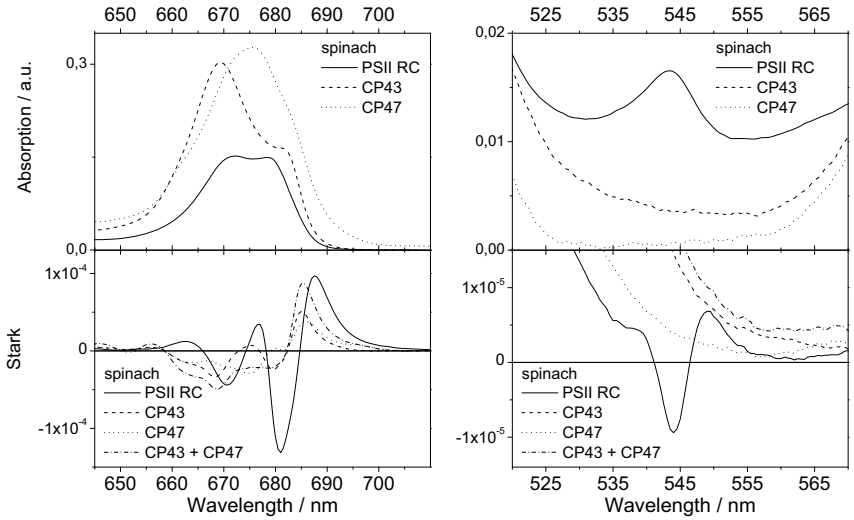

Figure A1. Simultaneously recorded 77 K absorption and Stark spectra of spinach PSII RC, CP43 and CP47 complexes. (*Left*) Q_Y absorption region, (*right*) Pheophytin Q_X absorption region. The absorption and Stark spectra are normalized to the integrated area of the absorption spectra in the 645 – 710 nm range. The absorption and Stark amplitudes can be directly compared with the *Syn*. amplitudes. The Stark spectra were recorded at $\chi = 54.7^{\circ}$ and an external electric field strength of 2.25×10^5 V cm^{-1}.

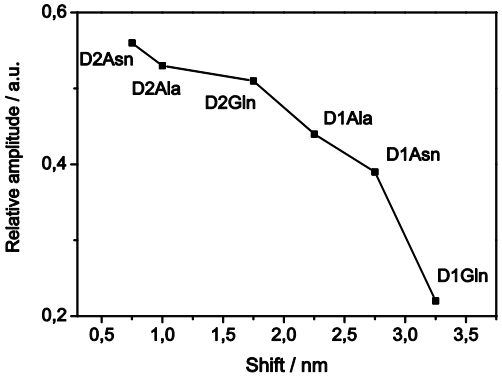

Figure A2. Relative amplitude of the blue Stark minimum (at 673.23 nm in WT) in the mutants with respect to the blue shift of the minimum position (with respect to WT).

REFERENCES

1. Zouni, A., Witt, H. T., Kern, J., Fromme, P., Krauss, N., Saenger, W., and Orth, P. (2001) Crystal structure of photosystem II from *Synechococcus elongatus* at 3.8 Å resolution, *Nature 409*, 739-743.
2. Ferreira, K. N., Iverson, T. M., Maghlaoui, K., Barber, J., and Iwata, S. (2004) Architecture of the photosynthetic oxygen-evolving center, *Nature 303*, 1831-1838.
3. Loll, B., Kern, J., Saenger, W., Zouni, A., and Biesiadka, J. (2005) Towards complete cofactor arrangement in the 3.0 Å resolution structure of photosystem II, *Nature 438*, 1040-1044.
4. Guskov, A., Kern, J., Gabdulkhakov, A., Broser, M., Zouni, A., and Saenger, W. (2009) Cyanobacterial photosystem II at 2.9-Å resolution and the role of quinones, lipids, channels and chloride, *Nat. Struct. Mol. Biol. 16*, 334-342.
5. Barter, L. M. C., Durrant, J. R., and Klug, D. R. (2003) A quantitative structure-function relationship for the photosystem II reaction center: supramolecular behavior in natural photosynthesis, *Proc. Natl. Acad. Sci. U.S.A. 100*, 946-951.
6. Durrant, J. R., Klug, D. R., Kwa, S. L. S., van Grondelle, R., Porter, G., and Dekker, J. P. (1995) A multimer model for P680, the primary electron donor of photosystem II, *Proc. Natl. Acad. Sci. U.S.A. 92*, 4798-4802.
7. van Brederode, M. E., and van Grondelle, R. (1999) New and unexpected routes for ultrafast electron transfer in photosynthetic reaction centers, *FEBS Lett. 455*, 1-7.
8. van Brederode, M. E., van Mourik, F., van Stokkum, I. H. M., Jones, M. R., and van Grondelle, R. (1999) Multiple pathways for ultrafast transduction of light energy in the photosynthetic reaction center of *Rhodobacter sphaeroides*, *Proc. Natl. Acad. Sci. U.S.A. 96*, 2054-2059.
9. Novoderezhkin, V. I., Andrizhiyevskaya, E. G., Dekker, J. P., and van Grondelle, R. (2005) Pathways and timescales of primary charge separation in the Photosystem II reaction center as revealed by simultaneous fit of time-resolved fluorescence and transient absorption, *Biophys. J. 89*, 1464-1481.
10. Novoderezhkin, V. I., Dekker, J. P., and van Grondelle, R. (2007) Mixing of exciton and charge transfer states in Photosystem II reaction centers: Modeling of Stark spectra with Modified Redfield Theory, *Biophys. J. 93*.
11. Romero, E., van Stokkum, I. H. M., Novoderezhkin, V. I., Dekker, J. P., and van Grondelle, R. (2010) Two different charge separation pathways in photosystem II, *Biochemistry 49*, 4300-4307.

12. Novoderezhkin, V., Romero, E., Dekker, J. P., and van Grondelle, R. (2011) Multiple charge separation pathways in photosystem II: modeling of the transient absorption kinetics, *Chem. Phys. Chem.* DOI: 10.1002/cphc.201000830

13. Boxer, S. G. (1996) Stark spectroscopy of photosynthetic systems, In *Biophysical Techniques in Photosysnthesis* (Hoff, J. A. a. A. J., Ed.), pp 177-189, Kluwer Academic Publishers.

14. Bublitz, G. U., and Boxer, S. G. (1997) Stark spectroscopy: applications in chemistry, biology, and material science, *Annu. Rev. Phys. Chem. 48*, 213-242.

15. Liptay, W. (1974) In *Excited states* (Lim, E., Ed.), pp 129-229, Academic Press, New York.

16. Frese, R. N., Germano, M., de Weerd, F. L., van Stokkum, I. H. M., Shkuropatov, A. Y., Shuvalov, V. A., van Gorkom, H. J., van Grondelle, R., and Dekker, J. P. (2003) Electric field effects on the chlorophylls, pheophytins, and *b*-carotenes in the reaction center of photosystem II, *Biochemistry 42*, 9205-9213.

17. Giorgi, L. B., Nixon, P. J., Merry, S. A. P., Joseph, M., Durrant, J. R., De Las Rivas, J., Barber, J., Porter, G., and Klug, D. R. (1996) Comparison of primary charge separation in the photosystem II reaction center complex isolated from wild-type and D1-130 mutants of the cyanobacterium *Synechocystis* PCC 6803, *J. Biol. Chem. 271*, 2093-2101.

18. Merry, S. A. P., Nixon, P. J., Barter, L. M. C., Schilstra, M., Porter, G., Barber, J., Durrant, J. R., and Klug, D. R. (1998) Modulation of quantum yield of primary radical pair formation in Photosystem II by site-directed mutagenesis affecting radical cations and anions, *Biochemistry 37*, 17439-17447.

19. Stewart, D. H., Nixon, P. J., Diner, B. A., and Brudvig, G. W. (2000) Assigment of the Q_y absorption bands of Photosystem II chromophores by low-temperature optical spectroscopy of wild-type and mutant reaction centers, *Biochemistry 39*, 14583-14594.

20. Diner, B. A., Schlodder, E., Nixon, P. J., Coleman, W. J., Rappaport, F., Lavergne, J., Vermaas, W. F. J., and Chisholm, D. A. (2001) Site-directed mutations at D_1-His198 and D_2-His197 of photosystem II in *Synechocystis* PCC 6803: Sites of primary charge separation and cation triplet stabilization, *Biochemistry 40*, 9265-9281.

21. Moore, L. J., Zhou, H., and Boxer, S. G. (1999) Excited-state electronic asymmetry of the special pair in photosynthetic reaction center mutants: absorption and Stark spectroscopy, *Biochemistry 38*, 11949-11960.

22. Shibuya, Y., Takahashi, R., Okubo, T., Suzuki, H., Sugiura, M., and Noguchi, T. (2010) Hydrogen bond interactions of the pheophytin electron acceptor and its radical anion in photosystem II as revealed by Fourier transform infrared difference spectroscopy, *Biochemistry 49*, 493-501.

23. Schlodder, E., Renger, T., Raszewski, G., Coleman, W. J., Nixon, P. J., Cohen, R. O., and Diner, B. A. (2008) Site-directed mutations at D1-Thr179 of photosystem II in *Synechocystis* sp. PCC 6803 modify the spectroscopic properties of the accessory chlorophyll in the D1-branch of the reaction center, *Biochemistry 47*, 3143-3154.

24. Stowell, M. H. B., McPhillips, T. M., Rees, D. C., Soltis, S. M., Abresch, E., and Feher, G. (1997) Light-induced structural changes in photosynthetic reaction center: implications for mechanism of electron-proton transfer, *Science 276*, 812-816.

25. Di Donato, M., Cohen, R. O., Diner, B. A., Breton, J., van Grondelle, R., and Groot, M. L. (2008) Primary charge separation in the photosystem II core from *Synechocystis*: A comparison of femtosecond visible/midinfrared pump-probe spectra of Wild-type and two P680 mutants, *Biophys. J. 94*, 4783-4795.

26. Groot, M.-L., Pawlowicz, N. P., van Wilderen, L. J. G. W., Breton, J., van Stokkum, I. H. M., and van Grondelle, R. (2005) Initial electron donor and acceptor in isolated photosystem II reaction centers identified with femtosecond mid-IR spectroscopy, *Proc. Natl. Acad. Sci. U.S.A. 102*, 13087-13092.

27. Holzwarth, A. R., Müller, M. G., Reus, M., Nowaczyk, M., Sander, J., and Rögner, M. (2006) Kinetics and mechanism of electron transfer in intact photosystem II and in the isolated reaction center: Pheophytin is the primary electron acceptor, *Proc. Natl. Acad. Sci. U.S.A. 103*, 6895-6900.

28. Raszewski, G., Saenger, W., and Renger, T. (2005) Theory of optical spectra of Photosystem II reaction centers: Location of the triplet state and the identity of the primary electron donor, *Biophys. J. 88*, 986-998.

29. Schlodder, E., Coleman, W. J., Nixon, P. J., Cohen, R. O., Renger, T., and Diner, B. A. (2007) Site-directed mutations at D_1-His198 and D_1-Thr179 of Photosystem II in *Synechocystis* PCC 6803: deciphering the spectral properties of the PSII reaction center, *Philos. T. R. Soc. B Published online*.

30. Kwa, S. L. S., Newell, W. R., van Grondelle, R., and Dekker, J. P. (1992) The reaction center of photosystem II studied with polarized fluorescence spectroscopy, *Biochim. Biophys. Acta 1099*, 193-202.

31. Beekman, L. M. P., Steffen, M., van Stokkum, I. H. M., Olsen, J. D., Hunter, C. N., Boxer, S. G., and van Grondelle, R. (1997) Characterization of the light-harvesting antennas of photosynthetic purple bacteria by Stark spectroscopy. 1. LH1 antenna complex and the B820 subunit from *Rhodospirillum rubrum*, *J. Phys. Chem. B 101*, 7284-7292.

32. Frese, R. N., Palacios, M. A., Azzizi, A., van Stokkum, I. H. M., Kruip, J., Rögner, M., Karapetyan, N. V., Schlodder, E., van Grondelle, R., and Dekker, J. P. (2002) Electric field effects on red chlorophylls, *b*-carotenes and P700 in cyanobacterial photosystem I complexes, *Biochim. Biophys. Acta 1554*, 180-191.

33. Lösche, M., Feher, G., and Okamura, M. Y. (1987) The Stark effect in reaction centers from *Rhodobacter sphaeroides* R-26 and *Rhodopseudomonas viridis*, *Proc. Natl. Acad. Sci. U.S.A. 84*, 7537-7541.

34. Lockhart, D. J., and Boxer, S. G. (1988) Stark effect spectroscopy of *Rhodobacter sphaeroides* and *Rhodopseudomonas viridis* reaction centers, *Proc. Natl. Acad. Sci. U.S.A. 85*, 107-111.

35. Middendorf, T. R., Mazzola, L., Lao, K., Steffen, M. A., and Boxer, S. G. (1993) Stark effect (electroabsorption) spectroscopy of photosynthetic reaction centers at 1.5 K: evidence that the special pair has a large excited-state polarizability, *Biochim. Biophys. Acta 1143*, 223-234.

36. Raszewski, G., Diner, B. A., Schlodder, E., and Renger, T. (2008) Spectroscopic properties of reaction center pigments in Photosystem II core complexes: Revision of the multimer model, *Biophys. J. 95*, 105-119.

37. Dekker, J. P., and van Grondelle, R. (2000) Primary charge separation in photosystem II, *Photosynth. Res. 63*, 195-208.

38. Nanba, O., and Satoh, K. (1987) Isolation of a photosystem II reaction center consisting of D-1 and D-2 polypeptides and cytochrome b-559, *Proc. Natl. Acad. Sci. U.S.A. 84*, 109-112.

39. Dekker, J. P., Bowlby, N. R., and Yocum, C. F. (1989) Chlorophyll and cytochrome *b-559* content of the photochemical reaction center of photosystem II, *FEBS Lett. 254*, 150-154.

40. Groot, M. L., Peterman, E. J. G., van Stokkum, I. H. M., Dekker, J. P., and van Grondelle, R. (1995) Triplet and fluorescing states of the CP47 antenna complex of photosystem II studied as a function of temperature, *Biophys. J. 68*, 281-290.

41. Groot, M.-L., Frese, R. N., de Weerd, F. L., Bromek, K., Pettersson, A., Peterman, E. J. G., van Stokkum, I. H. M., van Grondelle, R., and Dekker, J. P. (1999) Spectroscopic properties of the CP43 core antenna protein of photosystem II, *Biophys. J. 77*, 3328-3340.

42. Peterman, E. J. G., van Amerongen, H., van Grondelle, R., and Dekker, J. P. (1998) The nature of the excited state of the reaction center of photosystem II of green plants: A high-resolution fluorescence spectroscopy study, *Proc. Natl. Acad. Sci. U.S.A. 95*, 6128-6133.

43. Kwa, S. L. S., Eijckelhoff, C., van Grondelle, R., and Dekker, J. P. (1994) Site-selection spectroscopy of the reaction center complex of Photosystem II. 1. Triplet-minus-singlet absorption difference: Search for a second exciton band of P-680, *J. Phys. Chem. 98*, 7702-7711.

CHAPTER 6

Pigment-Protein Interactions for the Sites of Cation (P_{680}) and Anion (Phe_{D1}) Localization in the Photosystem II Reaction Center Studied by Light-Induced Fourier Transform Infrared (FTIR) Difference Spectroscopy

Elisabet Romero, Mariangela Di Donato, Peter J. Nixon, Jan P. Dekker and Jacques Breton

Light-induced Fourier transform infrared (FTIR) difference spectroscopy has been applied to a series of photosystem II (PSII) preparations. The pigment-protein interactions in the neutral and ionic states for the sites of cation (P_{680}) and anion (Phe_{D1}) localization in the PSII reaction center complex (PSII RC) have been investigated. Firstly, we discriminate between pigment and protein vibrational bands in the light-induced P_{680}^{+}/P_{680} and Phe_{D1}^{-}/Phe_{D1} FTIR difference spectra by i) comparing these spectra for standard and globally labelled samples with ^{15}N isotops and by ii) comparing the experimentally observed band shifts upon isotopic labelling with the expected vibrational shifts for chlorophyll *a* and pheophytin *a* in vacuum upon isotopic exchange (in the neutral and ionic states) calculated at density functional theory (DFT) level. Secondly, we compare the light-induced P_{680}^{+}/P_{680} FTIR difference spectra for PSII preparations with variable antenna size (BBY membranes, core and RC complexes) in order to study the vibrational properties of P_{680} at different levels of *intactness* of the PSII preparation. Thirdly, we investigate the hydrogen bond network of Phe_{D1} in the neutral and reduced states by recording the light-induced Phe_{D1}^{-}/Phe_{D1} FTIR difference spectra for a series of site-directed mutants at position D_1-130. The results are discussed in terms of the roles that the pigment-protein interactions play in the energy dynamics of the PSII RC.

Manuscript in preparation

INTRODUCTION

Photosystem II (PSII) is a pigment-protein complex embedded in the thylakoid membrane of higher plants, algae and cyanobacteria. The PSII supercomplex contains several light-harvesting complexes (antennas) and the photochemically active reaction center (RC) (*1*). One of the main functions of the antenna complexes is to absorb light energy and transfer the excitation energy to the RC, where charge separation takes place (*2*). The charge separation process results in highly oxidative species able to drive water splitting to molecular oxygen. The electrochemical gradient created across the membrane ultimately powers the photosynthetic organism.

The isolated PSII RC contains six chlorophylls *a* (Chl), two pheophytins *a* (Phe), and two *β*-carotene molecules. Four Chls (P_{D1}, P_{D2}, Chl_{D1} and Chl_{D2}) and two Phes (Phe_{D1} and Phe_{D2}) are arranged in two symmetric branches (D_1 and D_2) in the center of the complex. Two additional Chls (Chl_{ZD1} and Chl_{ZD2}) are situated at opposing sides in the periphery of the complex. The two *β*-carotene molecules (Car_{D1} and Car_{D2}) are located between $Chls_Z$ and the center of the complex (*3-5*). It has been established that only the D_1 branch is active in charge separation (*6*).

The investigation of the charge separation mechanisms has lead to an extensive debate in the literature due to the spectral complexity and congestion in PSII. The dynamics of energy transfer and charge separation in PSII have been studied by several groups with several spectroscopic techniques in both the isolated PSII RC (*7-20*) and the more intact PSII core complex containing the RC complex and the antennas CP43 and CP47 (*19, 21-23*). Theoretical models aimed to describe the experimental data have also been developed (*24-28*). In the isolated PSII RC, it is accepted that the final charge separated state is the $P_{680}^{+}Phe_{D1}^{-}$ radical pair. Therefore, the sites of cation and anion localization are P_{680} and Phe_{D1}, respectively.

In the recent years, the functional role of the protein matrix in the charge separation dynamics has been investigated by several research groups. In the PSII RC of higher plants the disorder induced by the slow protein motions creates a distribution of energetically different RC complexes leading to two different pathways of charge separation. The selection of a specific charge separation pathway depends on protein conformation (*20*). For the main light-harvesting complex of higher plants, LHCII, a disordered exciton-Redfield model explains most of the experimentally observed fluorescence spectral shifts in single complexes. The largest spectral shifts could be due to special protein conformations (*29*). For the bacterial reaction center the role of the protein matrix in controlling the kinetics of initial electron transfer has been

demonstrated (*30*). In the photsystem I complex of cyanobacteria protein dynamics have been shown to induce variation of energy transfer pathways (*31*).

The study of the pigment-protein interactions in the PSII RC is crucial for the understanding of the charge separation mechanisms. Light-induced Fourier transform infrared (FTIR) difference spectroscopy allows the observation of the specific vibrations of the pigments involved in charge separation as well as their interactions with the protein matrix (*32*). The high extinction coefficient of the carbonyl groups (C=O) in the IR 1800-1600 cm^{-1} absorption region together with the known sensitivity of these modes to hydrogen-bonding effects (*33, 34*) provides a sensitive means of studying pigment-protein interactions. A series of illumination cycles (dark-light-dark) in combination with specific redox conditions allows the reversible photoaccumulation of the final PSII RC charge separation states P_{680}^{+} or Phe_{D1}^{-}. The calculation of the light-minus-dark spectrum yields a highly structured light-induced FTIR difference spectrum which shows all molecular changes associated with the formation of the cation (P_{680}^{+}) or anion (Phe_{D1}^{-}). Hence, the spectrum is virtually free from contributions from the background absorption. The spectrum contains the specific vibrations of the pigments under study (P_{680}^{+}/P_{680} or Phe_{D1}^{-}/Phe_{D1}) as well as the protein response associated to the formation of P_{680}^{+} or Phe_{D1}^{-}. Therefore, in the light-induced FTIR difference spectrum the negative bands correspond to vibrational modes of the protein and the pigment in the neutral state which change due to the light-induced reaction. The positive bands correspond to protein and pigment vibrations related to the formation of the cation (P_{680}^{+}) or anion (Phe_{D1}^{-}).

However, it is not straightforward to completely extract and interpret all the information contained in a light-induced FTIR difference spectrum. The first step in the interpretation of the FTIR spectrum is the assignment of vibrational bands to specific modes of the pigment or the protein. One of the strategies for an empirical assignment consists on isotope labelling of particular atoms and comparison of the observed with calculated frequency shifts. In this work, in order to distinguish between pigment and protein modes, altered upon P_{680}^{+} or Phe_{D1}^{-} formation, we compare the light-induced (P_{680}^{+}/P_{680} or Phe_{D1}^{-}/Phe_{D1}) FTIR difference spectra of unlabelled (^{14}N) PSII RC complexes with globally labelled ^{15}N preparations. The ^{15}N labelling is uniform, all nitrogen atoms from both pigments and protein in the PSII RC are isotopically exchanged. Due to the larger mass of the ^{15}N isotope with respect to ^{14}N, the frequency (ν) of the modes involving the N atom will downshift in the ^{15}N preparations according to $\nu = 1/2\pi\,(F/\mu)^{1/2}$ (where F is the force constant and μ is the reduced mass).

Regarding the protein modes, the amide I (C=O stretching coupled to C-N stretching, 1800-1590 cm^{-1}) and amide II (C-N stretching, N-H bending, ca. 1550 cm^{-1}) modes (*32*) are expected to downshift upon ^{15}N exchange by 1-3 cm^{-1} and by ≈15 cm^{-1}, respectively (*35*). Concerning the P_{680} and Phe_{D1} pigments, a theoretical estimation of the vibrational frequencies of isolated Chl and Phe molecules, both in the neutral and ionic states, has been carried out at DFT/6-31g level for both the ^{14}N and ^{15}N molecules. The discrimination between protein and pigment bands, by comparing the observed and calculated isotopic shifts, will facilitate the interpretation of the steady-state and time-resolved infrared data.

The site of cation localization, P_{680}, has an extremely high redox potential of 1100-1300 mV (*36-38*) which converts PSII in the unique molecular machinery able to oxidize water (for which a minimum redox potential of +820 mV is required (*39*)). Electrostatic energy computations (*37*) indicate that the enormous upshift of the redox potential of P_{680} with respect to that of a monomeric Chl *a* in solution (of +830 mV) (*40*) is mainly due to the D_1-D_2 protein environment, i.e., the P_{680} protein binding pocket.

The light-induced P_{680}^+/P_{680} FTIR difference spectrum has already been obtained since quite long time in different laboratories (*41-45*). However, a definitive assignment of all the bands pertaining to P_{680}^+ which leads to the identification of the site of cation localization in one or more Chls is still missing. In particular there is no precise assignment for the 13^1-keto carbonyl bands of the two P_{D1} and P_{D2} pigments which may form P_{680}^+, which would be of considerable interest, considered that the amount of up-shift observed for these bands upon oxidation can give an indication about the amount of localization of the positive charge between the two halfs of P_{680}^+.

A detailed investigation on the vibronic properties of P_{680} in different preparations as PSII–enriched membranes (BBY) from spinach, PSII core from cyanobacteria and RC from spinach based on the analysis of light-induced P_{680}^+/P_{680} FTIR difference spectra has been reported (*45*). The results of this study suggest that the vibronic properties of P_{680}^+ are altered in isolated RC preparations when compared with more intact native preparations as membranes or cores. According to these authors the positive charge on P_{680}^+ is delocalized over P_{D1} and P_{D2} in the RC complexes, while it is mostly localized on one Chl (70-80 %) in the more intact preparations. This finding would imply that the presence of the primary electron acceptor Q_A or antennas and other proteins which are contained in core or membrane preparations, but not in the isolated RC preparation affect the redox potential of P_{680}, and are, at least in part, responsible of its ability to oxidize water.

Here we have re-examined this issue, and tried to move a further step towards the precise assignment of vibrational bands in the light-induced P_{680}^{+}/P_{680} FTIR difference spectrum.

For the site of anion localization, Phe_{D1}, we have studied the effect of site-directed mutation at position D_1-130 on the RC from cyanobacteria to describe the pigment-protein interactions in comparison with the wild-type (WT). The residue in position D_1-130 has been proposed to be hydrogen bonded to the 13^1-keto carbonyl of Phe_{D1} in RCs from higher plants (*46*) and cyanobacteria (*47*). The interactions with the protein environment of the 13^1-keto carbonyl of $Phe_{D1,}$ which is conjugated with the π-electron system of the macrocycle, has been shown to determine the quantum yield of radical pair formation (*48*) and, therefore, the efficiency of charge separation. The comparison of the light-induced Phe_{D1}^{-}/Phe_{D1} FTIR difference spectra of a cyanobacterial RCs WT and site-directed mutants with a higher plant RC allows the description of the pigment-protein interactions in both organisms, as well as the differences between them.

In this study, we aim to describe the pigment-protein interactions for the site of cation (P_{680}^{+}) and anion (Phe_{D1}^{-}) localization in PSII by light-induced FTIR difference spectroscopy. For the site of cation (P_{680}^{+}) localization a comparative study of different PSII preparations with variable antenna size is reported. For the site of anion (Phe_{D1}^{-}) localization a comparative study of WT and site-directed mutants is presented. The results are discussed in terms of the roles that the pigment-protein interactions play in the energy dynamics of the PSII RC.

MATERIALS AND METHODS

Sample preparation. BBY membranes were prepared as described elsewhere (*49, 50*) and were depleted of Q_A by treatment with 100 mM sodium dithionite and 30 μM benzyl violagen followed by dark incubation at 0 ^{0}C for ≈5 hours under Ar gas flow (*51*). PSII cores from spinach and from *Synechocystis* sp. PCC 6803 were prepared as described elsewhere (*6, 50*). Q_A-depleted BBY membranes from spinach were suspended in a BisTris buffer at pH 6.0 containing 50 mM BisTris, 20 mM $MgCl_2$, 5 mM $CaCl_2$, 10 mM $MgSO_4$, 0.4 M sucrose in the presence of 100 μl of 1 M potassium ferricyanide solution and centrifuged for 10 minutes at 120000 g. The resultant pellet was squeezed between two CaF_2 plates. PSII core samples from spinach were suspended in a Tris buffer at pH 6.5 containing 20 mM Tris and 0.06 % *β*-DM. An aliquot of 30 μl of this sample was mixed with 5 μl of 50 mM SiMo, loaded on a CaF_2 plate and slightly dried under N_2 gas flow before being covered with a second CaF_2 plate. PSII core form *Synechocystis* sp. PCC 6803 was suspended in a MES buffer at pH 6.0 containing 50 mM MES, 20 mM $CaCl_2$, 5 mM $MgCl_2$ and 0.03% *β*-DM in D_2O. An aliquot of 10 μl of this sample was mixed with 5 μl of 50 mM SiMo solution and loaded on a CaF_2 plate. The sample was partially dried under N_2 gas flow before being covered with a second plate. PSII RC samples were prepared from spinach as described in (*52*) and were suspended in a BisTris buffer at pH 6.5 containing 20 mM BisTris and 0.06 % *β*-DM. PSII RC samples were isolated from *Synechocystis* sp. PCC 6803 as described in (*48*) and were suspended in a BisTris buffer at pH 6.5 containing 20 mM BisTris and 0.06 % *β*-DM. The samples for the light-induced P_{680}^+/P_{680} FTIR difference spectra were prepared in two different ways. In one case 10 μl of sample were mixed with 5 μl of SiMo 50 mM, while in the other case 10 μl of RC were mixed with 1 μl of 500 mM potassium ferrycianide solution and 0.12 μl of 50 mM SiMo solution before being slightly dried under N_2 gas flow and loaded between two CaF_2 plates. The temperature was set to 250 K for BBY membranes and PSII core form *Synechocystis* and 230 K for spinach core and RC. The light-induced Phe_{D1}^-/Phe_{D1} FTIR difference spectra were recorded for both ^{14}N and ^{15}N spinach RC samples in the presence of a reducing reagent (100 mM DTT and 20 mM TMPD) at 260 K. An aliquot of 8 μl of RC sample was mixed with 5 μl of reducing reagent and partially dried under Ar gas flow.

Light-induced FTIR difference spectroscopy. FTIR difference spectra were recorded on a Nicolet 60SX and Magna 860 spectrophotometer equipped with a MCT detector and a N_2 gas flow cryostat. Difference spectra were calculated from data sets consisting of ≈90000 interferograms recorded before and after continuous red light illumination (630 nm). The spectral resolution was 4 cm^{-1}.

RESULTS AND DISCUSSION

Quantum chemical calculations: *Chl and Phe band shifts upon global ^{15}N isotope labelling*

Geometry optimization and frequency calculations for chlorophyll *a* (Chl *a*) and pheophytin *a* (Phe *a*) for both the standard ^{14}N and the ^{15}N molecules in the neutral and ionic states were carried out at DFT level, using the B3LYP hybrid exchange correlation potential (*53-56*) and the standard 6-31g basis set. Calculations were executed with the Gaussian 98 software package (*57*).

Table 1 and 2 show the more intense calculated vibrational modes (with assignment for C=O modes) for Chl *a* and Chl a^+ and for Phe *a* and Phe a^-, respectively, both with ^{14}N and ^{15}N isotope substitution. In all cases both the 13^1-keto carbonyl bands and the 13^2-ester bands are quite localized modes, except for Phe a^-, where the ester mode is mixed with ring modes. In both cases, Chl and Phe, the calculations indicate that the 13^1-keto frequency is higher than the 13^2-ester frequency, while both the experimental assignments (*46*) and more precise calculations (*47*) show that their trend is the opposite. This is probably due to the not extensive basis set used here and the lack of diffuse and polarization functions, which are important in particular to describe charged states. A precise calculation of vibrational frequencies is behind the scope of this work, where calculations are only performed to give an indication of the isotope effect on the modes of the chromophores. In this regard, our results show that only vibrational modes involving nitrogen atoms are affected by the isotopic substitution, while both the 13^1-keto carbonyl bands and the 13^2-ester bands, which are quite localized modes, are not shifted, and that the most affected modes are at frequencies lower than 1100 cm^{-1}, in a region of minor interest for the spectral analysis.

The calculated vibrational frequencies values for Chl and Phe in vacuum are upshifted with respect to the Chl and Phe vibrational frequencies in the PSII RC. In order to correct for this difference the calculated values have been multiplied by a constant factor of 0.966, which is a common practice for DFT calculations and does not affect the calculated isotope shift, since the calculation error is the same independently on which nitrogen isotope is used (*47*).

Table 1. DFT calculated vibrational modes (in cm^{-1}) for Chl *a* and Chl a^+ in vacuum with ^{14}N and ^{15}N isotope substitution (see text for details).

Chlorophyll			**Chlorophyll$^+$**		
N^{14}	N^{15}	shift	N^{14}	N^{15}	shift
1674 (13^1-keto)	1673	1	1688 (13^1-keto)	1688	0
1650 (13^2-ester)	1650	0	1646 (13^2-ester)	1646	0
1632	1632	0	1557	1556	1
1602	1602	0	1552	1551	1
1549	1549	0	1470	1470	0
1470	1470	0	1420	1417	3
1383	1381	2	1397	1394	3
1313	1309	4	1298	1294	4
1287	1285	2	1182	1180	2
1020	1009	11	981	974	7
1008	996	12	971	962	9
1001	987	14			
980	973	7			
977	969	8			

All frequencies have been scaled by 0.966

Table 2. DFT calculated vibrational modes (in cm^{-1}) for Phe *a* and Pheo a^- in vacuum with ^{14}N and ^{15}N isotope substitution (see text for details).

Pheophytin			**Pheophytin$^-$**		
N^{14}	N^{15}	shift	N^{14}	N^{15}	shift
1676 (13^1-keto)	1676	0	1638 (13^1-keto)	1637	1
1655 (13^2-ester)	1655	0	1629 (13^2-ester+ring)	1629	0
1549	1546	3	1624	1623	1
1543	1538	5	1577	1572	5
1477	1474	3	1486	1484	2
1379	1377	2	1435	1434	1
1293	1292	1	1353	1350	3
1214	1209	5	1318	1313	5
1148	1147	1	1123	1119	4
1058	1055	3	951	946	6
988	985	3	946	938	8
939	931	8			

All frequencies have been scaled by 0.966

Effect of ^{15}N isotope labelling on the FTIR absorption and light-induced FTIR difference spectra

The FTIR absorption of the standard (^{14}N) and the globally ^{15}N labeled spinach RC preparations for both the light-induced P_{680}^{+}/P_{680} and Phe_{D1}^{-}/Phe_{D1} FTIR difference experiments are shown in Figures 1 and 2, respectively. Upon ^{15}N exchange the amide I absorption band (C=O stretching coupled to C-N stretching), in the 1800-1590 cm^{-1} range, downshifts by 1 cm^{-1} due to the coupling with the C-N stretching mode, while the amide II band (N-H bending coupled to C-N stretching), in the 1580-1485 cm^{-1} range, downshifts by 14 cm^{-1}, as reported before (*35*).

In the light-induced FTIR difference spectra, the presence of band shifts upon isotopic exchange in the amide region, where no pigment frequency shifts are expected (as indicated by the DFT calculations, Table 1 and 2) indicates that the shifted bands correspond to protein vibrations (amide I and II).

Effect of ^{15}N isotope labelling on the light-induced P_{680}^{+}/P_{680} FTIR difference spectrum

Figure 1 shows the light-induced P_{680}^{+}/P_{680} FTIR difference spectra in the 1775-1200 cm^{-1} spectral range at 230 K of isolated PSII RC from spinach that were either unlabelled or globally labelled with ^{15}N isotopes. Similar spectra on the same unlabelled PSII RC preparations at 230 K have been previously reported (*41*). The vibrational shifts upon global ^{15}N isotopic labelling are best visualized by calculating the double-difference spectrum (^{14}N minus ^{15}N, Figure 1) after normalization of the spectra which produces the smallest peak-to-peak amplitude for all the bands.

1750 – 1650 cm^{-1} region. In this spectral region, where the C=O absorbs, both Chl and protein contributions are expected. According to the calculation (Table 1), no significant Chl shift upon isotopic labelling occurs in this region. The positive bands at 1724, 1710, 1667 cm^{-1} and the negative bands at 1702, 1680, 1652 cm^{-1} have been assigned to the 13^1-keto C=O vibration of P_{680} in the oxidized and neutral state, respectively (*41*). Only two of these bands, 1710(+) and 1702(-) cm^{-1}, are downshifted by 1 cm^{-1} upon ^{15}N exchange. These shifts appear clearly visible in the strong negative feature centred at 1705 cm^{-1} in the double-difference spectrum. The shifts for these P_{680} bands are due to the underlined changes due to the contribution of the amide I protein modes which also absorb in this range.

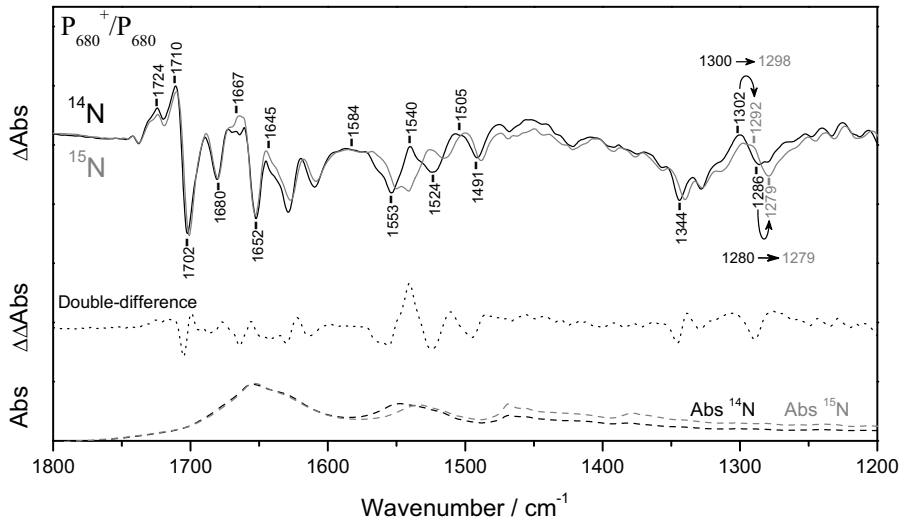

Figure 1. Light-induced P_{680}^{+}/P_{680} FTIR difference spectra of PSII RC from spinach at 230 K: unlabelled RC (*solid black line*) and ^{15}N labelled RC (*solid grey line*). Double-difference spectrum, unlabelled (^{14}N) minus ^{15}N labelled (*dotted line*). FTIR absorption spectra at 230 K: unlabelled RC (*dashed black line*) and ^{15}N labelled RC (*dashed grey line*). About 90000 interferograms were added. The band frequency is given in ± 1 cm^{-1}. The spectral resolution is 4 cm^{-1}.

In the 1675-1640 cm^{-1} range no shift is observed despite the intense amide I absorption indicating that the broad positive band centred at 1667 cm^{-1} and the narrow bands at 1652(-) and 1645(+) cm^{-1} correspond exclusively to P_{680}.

1650 – 1350 cm^{-1} region. From 1630 to 1600 cm^{-1} a ≈ 2 cm^{-1} shift is observed for both negative and positive bands indicating that these bands correspond to amide I protein vibrations which are influenced by the formation of P_{680}^{+}. In the 1580-1480 cm^{-1} range (amide II absorption region), shifts of up to 15 cm^{-1} are observed in agreement with the shift observed in the absorption spectra. These shifts also appear in the double-difference spectrum. The broad positive band centred around 1584 cm^{-1} is, in its lower energy side, downshifted by 6 cm^{-1}. The bands at 1563(-), 1553(-), 1540(+), 1524(-), 1505(+) and 1491(-) cm^{-1} are downshifted by 13, 12, 15, 8, 6 and 3 cm^{-1}, respectively, indicating that they correspond to protein amide II modes. From 1480 to 1390 cm^{-1} no shift is observed in the spectra. From 1480 to 1350 weak bands with no clear shifts are observed.

1350 –1200 cm^{-1} region. The negative band centred at 1344 cm^{-1} downshifts to 1340 cm^{-1} which appears as a differential signal, 1346(-)/1338(+) cm^{-1}, in the double-difference spectrum. No shift is expected for Chl in this region suggesting that these bands correspond to protein modes. The positive and negative signals in the 1310-1265 cm^{-1} range display a complex lineshape. For the unlabelled sample the positive band is a singlet (1300 cm^{-1}) and the negative band is a doublet (1286 and 1280 cm^{-1}). For the labelled sample the positive band is a doublet (1298 and 1292 cm^{-1}) and the negative band is a singlet (1279 cm^{-1}). The comparison of both spectra suggests, on the one hand, that for the unlabelled sample the high energy side of the positive singlet (around 1302 cm^{-1}) downshifts to 1292 cm^{-1} while the high energy negative band at 1286 cm^{-1} downshifts to 1279 cm^{-1} which corresponds to a 7-10 cm^{-1} shift for both bands upon isotopic labelling. On the other hand, for the unlabelled sample the positive band at 1300 cm^{-1} downshifts to 1298 cm^{-1} and the negative band at 1280 cm^{-1} downshifts to 1279 cm^{-1} which corresponds to a 1-2 cm^{-1} shift for both bands upon isotopic labelling. According to the DFT calculations (Table 1), the expected shifts for the Chl modes in this spectral range are 2-4 cm^{-1} which agrees with the shift observed for the positive and negative bands at 1300 and 1280 cm^{-1}, respectively. Therefore, we conclude that for the unlabelled sample, the high energy side of the positive and negative bands (around 1302 and 1286 cm^{-1}, respectively) correspond to protein modes while the low energy side of the positive and negative bands (at 1300 and 1280 cm^{-1}, respectively) correspond to Chl modes.

Effect of ^{15}N isotope labelling on the light-induced Phe_{D1}^{-}/Phe_{D1} FTIR difference spectrum

Figure 2 shows the light-induced Phe_{D1}^{-}/Phe_{D1} FTIR difference spectra in the 1750-1150 cm^{-1} spectral range at 230 K of isolated PSII reaction centers from spinach that were either unlabelled or globally labelled with ^{15}N isotopes, together with the double-difference spectrum (^{14}N minus ^{15}N). Similar spectra, measured at 240K on unlabeled PSII RC preparations, have been previously reported in the 1800-1350 cm^{-1} spectral range (*46*).

1750 – 1600 cm^{-1} region. In this spectral region, where the C=O absorbs, both Chl and protein contributions are expected. The two bands, negative at 1740 cm^{-1} and positive at 1730 cm^{-1} (1740(-)/1730(+)), are assigned to a free 13^2-ester C=O of Phe_{D1}, in the neutral and reduced state, respectively (see site-directed mutants section). None of these two bands shift upon isotopic exchange (Figure 2) which is in agreement with the DFT calculations for Phe_{D1} in the neutral and reduced states (Table 2).

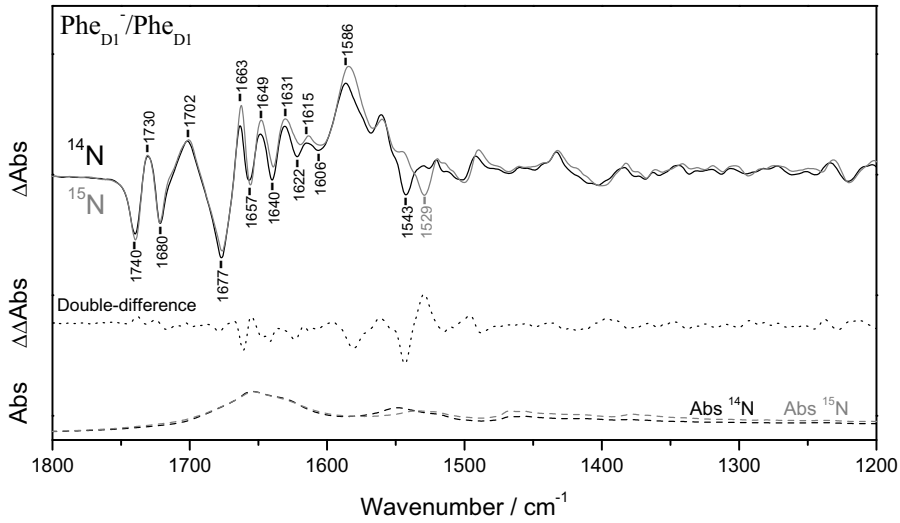

Figure 2. Light-induced Phe_{D1}^-/ Phe_{D1} FTIR difference spectra of PSII RC from spinach at 260 K: unlabelled RC (*solid black line*) and ^{15}N labelled RC (*solid grey line*). Double-difference spectrum, unlabelled (^{14}N) minus ^{15}N labelled (*dotted line*). FTIR absorption spectra at 230 K: unlabelled RC (*dashed black line*) and ^{15}N labelled RC (*dashed grey line)*. About 90000 interferograms were added. The band frequency is given in ± 1 cm^{-1}. The spectral resolution is 4 cm^{-1}.

The signals at 1722(-)/1702(+) cm^{-1} assigned to the hydrogen bonded 13^2-ester C=O vibration from Phe_{D1} in the neutral and reduced state, respectively (see site-directed mutants section) are not shifted upon ^{15}N labelling, in agreement with the DFT calculations (Table 2). For the intense bands at 1677(-)/1586(+) cm^{-1} assigned to the Phe_{D1} 13^1-keto C=O (*46, 47*), no shift is observed in the neutral state while a 2 cm^{-1} shift is observed in the reduced state. According to the DFT calculations and the distance between the 13^1-keto C=O and the closest nitrogen atom, the 13^1-keto C=O bands are not expected to shift upon isotope exchange. The observation of a 2 cm^{-1} shift in the reduced state indicates that in the 1600-1570 cm^{-1} region the amide I vibration of the protein backbone is also contributing. The bands in the amide I range at 1663(+), 1657(-), 1649(+), 1640(-) cm^{-1} are downshifted by 1 cm^{-1} while the bands at 1631(+), 1622(-), 1615(+), 1606(-) cm^{-1} are downshifted by 2 cm^{-1}. These shift values indicate that the differential signals in the 1670-1600 cm^{-1} range are associated mainly to amide I modes perturbed by Phe_{D1}^- formation.

1600 – 1150 cm^{-1} region. The larger shift is, as expected, observed in the amide II region. The bleach at 1543 cm^{-1} is downshifted by 14 cm^{-1} upon ^{15}N exchange as clearly visible in the double-difference spectra in the differential signal 1555(-)/1540(+) cm^{-1}. The weak bands in the 1500-1150 cm^{-1} region are downshifted by 2 – 5 cm^{-1}. These bands most likely represent ring modes of Phe_{D1}.

Comparison of the light-induced P_{680}^+/P_{680} FTIR difference spectra of PSII preparations with variable antenna size

Figure 3 shows the comparison of the light-induced P_{680}^+/P_{680} FTIR difference spectrum recorded for BBY membranes (at 250 K), PSII core and RC (at 230 K) from spinach. The P_{680}^+/P_{680} spectrum for the RC complex has been obtained in the presence of 50 mM SiMo. In contrast with what was reported in reference (*45*), we notice that all the three spectra are very similar, in particular the core and RC spectra are virtually identical. The differences noticed in the previously published spectra for the chlorophyll marker bands in the three preparations are strongly reduced in our spectra. For instance, in the previously reported FTIR spectra a positive signal at 1310 cm^{-1} due to P_{680}^+ in membranes and cores was shifted by 12 cm^{-1} in RC. In the spectra shown in Figure 3, the positive band at 1308 cm^{-1} in the membrane preparation is very broad. In the core spectra it begins to separate in two bands, at 1300 and 1312 cm^{-1}, while in the RC only the 1300 cm^{-1} band is clearly visible, and the 1312 cm^{-1} band is reduced to a shoulder. The most likely explanation for those changes is that this band corresponds not only to chromophore modes but also to protein modes. In this case, the differences observed in the spectra arise from differences in the protein content among the three PSII preparations. This explanation is supported by the ^{14}N *vs* ^{15}N data (Figure 1), indicating that the bands in the 1310-1265 cm^{-1} range correspond partly to a protein mode.

The most informative spectral region for understanding details on the vibronic structure of P_{680}^+ is the 1710-1680 cm^{-1} region where the 13^1-keto C=O groups of chlorophyll absorb. In all the three spectra reported in Figure 3 a strong negative band at 1701 cm^{-1} is observed which, in agreement with previous studies (*41, 43*), is assigned to the 13^1-keto C=O of P_{680} in the neutral state. It is possible that both the P_{D1} and P_{D2} 13^1-keto contribute to this band, meaning that they are located in a similar protein environment and free from hydrogen bonds. When charge separation occurs, and P_{680} is oxidized, the 13^1-keto C=O frequency upshifts, giving rise, in the spectra of all the three preparations, to a doublet positive signal at 1724 and 1710 cm^{-1}.

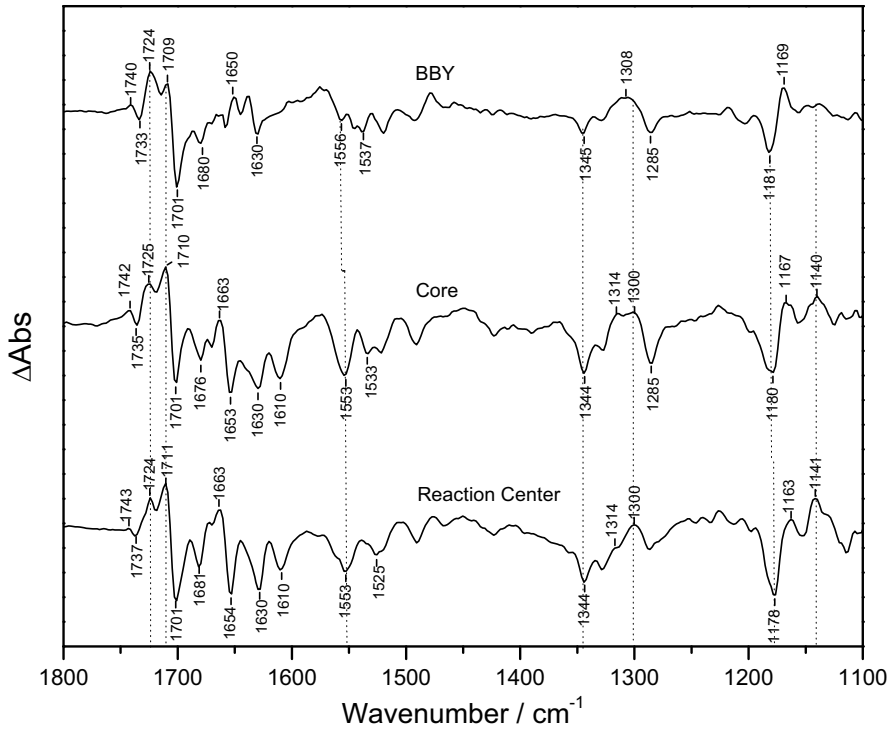

Figure 3. Light-induced P_{680}^{+}/P_{680} FTIR difference spectra of spinach PSII preparations with variable antenna size at 230 K: BBY membranes (*top line*), core (*middle line*) and RC (*bottom line*). The band frequency is given in ± 1 cm^{-1}. The spectral resolution is 4 cm^{-1}.

This observation contrasts what was reported in (*45*), where in the case of the RC preparation a single positive band at 1712 cm^{-1} was observed, suggesting that the positive charge distribution among the two chlorophylls (P_{D1} and P_{D2}) forming P_{680}^{+} is different in isolated reaction centers with respect to the more intact preparations.

Since the discrepancy between the spectra reported in Figure 3 and the previously published results could be due to the use of a different redox mediator, we also performed the measurements using the same experimental conditions as reported in (*45*). Figure 4 shows the comparison of the light-induced P_{680}^{+}/P_{680} FTIR difference spectra measured for the spinach RC at 230 K obtained i) in the presence of SiMo as a redox mediator and ii) by using ferricyanide in the presence of a small amount of SiMo as redox mediator, as reported in (*45*). As it can be clearly seen in Figure 4, the two RC spectra, obtained using different experimental conditions, are virtually identical.

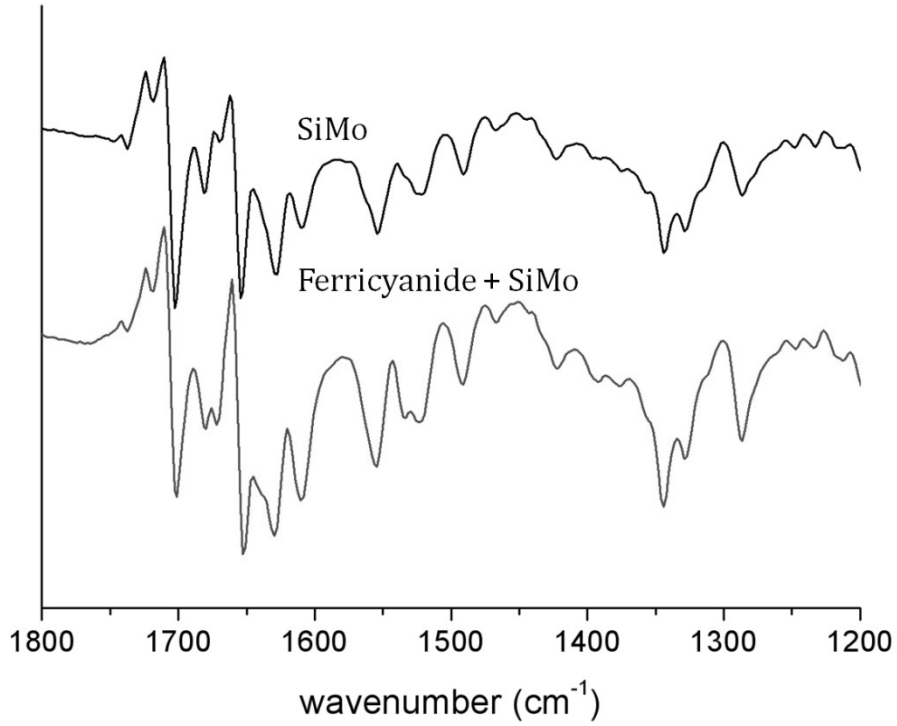

Figure 4. Light-induced P_{680}^{+}/P_{680} FTIR difference spectra of spinach RC obtained in the presence of different redox mediators: SiMo (*top line*) and ferricyanide plus SiMo (*bottom line*). The spectral resolution is 4 cm^{-1}.

In particular, they both show a positive doublet at 1724 and 1709 cm^{-1}, due to the upshifted 13^1-keto C=O signal upon oxidation of $P_{680,}$ although a difference in the relative the intensity of the two bands can be noted. Finally, in order to check if the presence of the doublet can be related to differences between plant or cyanobacteria samples, we also compared the P_{680}^{+}/P_{680} FTIR difference spectra for core and RC preparations from *Synechocystis* at 250 and 230 K, respectively, in the presence of SiMo as redox mediator (Figure 5). Once again, the spectra of core and RC preparations are very similar between each other and also similar to the corresponding spinach spectrum. Both spectra show a positive doublet in the 13^1-keto C=O region, but, differing in that from the corresponding spinach spectrum, two prominent negative bands at 1696 and 1681 cm^{-1} are observed in the neutral 13^1-keto C=O region, possibly suggesting that the protein environment of the carbonyl groups of P_{D1} and P_{D2} is more asymmetric in cyanobacterial systems than in plant preparations.

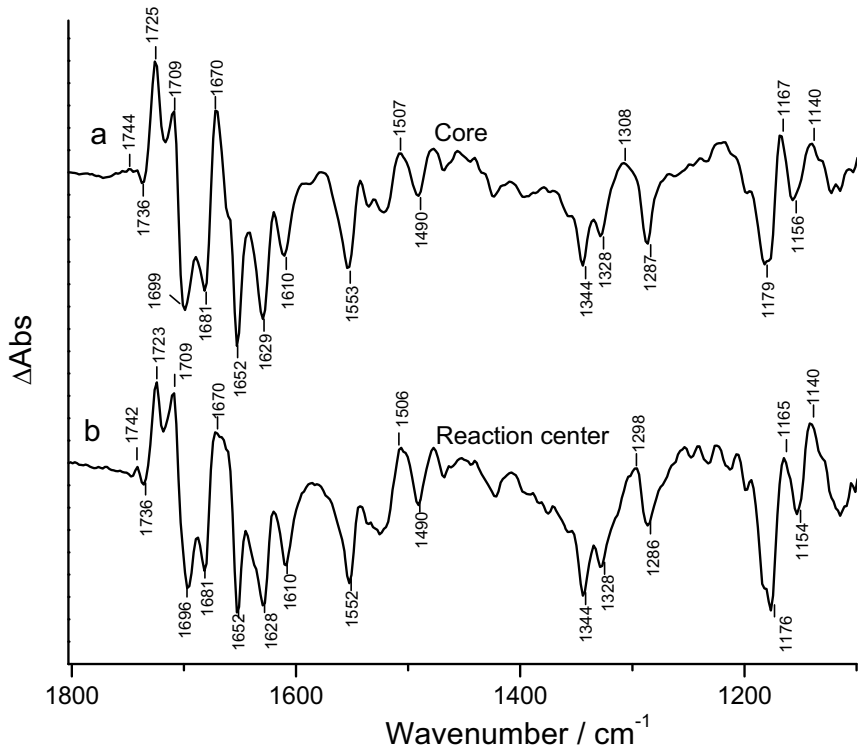

Figure 5. Light-induced P_{680}^{+}/P_{680} FTIR difference spectra of *Synechocystis* core at 250 K (*top line*) and RC at 230 K (*bottom line*) obtained in the presence SiMo as a redox mediator. The band frequency is given in ± 1 cm^{-1}. The spectral resolution is 4 cm^{-1}.

Conclusions. On the basis of all the comparisons reported above we can conclude that the vibronic structure of P_{680}^{+} and the amount of charge localization on the two chlorophyll forming the dimer in the isolated RC are very similar to that observed in more intact preparations.

Effect of site-directed mutation at position D_1-Gln130 on the light-induced Phe_{D1}^-/Phe_{D1} FTIR difference spectra of Synechocystis reaction centers and comparison with spinach

The X-ray crystal structure of cyanobacterial PSII core complexes (*3-5*) (Figure 6) shows that the glutamine (Gln) residue in position D_1-130 in the WT RC is at hydrogen bond distance from the 13^1-keto carbonyl of Phe_{D1}. This residue is exchanged by glutamic acid (Glu) in the D_1-Gln130Glu mutant and by leucine (Leu) in the D_1-Gln130Leu mutant. The mutations are expected to alter the hydrogen bond interaction between the amino acid in position D_1-130 and the 13^1-keto carbonyl of Phe_{D1}: no H-bond interaction is possible with leucine while a stronger H-bond is created with glutamic acid (with respect to Gln). In spinach the residue in position D_1-130 is glutamic acid as well as in the *Syn*. D_1-Gln130Glu mutant which can be considered as a "spinach-like" RC.

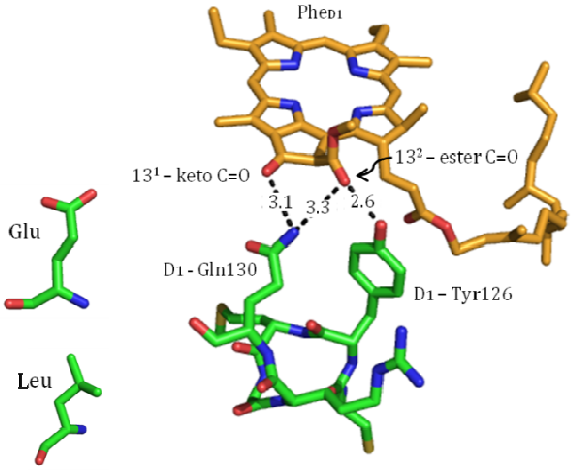

Figure 6. Relative position of the 13^1-keto and 13^2-ester carbonyl of Phe_{D1} with respect to the protein residues in position D_1-130 and D_1-126 (adapted from (*5*)). The chemical structure of the introduced residues (Glu and Leu) are shown at the left. Color code: Phe_{D1} (orange), protein (green), oxygen (red) and nitrogen (blue). Distances shown in Å.

The light-induced Phe_{D1}^-/Phe_{D1} FTIR difference spectra of reaction centers (RCs) isolated from higher plants (spinach) and of RC preparations isolated from cyanobacteria (*Synechocystis* sp. PCC 6803 (*Syn.*)): WT, D_1-Gln130Glu and D_1-Gln130Leu mutants at 240 K are shown in Figure 7. The negative bands in the spectra correspond to vibrations from the Phe_{D1} state and the positive bands from the Phe_{D1}^- state.

In the 1750-1700 cm^{-1} range, where the 13^2-ester carbonyl vibrations of Phe_{D1} are expected to contribute, two negative bands with different relative amplitude are observed for all RCs (Figure 7). The negative band at 1739 cm^{-1}

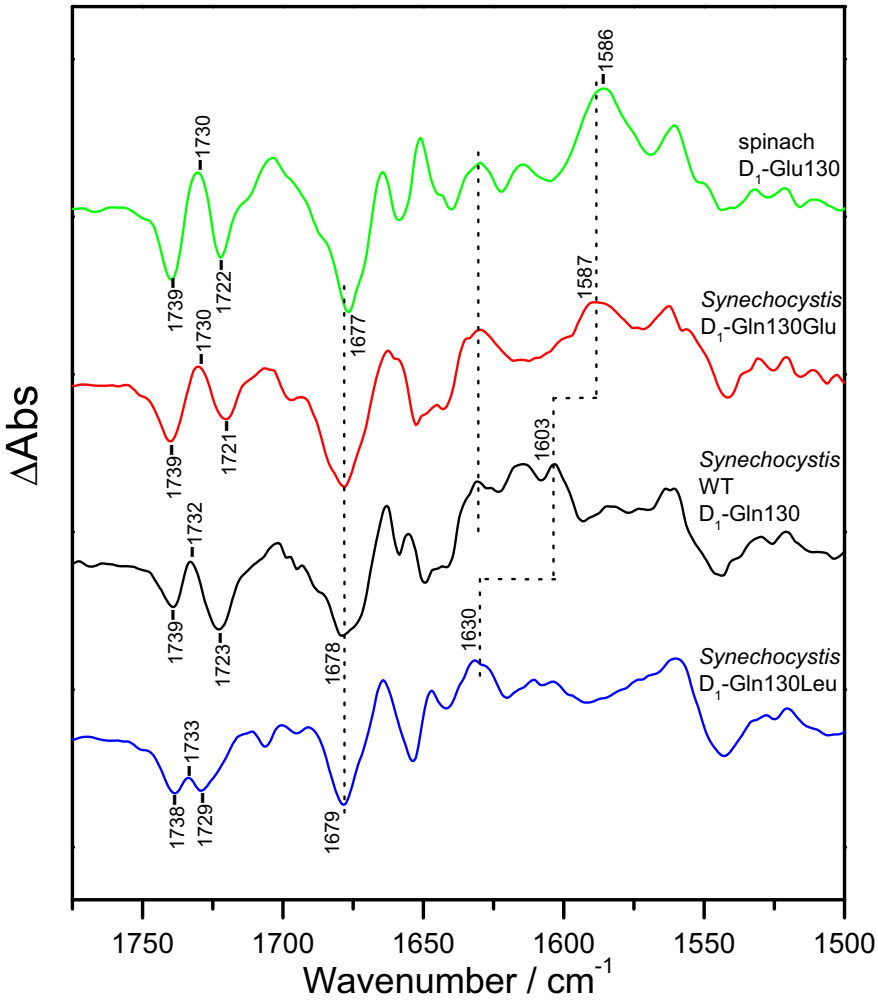

Figure 7. Light-induced Phe_{D1}^-/ Phe_{D1} FTIR difference spectra of PSII RC at 240K from spinach (D_1-Glu130) (*green*) and *Synechocystis*: D_1-Gln130Glu mutant (*red*), WT (D_1-Gln130) (*black*) and D_1-Gln130Leu mutant (*blue*). The band frequency is given in ± 1 cm^{-1}. The spectral resolution is 4 cm^{-1}.

in WT is observed at almost the same position in all RCs. In a FTIR study on RCs from a higher plant (pea), this band was assigned to the contribution from the protonated carboxylic group Glu at position D_1-130 (*46*). However, the spectra displayed in Figure 7 shows that the 1739 cm^{-1} band is present in the *Syn*. WT and in the D_1-Glu130Leu mutant (which do not contain Glu, but Gln and Leu, respectively) confirming that this band does not correspond to Glu in position D_1-130.

The 1739 cm^{-1} band (as well as in Phe *a* (*46*)) downshifts upon Phe_{D1} reduction depending on the residue at position D_1-130: 5 cm^{-1} for D_1-Gln130Leu, 7 cm^{-1} for WT and 10 cm^{-1} for D_1-Gln130Glu and spinach, suggesting that the amino acid in position D_1-130 influences the Phe_{D1} 13^2-ester C=O vibrational properties in the reduced state.

The light-induced FTIR difference spectra for pheophytin *a* (Phe *a*), Phe a^-/Phe *a*, and the comparison with its pyro derivative (lacking the 13^2-ester group) in a non-hydrogen bonding solvent (THF) shows that a negative band at 1743 cm^{-1} is present for Phe *a* but absent for its pyro derivative, which indicates that the 1743 cm^{-1} corresponds to the non-hydrogen bonded 13^2-ester C=O vibration of Phe *a* in solution (*46*). The observations discussed above suggest that the 1739 cm^{-1} negative band corresponds to a free (non-hydrogen bonded) 13^2-ester C=O of Phe_{D1} (the 4 cm^{-1} downshift of Phe_{D1} with respect to Phe *a* is attributed to the higher polarity of the protein environment with respect to the THF solution).

The second negative band in the 1750-1700 cm^{-1} range is at 1723 cm^{-1} in WT. This band could be attributed, in relation with the free 13^2-ester C=O vibration at 1739 cm^{-1}, to a H-bonded 13^2-ester C=O. In cyanobacterial RCs, Tyrosine 126 (Tyr126), which contains an –OH group, is within H-bond distance (2.58 Å) to the 13^2-ester C=O (*5*), making Tyr126 a good candidate for establishing a H-bond interaction with the 13^2-ester C=O. However, the 1723 cm^{-1} band in WT is sensitive to mutations at position D_1-130: it upshifts to 1729 cm^{-1} in D_1-Gln130Leu and downshifts to 1721 (1722) cm^{-1} in D_1-Gln130Glu (and in the spinach RC) upon mutation. It is interesting to note the significant 6 cm^{-1} downshift when the possible H-bond interaction between the 13^2-ester C=O and the D_1-130 residue is eliminated (upon Gln replacement by the non-hydrogen bonding Leu) in contrast with the small 1-2 cm^{-1} upshift when this possible interaction is strengthen (upon Gln replacement by Glu). Furthermore the relative intensity of the two negative bands at 1739 and 1723 cm^{-1} is also affected by the mutations at position D_1-130. The observed amplitude ratios are: 1:1 for D_1-Gln130Leu, 1:2 for WT and 3:2 for D_1-Gln130Glu and spinach. These observations suggest that the residue at position D_1-130 influences the hydrogen bond network of the 13^2-ester C=O, most likely by establishing an H-bond interaction with the 13^2-ester C=O. For the D_1-Gln130Leu mutant the residue at position Tyr126 could establish the H-bond interaction. In this case the Tyr126 residue establishes a weaker H-bond with the 13^2-ester carbonyl than the Gln and Glu in WT and D_1-Gln130Glu, respectively, due to the large electron density of the Tyr126 phenyl group. The presence of two bands attributable to the 13^2-ester C=O absorption points to the possible heterogeneity of its hydrogen-bonding status,

which has already been proposed in the case of the purple bacteria reaction centers (*58*). The authors of that work, by comparing the bacteriopheophytin light-induced H_A^-/H_A FTIR difference spectra of WT (L-Glu104) and two mutants (L-Glu104Gln and M-Trp250Phe), found three distinct subpopulations of H_A which appears to be related to differences in hydrogen-bonding interactions between the H_A carbonyls in ring V and the protein. In this case, in one subpopulation the 13^2-ester carbonyl is free from H-bond while in the other two subpopulations different H-bond networks to the 13^2-ester carbonyl leads to two negative bands in the spectra (*58*). In a similar manner, in the PSII RC of *Syn*. WT and plants two different subpopulations may exist: with and without 13^2-ester carbonyl H-bond interaction with the residue at position D_1-130, corresponding to the bands at 1723 and 1739 cm^{-1}, respectively.

The 13^1-keto carbonyl vibrations of Phe_{D1} are expected to be found in the 1700-1550 cm^{-1} region. In order to interpret the spectral changes upon mutation at position D_1-130, i.e., upon modification of the H-bond strength to the 13^1-keto C=O of Phe_{D1}, it is helpful to recall the position of the 13^1-keto carbonyl bands for Phe *a* in a non-hydrogen bonding solvent (THF) (*46*). The light-induced Phe a^-/Phe *a* FTIR difference spectrum shows a negative and a positive band at 1706(-)/1656(+) cm^{-1} (at (1701(-)/1649(+) cm^{-1} for the pyro derivative) which correspond to a 50 cm^{-1} upshift upon reduction of the 13^1-keto C=O vibration of Phe *a* free from H-bond interactions. In the RCs spectra shown in Figure 7, the negative band corresponding to the 13^1-keto C=O of Phe_{D1} in the neutral form is at 1679 cm^{-1} for D_1-Gln130Leu, at 1678 cm^{-1} for WT and D_1-Gln130Glu, and at 1677 cm^{-1} for spinach RC, in agreement with the literature (*46, 47*). The careful comparison of the spectral shapes and the expected H-bond strength trend: no H-bond for D_1-Gln130Leu, H-bond for WT and stronger H-bond for D_1-Gln130Glu and spinach with respect to WT; lead us to the assignment of the 13^1-keto carbonyl of Phe_{D1} in the reduced state to 1630 cm^{-1} for D_1-Gln130Leu, 1615 cm^{-1} for WT, 1587 cm^{-1} for D_1-Gln130Glu and 1586 cm^{-1} for the spinach RC (Figure 7). For the D_1-Gln130Leu mutant, the shift upon reduction is 49 cm^{-1}, the same shift observed for the 13^1-keto carbonyl band of Phe *a* in solution which indicates that in this mutant the 13^1-keto carbonyl of Phe_{D1} is free from H-bond interactions. The 27 cm^{-1} overall shift of the transition 1679(-)/1630(+) cm^{-1} for Phe_{D1} with respect to 1706(-)/1656(+) cm^{-1} for Phe *a* is explained by the polar protein environment which stabilizes this transition. This effect, although less significant, is also found in the free 13^2-ester C=O vibration at 1739 cm^{-1} (see above) and suggests that the 13^1-keto C=O is more sensitive to the protein environment than the 13^2-ester C=O.

For the WT, the band assigned to the 13^1-keto C=O of Phe_{D1} in the reduced state is at 1603 cm^{-1}, which corresponds to a 75 cm^{-1} shift upon reduction. In a recent FTIR work on PSII cores from cyanobacteria and BBY membranes from spinach (*47*), the spectral differences between WT (D_1-Gln130), a preparation with Glu at position D_1-130 (D_1-Glu130) and spinach (D_1-Glu130), lead to the assignment of a positive band at 1605 cm^{-1} to the 13^1-keto carbonyl of Phe_{D1} in the reduced state. In that work the 1605 cm^{-1} positive band downshifts to 1587 cm^{-1} and 1586 cm^{-1} for the D_1-Glu130 and the spinach preparations, respectively, which corresponds to a 77, 95 and 92 cm^{-1} downshift upon reduction for WT, and the D_1-Glu130 and the spinach preparations, respectively. This assignment was supported by density functional theory (DFT) calculations (*47*).

In the present work, the trend is also clear; the shift of the 13^1-keto C=O of Phe_{D1} upon reduction is 49 cm^{-1} for the free 13^1-keto C=O (D_1-Gln130Leu), 75 cm^{-1} for the 13^1-keto C=O H-bonded with Gln (WT) and 91 cm^{-1} for the 13^1-keto C=O H-bonded with Glu (D_1-Gln130Glu and spinach RC) (Figure 7). These values are in agreement with the experimental and calculated values presented recently (*47*). Nevertheless, the availability of the D_1-Gln130Leu mutant is an advantage with respect to previously reported work and provides the keys to the novel findings of this work.

Two unexpected conclusions can be drawn from the comparison of the spectral features assigned to the 13^1-keto C=O of Phe_{D1} (Figure 7). On one hand, the negative band assigned to the H-bonded 13^1-keto carbonyl of Phe_{D1} in the neutral state is virtually at the same position for all RCs, even for the D_1-Gln130Leu mutant where no H-bond is possible between the 13^1-keto carbonyl and the residue at position D_1-130. In this case, a water molecule could provide the H-bond interaction. However, the fact that the downshift upon Phe_{D1} reduction is exactly the same as found for the reduction of Phe *a* in a non-hydrogen bonding solvent (*46*), lead us to consider that a water molecule is not interacting with the 13^1-keto C=O of Phe_{D1}. Therefore, we propose that the 13^1-keto C=O of Phe_{D1} is not H-bonded in the neutral state in any of the RCs studied here, which implies that the H-bond interaction is only established in the Phe_{D1} reduced state. On the other hand, the 1630 cm^{-1} positive band assigned to the free, non-hydrogen bonded 13^1-keto carbonyl of Phe_{D1}^- in the D_1-Gln130Leu mutant, is clearly present in the spectra of all the RCs samples studied here. Although the effect of the isotopic exchange (^{14}N by ^{15}N) indicates that the protein amide I contributes to the 1630 cm^{-1} positive band in the spinach RC FTIR difference spectrum, we cannot rule out the possibility that this band is the composite of contributions from both protein and Phe_{D1}.

Therefore, this observation indicates the presence of different subpopulations in the sample ensemble: a subpopulation with the 13^1-keto C=O H-bonded to the D_1-130 residue and a subpopulation with the 13^1-keto C=O free from H-bond interactions. This scenario is in line with the same two subpopulations previously observed for the 13^2-ester C=O (see above).

Conclusions. Therefore, we conclude that two different subpopulations with different H-bond interactions to both the 13^2-ester and 13^1-keto carbonyl are present in the RC ensemble. In one subpopulation, the 13^2-ester carbonyl is free from H-bond (1739 cm^{-1} negative band in WT) and the 13^1-keto carbonyl is H-bonded to residue D_1-130 (1603 cm^{-1} positive band in WT). In the other subpopulation, the 13^2-ester carbonyl is H-bonded to residue D_1-130 (1723 cm^{-1} negative band in WT) and the 13^1-keto carbonyl is free from H-bond interactions (1630 cm^{-1} positive band in WT).

The presence of two different subpopulations in the *Syn*. and spinach RCs can be rationalized by the presence of static disorder in the pigment-protein complexes. The system is in continuous movement: fast nuclear motions (intra- and interpigment vibrations, protein vibrations) and slow conformational motions of the protein produce slight different protein conformations which, however, have important implications in the energy dynamics of the system. Recently, we have demonstrated by time-resolved absorption spectroscopy the presence of two different pathways of charge separation in the spinach RC. In one pathway, the so-called Chl_{D1} path, Phe_{D1} is the primary electron acceptor and Chl_{D1} is the primary electron donor; while in the other pathway, the P_{D1} path, Chl_{D1} is the primary electron acceptor and P_{D1} is the primary electron donor ((*20*) and Chapter 2 of this Thesis). The findings presented here are directly related with the presence of two different pathways of charge separation in photosystem II. The subpopulation with the 13^2-ester carbonyl free from H-bond and the 13^1-keto carbonyl H-bound to residue D_1-130 corresponds with the Chl_{D1} path. The H-bond interaction with Phe_{D1} 13^1-keto carbonyl converts the Phe_{D1} cofactor in a good electron acceptor. Conversely, in the other subpopulation where the Phe_{D1} 13^1-keto carbonyl is free from H-bond interactions, the Chl_{D1} cofactor could act as the primary electron acceptor.

ACKNOWLEDGEMENT

The authors thank Nicolas Gilles, Hervé Bottin, and Pierre Sétif for isotopically labelled spinach cultures; and Henny van Roon for the expert preparation of the spinach reaction center samples.

REFERENCES

1. Dekker, J. P., and Boekema, E. J. (2005) Supramolecular organization of thylakoid membrane proteins in green plants, *Biochim. Biophys. Acta 1706*, 12-39.

2. Dekker, J. P., and van Grondelle, R. (2000) Primary charge separation in photosystem II, *Photosynth. Res. 63*, 195-208.

3. Ferreira, K. N., Iverson, T. M., Maghlaoui, K., Barber, J., and Iwata, S. (2004) Architecture of the photosynthetic oxygen-evolving center, *Nature 303*, 1831-1838.

4. Loll, B., Kern, J., Saenger, W., Zouni, A., and Biesiadka, J. (2005) Towards complete cofactor arrangement in the 3.0 Å resolution structure of photosystem II, *Nature 438*, 1040-1044.

5. Guskov, A., Kern, J., Gabdulkhakov, A., Broser, M., Zouni, A., and Saenger, W. (2009) Cyanobacterial photosystem II at 2.9-Å resolution and the role of quinones, lipids, channels and chloride, *Nat. Struct. Mol. Biol. 16*, 334-342.

6. Diner, B. A., Schlodder, E., Nixon, P. J., Coleman, W. J., Rappaport, F., Lavergne, J., Vermaas, W. F. J., and Chisholm, D. A. (2001) Site-directed mutations at D_1-His198 and D_2-His197 of photosystem II in *Synechocystis* PCC 6803: Sites of primary charge separation and cation triplet stabilization, *Biochemistry 40*, 9265-9281.

7. van Dorssen, R. J., Breton, J., Plijter, J. J., Satoh, K., van Gorkom, H. J., and Amesz, J. (1987) Spectroscopic properties of the reaction center and of the 47 kDa chlorophyll protein of Photosystem II, *Biochim. Biophys. Acta 893*, 267-274.

8. Durrant, J. R., Hastings, G., Joseph, D. M., Barber, J., Porter, G., and Klug, D. R. (1992) Subpicosecond equilibration of excitation energy in isolated photosystem II reaction centers, *Proc. Natl. Acad. Sci. U.S.A. 89*, 11632-11636.

9. Schelvis, J. P. M., van Noort, P. I., Aartsma, T. J., and van Gorkom, H. J. (1994) Energy transfer, charge separation and pigment arrangement in the reaction center of photosystem II, *Biochim. Biophys. Acta 1184*, 242-250.

10. Visser, H. M., Groot, M.-L., van Mourik, F., van Stokkum, I. H. M., Dekker, J. P., and van Grondelle, R. (1995) Subpicosecond transient absorption difference spectroscopy on the reaction center of Photosystem II: radical pair formation at 77 K, *J. Phys. Chem. 99*, 15304-15309.

11. Müller, M. G., Hucke, M., Reus, M., and Holzwarth, A. R. (1996) Primary processes and structure of the Photosystem II reaction center. 4. Low-intensity femtosecond transient absorption spectra of D_1-D_2-cyt-b_{559} reaction centers, *J. Phys. Chem. 100*, 9527-9536.

12. Groot, M.-L., van Mourik, F., Eijckelhoff, C., van Stokkum, I. H. M., Dekker, J. P., and van Grondelle, R. (1997) Charge separation in the reaction center of photosystem II studied as a function of temperature, *Proc. Natl. Acad. Sci. U.S.A. 94*, 4389-4394.

13. Peterman, E. J. G., van Amerongen, H., van Grondelle, R., and Dekker, J. P. (1998) The nature of the excited state of the reaction center of photosystem II of green plants: A high-resolution fluorescence spectroscopy study, *Proc. Natl. Acad. Sci. U.S.A. 95*, 6128-6133.

14. Greenfield, S. R., Seibert, M., and Wasielewski, M. R. (1999) Time-resolved absorption changes of the pheophytin Q_x band in isolated photosystem II reaction centers at 7 K: Energy transfer and charge separation, *J. Phys. Chem. B 103*, 8364-8374.

15. Andrizhiyevskaya, E. G., Frolov, D., van Grondelle, R., and Dekker, J. P. (2004) On the role of the CP47 core antenna in the energy transfer and trapping dynamics of photosystem II, *Phys. Chem. Chem. Phys. 6*, 4810-4819.

16. van Mourik, F., Groot, M.-L., van Grondelle, R., Dekker, J. P., and van Stokkum, I. H. M. (2004) Global and target analysis of fluorescence measurements on photosystem 2 reaction centers upon red excitation, *Physical Chemistry Chem. Phys. 6*, 4820-4824.

17. Germano, M., Gradinaru, C. C., Shkuropatov, A. Y., van Stokkum, I. H. M., Shuvalov, V. A., Dekker, J. P., van Grondelle, R., and van Gorkom, H. J. (2004) Energy and electron tranfer in photosystem II reaction centers with modified pheophytin composition, *Biophys. J. 89*, 1664-1672.

18. Groot, M.-L., Pawlowicz, N. P., van Wilderen, L. J. G. W., Breton, J., van Stokkum, I. H. M., and van Grondelle, R. (2005) Initial electron donor and acceptor in isolated photosystem II reaction centers identified with femtosecond mid-IR spectroscopy, *Proc. Natl. Acad. Sci. U.S.A. 102*, 13087-13092.

19. Holzwarth, A. R., Müller, M. G., Reus, M., Nowaczyk, M., Sander, J., and Rögner, M. (2006) Kinetics and mechanism of electron transfer in intact photosystem II and in the isolated reaction center: Pheophytin is the primary electron acceptor, *Proc. Natl. Acad. Sci. U.S.A. 103*, 6895-6900.

20. Romero, E., van Stokkum, I. H. M., Novoderezhkin, V. I., Dekker, J. P., and van Grondelle, R. (2010) Two different charge separation pathways in photosystem II, *Biochemistry 49*, 4300-4307.

21. Andrizhiyevskaya, E. G., Bautista, J. A., Diner, B. A., van Grondelle, R., and Dekker, J. P. (2005) Energy transfer and trapping in photosynthetic complexes with variable antenna size, VU University Amsterdam, Amsterdam.

22. Miloslavina, Y., Szczepaniak, M., Müller, M. G., Sander, J., Nowaczyk, M., Rögner, M., and Holzwarth, A. R. (2006) Charge separation kinetics in intact photosystem II core particles is trap-limited. A picosecond fluorescence study, *Biochemistry 45*, 2436-2442.

23. van der Weij-de Wit, C. D., van Stokkum, I. H. M., van Grondelle, R., and Dekker, J. P. (In press) Charge separation is virtually irreversible in photosystem II core complexes with oxidized primary quinone acceptor, *J. Phys. Chem.*

24. Durrant, J. R., Klug, D. R., Kwa, S. L. S., van Grondelle, R., Porter, G., and Dekker, J. P. (1995) A multimer model for P680, the primary electron donor of photosystem II, *Proc. Natl. Acad. Sci. U.S.A. 92*, 4798-4802.

25. Novoderezhkin, V. I., Andrizhiyevskaya, E. G., Dekker, J. P., and van Grondelle, R. (2005) Pathways and timescales of primary charge separation in the Photosystem II reaction center as revealed by simultaneous fit of time-resolved fluorescence and transient absorption, *Biophys. J. 89*, 1464-1481.

26. Novoderezhkin, V. I., Dekker, J. P., and van Grondelle, R. (2007) Mixing of exciton and charge transfer states in Photosystem II reaction centers: Modeling of Stark spectra with Modified Redfield Theory, *Biophys. J. 93*.

27. Raszewski, G., Diner, B. A., Schlodder, E., and Renger, T. (2008) Spectroscopic properties of reaction center pigments in Photosystem II core complexes: Revision of the multimer model, *Biophys. J. 95*, 105-119.

28. Raszewski, G., Saenger, W., and Renger, T. (2005) Theory of optical spectra of Photosystem II reaction centers: Location of the triplet state and the identity of the primary electron donor, *Biophys. J. 88*, 986-998.

29. Krüger, T. P. J., Novoderezhkin, V. I., Ilioaia, C., and van Grondelle, R. (2010) Fluorescence spectral dynamics of single LHCII trimers, *Biophys. J. 98*, 3093-3101.

30. Wang, H., Lin, S., Allen, J. P., Williams, J. C., Blankert, S., Laser, C., and Woodbury, N. W. (2007) Protein dynamics control the kinetics of initial electron transfer in photosynthesis, *Science 316*, 747-750.

31. Brecht, M., Radics, V., Nieder, J. B., and Bittl, R. (2009) Protein dynamics-induced variation of excitation energy transfer pathways, *Proc. Natl. Acad. Sci. U.S.A. 106*, 11857-11861.

32. Mäntele, W. (1996) Infrared and Fourier-transform infrared spectroscopy, In *Biophysical techniques in photosynthesis* (Hoff, J. A. a. A. J., Ed.), pp 137-160, Kluwer Academic Publishers.

33. Lutz, M., and Mäntele, W. (1991) In *Chlorophylls* (Scheer, H., Ed.), pp 855-902, CRC Press, Boca Raton, FL.

34. Socrates, G. (1994) *Infrared Charactheristic Group Frequencies*, 2nd ed., Wiley and Sons, New York.

35. Breton, J., Nabedryk, E., and Leibl, W. (1999) FTIR study of the primary electron donor of photosystem I (P700) revealing delocalization of the charge in $P700^{+}$ and localization of the triplet character in $^{3}P700$, *Biochemistry 38*, 11585-11592.

36. Rappaport, F., Guergova-Kuras, M., Nixon, P. J., Diner, B. A., and Lavergne, J. (2002) Kinetics and pathways of charge recombination in photosystem II, *Biochemistry 41*, 8518-8527.

37. Ishikita, H., Loll, B., Biesiadka, J., Saenger, W., and Knapp, E.-W. (2005) Redox potentials of chlorophylls in the photosystem II reaction center, *Biochemistry 44*, 4118-4124.

38. Rappaport, F., and Diner, B. A. (2008) Primary photochemistry and energetics leading to the oxidation of the $(Mn)_4Ca$ cluster and to the evolution of molecular oxygen in Photosystem II, *Coord. Chem. Rev. 252*, 259-272.

39. Blankenship, R. E., and Hartman, H. (1998) The origin and evolution of oxygenic photosynthesis, *Trends Biochem. Sci. 23*, 94-97.

40. Saji, T., and Bard, A. J. (1977) Electrogenerated chemiluminescence. 29. The electrochemistry and chemiluminescence of chlorophyll *a* in *N*,*N*-dimethylformamide solutions, *J. Am. Chem. Soc. 99*, 2235-2240.

41. Breton, J., Hienerwadel, R., and Nabedryk, E. (1997) FTIR difference spectrum of the photooxidation of the primary electron donor of photosystem II, In *Spectroscopy of Biological Molecules: Modern Trends* (P. Carmona, R. N., A. Hernanz, Ed.), p 101, Kluwer Academic Publishers, Dordrecht.

42. Sarcina, M., Breton, J., Nabedryk, E., Diner, B. A., and Nixon, P. J. (1998) FTIR studies on the P680 cation and triplet states in WT and mutant PSII reaction centers of *Synechocystis* 6803, In *Photosynthesis: Mechanisms and Effects* (Garab, G., Ed.), pp 1053-1056, Kluwer Academic Publishers, Dordrecht.

43. Noguchi, T., Tomo, T., and Inoue, Y. (1998) Fourier transform infrared study of the cation radical of P680 in the photosystem II reaction center: evidence for charge delocalization on the chlorophyll dimer, *Biochemistry 37*, 13614-13625.

44. Sugiura, M., Rappaport, F., Brettel, K., Noguchi, T., Rutherford, W. A., and Boussac, A. (2004) Site-directed mutagenesis of *Thermosynechococcus elongatus* photosystem II: The O_2-evolving enzime lacking the redox-active tyrosine D, *Biochemistry 43*, 13549-13563.

45. Okubo, T., Tomo, T., Sugiura, M., and Noguchi, T. (2007) Perturbation of the structure of P680 and the charge distribution on its radical cation in isolated reaction center complexes of photosystem II as revealed by Fourier transform infrared spectroscopy, *Biochemistry 46*, 4390-4397.

46. Nabedryk, E., Andrianambinintsoa, S., Berger, G., Leonhard, M., Mäntele, W., and Breton, J. (1990) Characterization of bonding interactions of the intermediary electron acceptor in the reaction center of photosystem II by FTIR spectroscopy, *Biochim. Biophys. Acta 1016*, 49-54.

47. Shibuya, Y., Takahashi, R., Okubo, T., Suzuki, H., Sugiura, M., and Noguchi, T. (2010) Hydrogen bond interactions of the pheophytin electron acceptor and its radical anion in photosystem II as revealed by Fourier transform infrared difference spectroscopy, *Biochemistry 49*, 493-501.

48. Giorgi, L. B., Nixon, P. J., Merry, S. A. P., Joseph, M., Durrant, J. R., De Las Rivas, J., Barber, J., Porter, G., and Klug, D. R. (1996) Comparison of primary charge separation in the photosystem II reaction center complex isolated from wild-type and D1-130 mutants of the cyanobacterium *Synechocystis* PCC 6803, *J. Biol. Chem. 271*, 2093-2101.

49. Berthold, D. A., Babcock, G. T., and Yocum, C. F. (1981) A highly resolved, oxygen-evolving photosystem II preparation from spinach thylakoid membranes, *FEBS Lett. 134*, 231-234.

50. van Leeuwen, P. J., Nieveen, M. C., van de Meent, E. J., Dekker, J. P., and van Gorkom, H. J. (1991) Rapid and simple isolation of pure photosystem II core and reaction center particles from spinach, *Photosynth. Res. 28*, 149-153.

51. van Mieghem, F. J. E., Nitschke, W., Mathis, P., and Rutherford, W. A. (1989) The influence of the quinone-iron electron acceptor complex on the reaction center photochemistry of photosystem II, *Biochim. Biophys. Acta 977*, 207-214.

52. Kwa, S. L. S., Newell, W. R., van Grondelle, R., and Dekker, J. P. (1992) The reaction center of photosystem II studied with polarized fluorescence spectroscopy, *Biochim. Biophys. Acta 1099*, 193-202.

53. Vosko, S. H., Wilk, L., and Nusair, M. (1980) Accurate spin-dependent electron liquid correlation energies for local spin density calculations: a critical analysis, *Can. J. Phys. 58*, 1200-1211.

54. Lee, C., Yang, W., and Parr, R. G. (1988) Development of the Colle-Salvetti correlation-energy formula into a functional of the electron density, *Phys. Rev. B 37*, 785-789.

55. Becke, A. D. (1993) Density-functional thermochemistry. III. The role of exact exchange, *J. Chem. Phys. 98*, 5648-5652.

56. Stephens, P. J., Devlin, F. J., Chabalowski, C. F., and Frisch, M. J. (1994) Ab initio calculation of vibrational absorption and circular dichroism spectra using density functional force fields, *J. Phys. Chem. 98*, 11623-11627.

57. Frisch, m. J., Trucks, G. W., Schlegel, H. B., Scuseria, G. E., Robb, M. A., Cheeseman, J. R., Zakrzewski, V. G., Montgomery, J. A. J., Stratmann, R. E., Burant, J. C., Dapprich, S., Millam, J. M., Daniels, A. D., Kudin, K. N., Strain, M. C., Farkas, O., Tomasi, J., Barone, V., Cossi, M., Cammi, R., Mennucci, B., Pomelli, C., Adamo, C., Clifford, S., Ochterski, J., Petersson, G. A., Ayala, P. Y., Cui, Q., Morokuma, K., Malick, D. K., Rabuck, A. D., Raghavachari, K., Foresman, J. B., Cioslowski, J., Ortiz, J. V., Stefanov, B. B., Liu, G., Liashenko, A., Piskorz, P., Komaromi, I., Gomperts, R., Martin, R. L., Fox, D. J., Keith, T., Al-Laham, M. A., Peng, C. Y., Nanayakkara, A., Gonzalez, C., Challacombe, M., Gill, P. M. W., Johnson, B., W. Chen, W., Wong, M. W., Andres, J. L., Gonzalez, C., Head-Gordon, M., Replogle, E. S., and Pople, J. A. (1998) Gaussian 98, Revision A.6, Gaussian, Inc., Pittsburgh PA.

58. Breton, J., Bibikova, M., Oesterhelt, D., and Nabedryk, E. (1999) Conformational heterogeneity of the bacteriopheophytin electron acceptor H_A in reaction centers from *Rhodopseudomonas viridis* revealed by Fourier transform infrared spectroscopy and site-directed mutagenesis, *Biochemistry 38*, 11541-11552.

CHAPTER 7

The Origin of the Low-Energy Form of Photosystem I Light-Harvesting Complex Lhca4: Mixing of the Lowest Exciton with a Charge-Transfer State

Elisabet Romero, Milena Mozzo, Ivo H. M. van Stokkum, Jan P. Dekker, Rienk van Grondelle, and Roberta Croce

The peripheral light-harvesting complex of photosystem I contains red chlorophylls (Chls) that, unlike the typical antenna Chls, absorb at lower energy than the primary electron donor P700. It has been shown that the red-most absorption band arises from two excitonically coupled Chls, although this interaction alone cannot explain the extreme red-shifted emission (25 nm, ≈480 cm^{-1} for Lhca4 at 4 K) that the red Chls present. Here, we report the electric field-induced absorption changes (Stark effect) on the Q_Y region of the Lhca4 complex. Two spectral forms, centered around 690 nm and 710 nm, were necessary to describe the absorption and Stark spectra. The analysis of the lowest energy transition yields a high value for the change in dipole moment, $\Delta\mu_{710nm} \approx 8\ D\ f^{-1}$, between the ground and excited states as compared with monomeric, $\Delta\mu$ = 1 D, or dimeric, $\Delta\mu$ = 5 D, Chl *a* in solution. The high value of the $\Delta\mu$ demonstrates that the origin of the red-shifted emission is the mixing of the lowest exciton state with a charge-transfer state of the dimer. This energetic configuration, an excited state with charge-transfer character, is very favorable for the trapping and dissipation of excitations and could be involved in the photoprotective mechanism(s) of the photosystem I complex.

This chapter is based on the publication:

Elisabet Romero, Milena Mozzo, Ivo H. M. van Stokkum, Jan P. Dekker, Rienk van Grondelle, and Roberta Croce. (2009) The Origin of the Low-Energy Form of Photosystem I Light-Harvesting Complex Lhca4: Mixing of the Lowest Exciton with a Charge-Transfer State. *Biophys, J*. 96:L35-L37

Photosystem I (PSI) is a multisubunit pigment-protein complex located in the thylakoid membrane of higher plants and algae where one of the first steps of solar energy conversion by light-driven electron transport takes place. It consists of two separable subunits: the PSI core and the peripheral light-harvesting complex I. The light-harvesting complex I, responsible for the absorption of light and the transfer of energy to the PSI core, contains in plants four subunits: Lhca1, 2, 3 and 4 (*1,2*). The most striking spectroscopic feature of PSI is the presence of red chlorophylls (Chls), i.e., Chls that absorb at longer wavelength than the primary electron donor P700, and that exhibit nontypical Chl behavior: a large absorption bandwidth (400–500 cm^{-1} at 4 K) due to both homogeneous and inhomogeneous broadening, and an extremely red-shifted emission (absorption at 708 nm and emission at 733 nm for Lhca4 at 4 K), i.e., 480 cm^{-1} (*3*), the most dramatic Stokes spectral shift observed in a photosynthetic complex so far. In higher plants, these forms are mainly associated with the outer antenna, although low energy absorption forms are also present in the core (*4*).

It has been shown that the red-most absorption band in the PSI complex arises from an excitonically coupled dimer of Chls (*5–8*), although this interaction alone cannot account for the extreme red-shifted emission and the large bandwidth. A complementary explanation for both effects is the presence of a charge-transfer (CT) state mixed with the lowest exciton state of the dimer (*9*). Although the involvement of a CT state in the spectroscopic properties of the red Chls has been proposed by several authors for both the red forms of the core and the antenna (*3,10–13*), no direct evidence has been provided to date. To reveal the origin of the red Chls is a key aspect in PSI research because of the very pronounced effect that these low energy forms have on the energy transfer and trapping in the whole complex (*14*).

In this study, we have focused our attention on Lhca4, the subunit with the red-most shifted emission. To investigate the CT character of its lowest exciton state, we have performed Stark spectroscopy, a technique extremely sensitive to the changes in the electronic charge distribution of pigments upon excitation. This technique monitors the spectral changes induced by an externally applied electric field in absorption or emission spectra. A detailed description of the theoretical background, experimental setup, and analytical methods of Stark spectroscopy is found elsewhere (*15*). In simple terms, for a randomly oriented sample, the Stark spectrum (Abs_{Fon} _ Abs_{Foff}) is described by the Liptay formalism as a linear combination of the zeroth, first, and second derivatives of the absorption spectrum (*16*). The molecular parameters change in polarizability, $\Delta\alpha$, and change in dipole moment, $\Delta\mu$, between the excited and

ground states, scale with the first and second derivatives, respectively, of the absorption spectrum. Thus, quantitative simultaneous analysis of the absorption and Stark spectra gives values for $\Delta\alpha$ and $\Delta\mu$ that are expressed in terms of the local field correction *f*, a parameter that accounts for the internal electric field felt by the chromophore because of the protein environment (theoretical calculations estimate $1.1 > f > 1.3$ (*15*)). A measure of the degree of charge separation between the ground and excited states is given by $\Delta\mu$, the key parameter to determine when the presence of CT states is investigated. $\Delta\alpha$ is related to the deformability of the electronic cloud of a molecule and provides information about the electronic properties of a chromophore interacting with the protein matrix.

The Liptay formalism, however, presents limitations when applied to photosynthetic systems: it is formulated for noninteracting molecules with isolated absorption bands with constant electrooptic parameters across each band and does not account for the field-induced mixing of (excitonic) states that can lead to new transitions. Another source of uncertainty when applying the Liptay formalism is the description of the absorption bands with Gaussian shapes that do not describe the vibrational side bands. Several examples of the failure of the method can be found in the literature (*17,18*). This problem can be overcome by combining the disordered exciton model with the modified Redfield Theory, in which more realistic band positions and band shapes are obtained from the simultaneous fit of absorption, fluorescence, linear dichroism, circular dichroism, and triplet-minus-singlet spectra (*19*). Although there are conceptual limitations underlying the Liptay formalism, it is useful, as a first approximation, for obtaining an estimation of the $\Delta\mu$ (the analytical limitations are more important for $\Delta\alpha$ (*15*)). By comparing the $\Delta\mu$ of interest with the $\Delta\mu$ for monomeric (1 D) and dimeric (5 D) Chl *a* in solution (the large increase upon dimerization was ascribed to the CT character of the dimer excited state) (*20*), it is concluded that for transitions arising from a dimer, when $\Delta\mu \geq 5\ \mathrm{D}\ f^{-1}$ the excited state is mixed with a CT state.

The absorption and Stark spectra of reconstituted Lhca4 prepared as in *Croce et al*. (*21*) are shown in Figure 1. Six skewed Gaussian bands are necessary to obtain a satisfactory simultaneous fit of the absorption and Stark spectra. When all the fitting parameters (position, full width at half maximum (FWHM), and skewness of the absorption bands) are free, the low energy form is fitted with a single broad band (centered at 700 nm, FWHM = 970 cm^{-1}) whose derivatives do not fully describe the red tail of the Stark spectrum (see Appendix). According to *Croce et al*. (*3*), a second emission form at 705 nm absorbing around 690 nm is present in Lhca4.

The inclusion of this second red absorption band substantially improves the quality of the fit. Several fits with similar quality are obtained when the position and the width of the lowest energy forms are fixed to 689–690 nm, FWHM = 550–800 cm^{-1}; and 708–711 nm, FWHM = 550–700 cm^{-1} (the rest of fitting parameters are free, see Appendix). The Gaussian deconvolution of the absorption spectra also satisfies two criteria obtained from fluorescence measurements (*3*): 1), the maximum of the red-most band is around 709 nm; and 2), the red-most band shows absorption in the range of 685–697 nm.

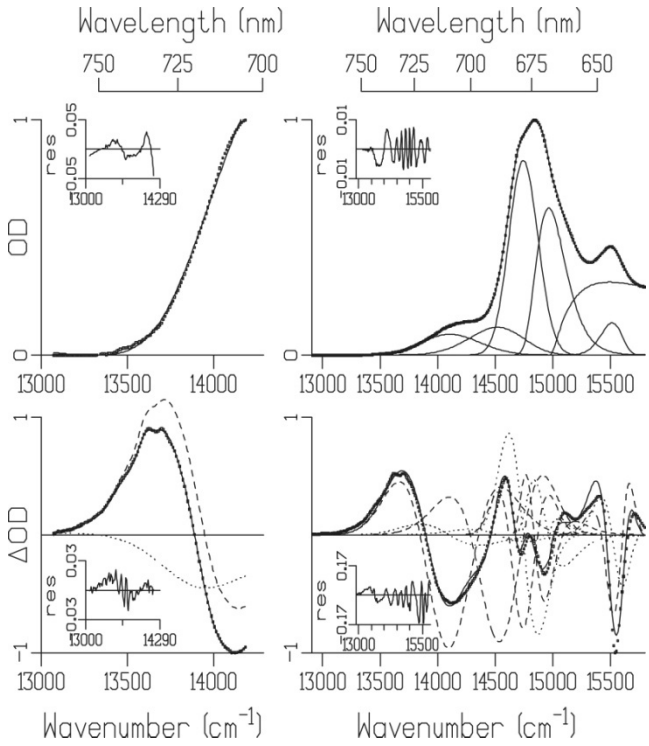

Figure 1. Normalized absorption (*upper panel*) and Stark (*lower panel*) spectra of Lhca4 at 77K. (*Dots*) data points, (*solid lines*) fit results, (*dashed lines*) second derivatives, (*dotted lines*) first derivatives. Insets show the residuals of the fit. Absorption spectrum fitted with a spline line shape (*left panels*) and with skewed Gaussians (*right panels*). The sample was in a glycerol buffer glass (57% glycerol v/v) containing 10 mM Hepes pH 7.5, 0.06% *β*-DM, sucrose ≈0.4 M. The Stark spectra was measured at magic angle $\chi = 54.7°$ (χ is the angle between the externally applied electric field and the polarization of the measuring light) and at a field strength of $F = 2.375 \times 10^5$ V cm^{-1}. The absorption maximum is OD 0.66 at 674 nm, the Stark minimum is $\Delta OD - 1.8 \times 10^{-4}$ at 643.5 nm.

The change in dipole moment between the excited and ground states for the red-most band is deducted from seven different fits in the 630–800 nm region (for a selection, see Appendix) and ranges from $\Delta\mu$ = 6.6 to 8.2 D f^{-1}. We also fitted the red side of the band with a spline line shape from 705 to 775 nm (Figure 1), where the overlap with the 690 nm band is small, obtaining $\Delta\mu$ = 8.2 D f^{-1}, which shows that the fit is consistent. The high $\Delta\mu$ indicates that the lowest exciton state has acquired a significant CT character or, in other words, the lowest exciton state is mixed with a CT state of the dimer. This mixing creates a vibronically broadened lowest excitonic state that couples strongly with phonons (protein lattice vibrations), resulting in a redistribution of oscillator strength, an homogeneously broad absorption band, and an extreme red-shifted emission.

The second red absorption band, centered around 690 nm, has a value for the change in dipole moment that ranges from $\Delta\mu$ = 3.8 to 6.8 D f^{-1}. This is most likely due to the spectral overlap and will not be further discussed here because it is out of the scope of this chapter.

The change in dipole moment for the bulk Chls ranges from $\Delta\mu$ = 0.7 to 1.1 D f^{-1}, which suggests that these are monomeric Chls. The broad band at the blue side of the spectra around 650 nm is necessary for the description of the absorption spectrum (it could account for the sum of the vibrational side bands of red and bulk Chls), although it does not contribute to the Stark spectrum ($\Delta\mu$ = 0.00 to 0.04 D f^{-1}). The Chls *b* absorbing at 644.5 nm have a change in dipole moment from $\Delta\mu$ = 1.7 to 1.8 D f^{-1}, which indicates that the Chls *b* behave differently from the bulk and red Chls.

We note that the mixing exciton-CT state and its strong coupling to phonons make the dimer an energetically very flexible system, highly dependent on protein vibrations and conformation. Thus, the protein could, by conformational changes (*22*), modulate the orientation and distance of the Chls forming the excitonically coupled dimer and the mixing with the CT state to switch between a system that transfers excitation energy to P700 and a system that dissipates excess excitation energy (photoprotective state).

In conclusion, we have demonstrated that the large bandwidth and the extreme red-shifted emission of the lowest energy form in the Lhca4 complex originates from the mixing of the lowest exciton state with a CT state of the excitonically coupled dimer.

APPENDIX

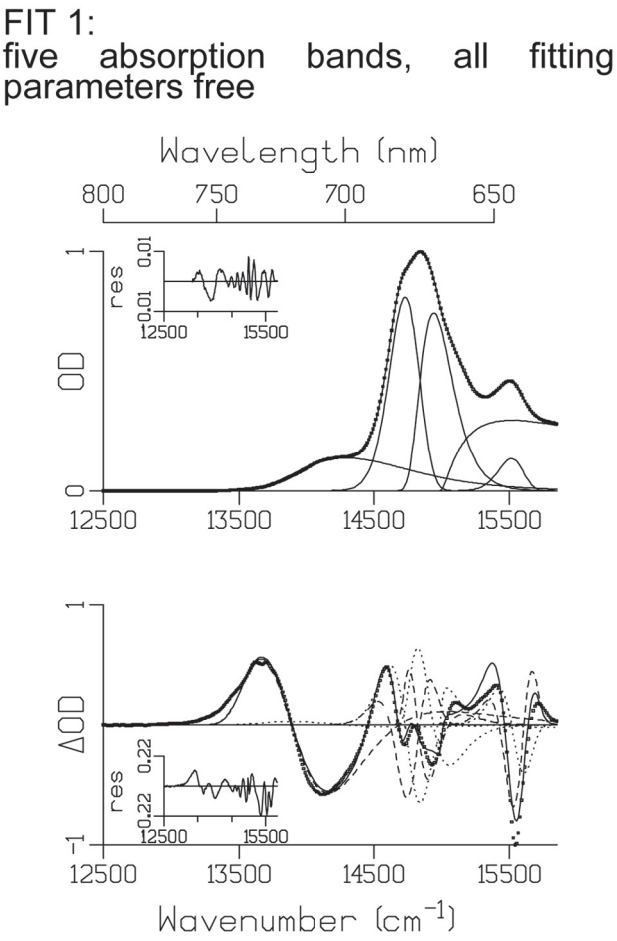

Figure S1. Absorption (*upper panel*) and Stark (*lower panel*) spectra of Lhca4 at 77K. (*Dots*) data points, (*solid lines*) fit results, (*dashed lines*) second derivatives, (*dotted lines*) first derivatives. Insets show the residuals of the fit.

TABLE 1 Fit 1: 5 absorption bands, all fitting parameters free

Band assignment	Maximum nm	FWHM cm^{-1}	$\Delta\mu$ D f^{1}
Red-most	699.5	970	6.8
"*Bulk*" Chls	679.0	260	0.8
"*Bulk*" Chls	669.5	280	0.8
Broad band	644.5	1470	0.1
Chl *b*	644.5	220	1.8

The errors are approximately 10%.

FIT 2:
Six absorption bands, position and FWHM of the lowest energy forms fixed

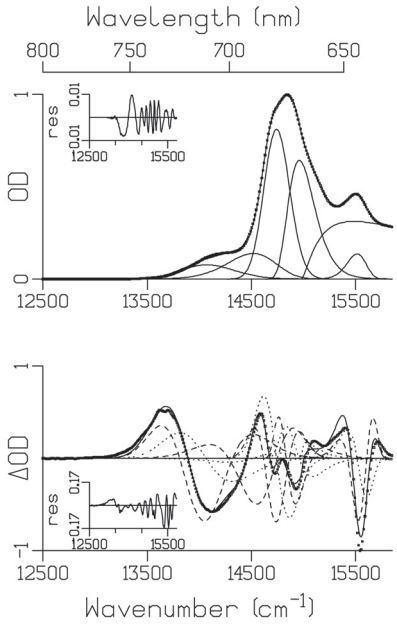

Figure S2. Absorption (*upper panel*) and Stark (*lower panel*) spectra of Lhca4 at 77K. (*Dots*) data points, (*solid lines*) fit results, (*dashed lines*) second derivatives, (*dotted lines*) first derivatives. Insets show the residuals of the fit.

FIT 3:
Six absorption bands, position and FWHM of the lowest energy forms fixed

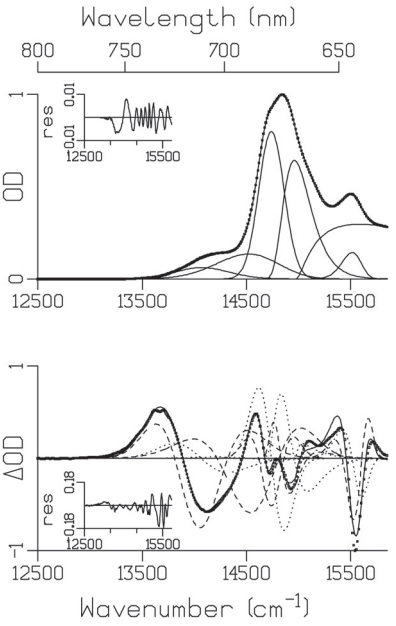

Figure S3. Absorption (*upper panel*) and Stark (*lower panel*) spectra of Lhca4 at 77K. (*Dots*) data points, (*solid lines*) fit results, (*dashed lines*) second derivatives, (*dotted lines*) first derivatives. Insets show the residuals of the fit.

TABLE 2 Fit 2: 6 absorption bands, 4 fitting parameters fixed

Band assignment	Maximum nm	FWHM cm^{-1}	$\Delta\mu$ D f^{-1}
Red-most	711.0	600	6.6
690nm band	689.0	550	3.8
"*Bulk*" Chls	678.5	290	1.0
"*Bulk*" Chls	668.5	300	0.9
Broad band	646.0	1360	0.0
Chl *b*	644.5	220	1.8

The errors are approximately 10%.

TABLE 3 Fit 3: 6 absorption bands, 4 fitting parameters fixed

Band assignment	Maximum nm	FWHM cm^{-1}	$\Delta\mu$ D f^{-1}
Red-most	711.0	600	7.7
690nm band	688.5	700	5.4
"*Bulk*" Chls	678.5	290	0.8
"*Bulk*" Chls	668.5	310	0.8
Broad band	642.0	1640	0.0
Chl *b*	644.5	220	1.7

The errors are approximately 10%.

REFERENCES

1. Nelson, N., and C. F. Yocum. (2006) Structure and function of photosystem I and II. *Annu. Rev. Plant Biol*. 57:521–565.
2. Jensen, P. E., R. Bassi, E. J. Boekema, J. P. Dekker, S. Jansson, et al. (2007) Structure, function and regulation of plant photosystem I. *Biochim. Biophys. Acta*. 1767:335–352.
3. Croce, R., A. Chojnicka, T. Morosinotto, J. A. Ihalainen, F. van Mourik, et al. (2007) The low-energy forms of Photosystem I light-harvesting complexes: spectroscopic properties and pigment-pigment interaction characteristics. *Biophys. J*. 93:2418–2428.
4. Croce, R., G. Zuchelli, F. M. Garlaschi, and R. C. Jennings. (1998) A Thermal Broadening Study of the Antenna Chlorophylls in PSI-200, LHCI, and PSI Core. *Biochemistry*. 37:17355–17360.
5. Gobets, B., H. van Amerongen, R. Monshouwer, J. Kruip, M. Rogner, et al. (1994) Polarized site-selected fluorescence spectroscopy of isolated Photosystem I particles. *Biochim. Biophys. Acta*. 1188:75–85.
6. Ihalainen, J. A., P. E. Ratsep, P. E. Jensen, H. V. Scheller, R. Croce, et al. (2003) Red spectral forms of chlorophylls in green plant PSI- a site-selective and high-pressure spectroscopy study. *J. Phys. Chem. B*. 107:9086–9093.
7. Morosinotto, T., J. Breton, R. Bassi, and R. Croce. (2003) The nature of a Chlorophyll ligand in Lhca proteins determines the far red fluorescence emission typical of Photosystem I. *J. Biol. Chem*. 278:20612–20619.
8. Morosinotto, T., M. Mozzo, R. Bassi, and R. Croce. (2005) Pigment pigment interactions in Lhca4 antenna complex of higher plants Photosystem I. *J. Biol. Chem*. 280:20612–20619.
9. Parson, W. W., and A. Warshel. (1978) Spectroscopic properties of photosynthetic reaction centers. 2. Application of the theory to Rhodopseudomonas viridis. *J. Am. Chem. Soc*. 109:6152–6163.
10. Melkozernov, A. N., S. Lin, and R. E. Blankenship. (2000) Excitation dynamics and heterogeneity of energy equilibration in the core antenna of Photosystem I from cyanobacterium Synechocystis sp. PCC6803. *Biochemistry*. 39:1489–1498.
11. Zazubovich, V., S. Matsuzaki, T. W. Johnson, J. M. Hayes, P. M. Chitnis, et al. (2002) Red antenna states of Photosystem I from cyanobacterium Synechococcus elongatus: a spectral hole burning study. *Chem. Phys*. 275:47–59.

12. Frese, R. N., M. A. Palacios, A. Azzizi, I. H. M. van Stokkum, J. Kruip, et al. (2002) Electric field effects on red chlorophylls, b-carotenes and P700 in cyanobacterial Photosystem I complexes. *Biochim. Biophys. Acta*. 1554:180–191.
13. Ihalainen, J. A., R. Croce, T. Morosinotto, I. H. M. van Stokkum, R. Bassi, et al. (2005) Excitation decay pathways of Lhca proteins: a timeresolved fluorescence study. *J. Phys. Chem. B*. 109:21150–21158.
14. Gobets, B., and R. van Grondelle. (2001) Energy transfer and trapping in Photosystem I. *Biochim. Biophys. Acta*. 1507:80–89.
15. Bublitz, G. U., and S. G. Boxer. (1997) Stark spectroscopy: applications in Chemistry, Biology and Materials Science. *Annu. Rev. Phys. Chem*. 48:213–242.
16. Liptay, W. (1974) Dipole moments and polarizabilities of molecules in excited electronic states. *In* Excited States., vol. 1 E. C. Lim, editor. Academic Press, New York and London. 129–229.
17. Moore, L., J. Zhou, and S. G. Boxer. (1999) Excited-state electronic assymetry of the special pair in photosynthetic reaction center mutants: Absorption and Stark spectroscopy. *Biochemistry*. 38:11949–11960.
18. Frese, R. N., M. Germano, L. de Weerd, I. H. M. van Stokkum, A. Y. Shkuropatov, et al. (2003) Electric field effects on the chlorophylls, pheophytins, and b-carotenes in the reaction center of PSII. *Biochemistry*. 42:9205–9213.
19. Novoderezhkin, V. I., J. P. Dekker, and R. van Grondelle. (2007) Mixing of exciton and charge-transfer states in Photosystem II reaction centers: modeling of Stark spectra with modified Redfield theory. *Biophys. J*. 93:1293–1311.
20. Krawczyk, R. (1991) Electrochromism of chlorophyll a monomer and special pair dimer. *Biochim. Biophys. Acta*. 1056:64–70.
21. Croce, R., T. Morosinotto, S. Castelletti, J. Breton, and R. Bassi. (2002) The Lhca antenna complexes of higher plants Photosystem I. *Biochim. Biophys. Acta*. 1556:29–40.
22. Brecht, M., V. Radics, J. B. Nieder, H. Studier, and R. Bittl. (2008) Red antenna states of Photosystem I from Synechocystis PCC 6803. *Biochemistry*. 47:5536–5543.

SUMMARY

The main objective of this Thesis is to investigate how photosynthetic organisms transform the energy of sunlight into electrochemical energy by means of the charge separation (CS) process, one of the key processes in photosynthetic energy conversion. The CS process occurs in the photosystem II reaction center (PSII RC), a pigment-protein complex embedded in the photosynthetic membrane of oxygen evolving organisms (cyanobacteria, algae and higher plants). The photosynthetic membrane network located inside a cellular organelle, the chloroplast, holds the whole photosynthetic machinery which is composed of many different pigment-protein complexes with different functions.

Light from the sun is collected and transferred to the photochemically active RC by light-harvesting complexes, the so-called antennas. Once the sunlight excitation energy reaches the RC, a series of energy and electron transfer reactions among the chromophores in the RC (six chlorophylls, two pheophytinsand two β-carotenes) and two electron acceptors (quinones) convert the sunlight energy into a charge separated state. This charge separated state, in turn, creates an electrochemical gradient across the photosynthetic membrane which ultimately powers the photosynthetic organism.

The CS process in PSII RC has been extensively studied since the first biochemical isolation of the PSII RC was achieved in 1987 by Nanba and Satoh. Despite the apparent simplicity of the isolated RC, the spectral congestion in the RC (the chlorophylls and pheophytins absorb at approximately the same energy) complicates the interpretation of the spectroscopic data and has led to a long and extensive debate in the literature regarding the mechanism and time scale of CS. In chapter 2 we present a detailed transient absorption study aimed to investigate the molecular mechanisms of CS. The design of the experiment provides the required data which after the application of global and target analysis leads us to demonstrate that CS can occur via two different pathways with participation from different sets of chromophores at every stage of the process. Each RC complex reaches a common final charge separated state following one of the two pathways depending on protein configuration. This result highlights the role of the protein in controlling the CS dynamics in the PSII RC.

In chapter 3 we further verify the idea of the two pathways by the physical modeling of the transient absorption kinetics using the modified Redfield-generalized Förster theory.

In chapter 4 we present an unexpected observation in the experimental data of chapter 2. Until this point, generally only the chlorophylls and pheophytins were considered to participate in the energy transfer reactions within the RC. Even so, we observe a perturbation in the energy of the two β-carotenes present in the RC when the peripheral chlorophylls, the so-called $Chls_Z$, are in the excited state. This observation suggests that the electronic states of the $Chls_Z$ and the β-carotenes are mixed. The $Chls_Z$ are located at opposing sides at the periphery of the complex (at ≈ 25 Å from the central chromophores which are separated by ≈ 10 Å from each other) and transfer excitation energy to the center of the complex in ≈ 20 ps (1 ps = 10^{-9} s). However, if the energy transfer time is calculated theoretically, much longer energy transfer times are obtained (up to 100 ps). The fact that the β-carotenes are not included in the theoretical calculations and the presence of their electronic mixing with the $Chls_Z$, lead us to hypothesize the involvement of the β-carotenes in accelerating the energy transfer process between the $Chls_Z$ and the chromophores in the center of the complex.

In chapter 5 we have assessed the properties of the electronic states which initiate CS by a combined approach: Stark spectroscopy (a extremely sensitive technique to the movement of charge associated with an electronic transition) applied to site-directed mutants (where the exchange of a single amino acid modifies the pigment-protein interactions of the naturally occurring organism, the so-called wild-type). The comparison of the Stark spectra of the wild-type PSII complex with eight different site-directed mutants allows us to demonstrate that the electronic states which initiate CS are collective excited states (excitons) mixed with charge transfer (CT) states. The CT character of these mixed states promotes ultrafast and efficient CS in the PSII RC. This work, in line with chapter 2, provides further evidence for the presence of two CS pathways and for the capacity of the protein to fine-tune the energy of the exciton and CT states and the degree of mixing between them which ultimately controls the CS dynamics.

In chapter 6 we examine the pigment-protein interactions directly by applying light-induced Fourier transform infrared (FTIR) difference spectroscopy. The comparison of several PSII preparations with different antenna size indicates that the vibrational properties of the RC complex are independent of the total size of the PSII complex, and do not change during the isolation procedure. The comparison of the wild-type RC with two site-directed mutants allows us to identify the specific pigment-protein interactions which may control the selection of a specific CS pathway in each RC.

In chapter 7 we move to the study of a different pigment-protein complex, a peripheral light-harvesting complex of photosystem I, Lhca4. A distinctive characteristic of this complex is the presence of red chlorophylls, which absorption and emission energy is much lower than for the typical antenna chlorophylls. Using Stark spectroscopy we have demonstrated that the low energy of the red chlorophylls in Lhca4 originates from the mixing of the lowest energy state with a CT state.

Overall, this Thesis deals with the study of the electronic structure and energy dynamics in photosynthetic pigment-protein complexes. Our main objective is to gain insight into the design principles which lead to their high efficiency in converting solar energy into electrochemical energy. The understanding of these design principles is very important in the present time, with vital issues as the energetic crisis and the climate change in front of us. Therefore, we need to find alternative strategies to the fossil fuels in order to fulfil our energetic demands with a clean energy source. Therefore, we hope the work presented in this Thesis contributes to the efforts of the scientific community for achieving the efficient and clean utilization of our largest energy source: the Sun.

SAMENVATTING

Het hoofddoel van dit proefschrift is het bestuderen hoe fotosynthetische organismen de energie van zonlicht omzetten in electrochemische energie door middel van ladingsscheiding (CS). CS is één van de cruciale processen van fotosynthetische energieomzetting. Het vindt plaats in het reactie centrum van fotosysteem II (PSII RC), een pigment-eiwit complex in de fotosynthetische membranen van zuurstof producerende organismen (cyanobacteriën, algen en hogere planten). Het netwerk van fotosynthetische membranen zit in een celorganel (de chloroplast), en bevat de complete fotosynthetische machinerie, die bestaat uit vele verschillende pigment-eiwit complexen met verschillende functies.

Lichtoogstende complexen, zogenaamde "antennes", absorberen zonlicht, en dragen de energie daarvan over aan het fotochemisch actieve RC. Wanneer deze excitatie energie het RC bereikt, leidt dit tot een serie energie- en electron-overdrachtsreacties tussen de chromoforen en electron-acceptoren in het RC (zes chlorofyllen, twee pheophytines, twee β-carotenen en twee quinonen). Hierdoor wordt de energie omgezet in een ladingsgescheiden toestand, die een electrochemische gradiënt creëert over het fotosynthetische membraan, en zodoende de fotosynthetische organismen van energie voorziet.

Het ladingsscheidingsproces (CS) in PSII RC is uitgebreid bestudeerd sinds de eerste biochemische isolatie in 1987 door Nanba en Satoh. Ondanks de schijnbare eenvoud van het geïsoleerde RC, is interpretatie van spectroscopische data complex, door de spectrale overlap van de chlorofyllen en pheophytines. Bijgevolg is er een lang en uitgebreid debat gaande over het mechanisme en de tijdsschaal van CS. In hoofdstuk 2 rapporteren we een gedetailleerde tijdsopgeloste absorptie spectroscopie studie naar de moleculaire mechanismen van CS. De opzet van het experiment en het gebruik van globale en "target" analyse, maakten het mogelijk om aan te tonen dat CS optreedt via twee verschillende routes. Verschillende combinaties van chromoforen zijn betrokken in elk stadium van het proces. De eiwitconfiguratie bepaalt welke van de twee routes wordt gevolgd, maar uiteindelijk bereikt ieder RC dezelfde ladingsgescheiden toestand. Dit resultaat laat goed de rol van het eiwit zien in het controleren van de CS dynamica in het PSII RC. In hoofdstuk 3 verifiëren we het concept van de twee CS routes, door geavanceerde fysische modellering van de tijdsopgeloste absorptie kinetiek, met behulp van "modified Redfield-generalized Förster theory".

In hoofdstuk 4 rapporteren we een onverwachte observatie in de experimenten in hoofdstuk 2. Tot dusverre werd algemeen aangenomen dat alleen de chlorofyllen en pheophytines deelnamen aan de energie-overdrachtsprocessen in het RC. Desalniettemin zien we een verstoring van de energie van de twee β-carotenen in het RC wanneer de perifere chlorofyllen ($Chls_Z$) geëxciteerd zijn. Dit suggereert dat de electronische toestanden van de $Chls_Z$ en de β-carotenen gemengd zijn. De $Chls_Z$ bevinden zich op tegenovergelegen zijden aan de periferie van het complex (op ≈ 25 Å van de centrale chromoforen, die ≈ 10 Å van elkaar zijn gescheiden). Energieoverdracht van $Chls_Z$ naar de centrale chromoforen duurt ≈ 10 ps (1 ps = 10^9 s), veel sneller dan de verwachte tijden (tot 100 ps) op basis van theoretische berekeningen. Het ontbreken van β-carotenen in die berekeningen, en hun electronische menging met $Chls_Z$, leidde tot de hypothese dat de β-carotenen betrokken zijn bij het versnellen van energieoverdracht tussen $Chls_Z$ en de chromoforen in het centrum van het complex.

In hoofdstuk 5 bestuderen we de eigenschappen van de electronische toestanden die CS initiëren met een gecombineerde aanpak: Stark spectroscopie (een extreem gevoelige techniek voor de beweging van lading tijdens een electronische overgang), toegepast op puntmutanten (waarbij de verandering van een enkel aminozuur de pigment-eiwit interacties verandert ten opzichte van de natuurlijke vorm, het wild-type). De Stark spectra van wild-type PSII is vergeleken met acht verschillende puntmutanten. Hieruit bleek dat de electronische toestanden die CS initiëren een mengsel zijn van collectief-geëxciteerde toestanden (excitonen) en ladingsgescheiden (CT) toestanden. Het CT karakter van deze gemende toestanden bevordert ultrasnelle en efficiënte CS in het PSII RC. Dit werk levert verder bewijs voor het bestaan van twee CS routes, en voor de mogelijkheid van het eiwit tot fijnafstelling van de energie van de exciton- en CT-toestanden en de mate van menging tussen deze toestanden. Zodoende beïnvloedt het eiwit de CS dynamica.

In hoofdstuk 6 bestuderen we de pigment-eiwit interacties op een directe manier, door het gebruik van licht-geïnduceerde Fourier-transformatie infrarood (FTIR) spectroscopie. Een vergelijking tussen verscheidene PSII preparaten met verschillende antenne-grootte wijst er op dat de vibrationele eigenschappen van het RC onafhankelijk zijn van de totale omvang van het PSII complex en niet veranderen tijdens de isolatieprocedure. Het vergelijken van het wild-type RC met twee puntmutanten maakte het mogelijk om de specifieke pigment-eiwit interacties te identificeren die wellicht bepalen welke CS route plaatsvindt in een RC.

In hoofdstuk 7 bestuderen we een ander pigment-eiwit complex, Lhca4, een perifeer lichtoogstend complex van fotosysteem I. Lhca4 onderscheidt zich door de aanwezigheid van rode chlorofyllen, met een absorptie- en emissie-energie die veel lager is dan voor doorsnee antenne chlorofyllen. Met Stark spectroscopie hebben we aangetoond dat de lage energie van de rode chlorofyllen veroorzaakt wordt door het mengen van de laagste energie-toestand met een CT toestand.

Al met al, beschrijft dit proefschrift onderzoek naar de electronische structuur en energie-dynamica in fotosynthetische pigment-eiwit complexen. Dit heeft als doel inzicht te verkrijgen in de ontwerpprincipes die leiden tot hun efficiënte omzetting van zonne-energie in electrochemische energie. Het begrijpen van deze principes is erg belangrijk in de huidige tijd, met nijpende problemen zoals de energiecrisis en klimaatverandering. Daarom moeten we schone alternatieve vinden voor fossiele brandstoffen. Vandaar dat we hopen dat het werk in dit proefschrift bijdraagt aan de inspanningen van de wetenschappelijke gemeenschap voor het bereiken van efficiënt en schoon gebruik van de onze grootste energiebron: de Zon.

List of Publications

Romero, E., Mozzo, M., van Stokkum, I. H. M., Dekker, J. P., van Grondelle, R., and Croce, R. (2009) The origin of the low-energy form of photosystem I light-harvesting complex Lhca4: mixing of the lowest exciton with a charge-transfer state, *Biophys J. 96(5)***:** L35–L37

Romero, E., van Stokkum, I. H. M., Novoderezhkin, V. I., Dekker, J. P., and van Grondelle, R. (2010) Two different charge separation pathways in photosystem II, *Biochemistry (Accelerated Publications) 49,* 4300-4307

Novoderezhkin, V. I., **Romero, E.**, Dekker, J. P., and van Grondelle, R. (2011) Multiple charge separation pathways in photosystem: modeling of the transient absorption kinetics, *ChemPhysChem*, *In press*

Romero, E., van Stokkum, I. H. M., Dekker, J. P., and van Grondelle, R. (2011) Ultrafast carotenoid band shifts correlated with Chl_z excited states in the photosystem II reaction center: are the carotenoids involved in energy transfer?, *Phys. Chem. Chem. Phys.* (*Communication*),
DOI: 10.1039/C0CP02896G

Boehm, M.[#], **Romero, E.**[#], Reisinger, V., Yu, J., Komenda, J., Eichacker, L. A., Dekker, J. P., and Nixon, P. J., (2011) Investigating the early stages of photosystem II assembly in *Synechocystis* sp. PCC 6803: isolation of CP47 and CP43 complexes, *J. Biol. Chem., In press*
[#]These authors contributed equally to this work

Romero, E., Diner, B. A., Nixon, P. J., Dekker, J. P., and van Grondelle, R., The electronic structure of photosystem II: Stark spectroscopy on site–directed mutants, *Manuscript in preparation*

Romero, E., Di Donato, M., Nixon, P. J., Dekker, J. P., and Breton, J., Pigment-protein interactions for the sites of cation (P_{680}) and anion (Phe_{D1}) localization in the photosystem II reaction center studied by light-induced Fourier transform FTIR difference spectroscopy, *Manuscript in preparation*

Romero, E., van Grondelle, R., and Dekker, J. P., Stark spectroscopy on photosystem II preparations with variable antenna size, *Manuscript in preparation*

Romero, E., Boehm, M., Nixon, P. J., and Dekker, J. P., The unusual temperature dependence of fluorescence for CP43 and CP47 antenna complexes isolated from *Synechocystis* sp. PCC 6803 is caused by aggregation, *Manuscript in preparation*

NAWOORD

Time has passed . . . . and here I am, writing the acknowledgement, the last part of my book . . . . it is time to look back and remember the people with who I have shared these past years . . . .

Let's start from the beginning . . . .

Once upon a time, there was a little girl and her name was Eli. She had experienced the scientific research during the time she was working for her master degree. It was there, in the darkness of the lab, where she said to herself: "I want to become a scientist!"

Eli also wanted to expand her horizons, she wanted new experiences . . . . so Eli started to look for fellowships outside Spain . . . . first in chemical sciences, no success, . . ., later in life sciences . . . . . and there it was: a biophysics position in The Netherlands. When she clicked on it, she saw it, it was in Amsterdam! The more info she was reading about the project, the more interested she was about it. Then she thought: this is the chance of my life, I really have to get this position!

And she did, she got it!!!!

Yes, I got it, a PhD position in the Marie Curie Training Network INTRO2. To be part of this project has been a wonderful experience: a lot of travelling to great labs and beautiful places, many courses given by researches among the best in their field, many talks given and attended in our INTRO2 meetings, lots of international conferences . . . . and yes, also a lot of parties and fun!!! All this taken together is an excellent environment to start a scientific career. Actually, this experience has been much better than I could have ever imagine, not only for my scientific but also for my personal development. And well, the responsible for this to happen has a name: Jan Dekker, my PhD supervisor. Jan, I would like to thank you for the great opportunity you offered me, for your wise advices, for our discussions in which I have learned really a lot, for being open and willing to listen to my (sometimes crazy) ideas. Jan, the man that never says no (at least to me), thank you for the freedom you gave me to find my own way.

Next I would like to thank Rienk. Well, I have to say that at the beginning, during my first months in the group, I was, let's say, a bit *afraid* about you. Actually, I am not sure why, maybe because of the respect I had (and I still have) for you, maybe because of your strong personality and your attitude, so direct that sometimes could be interpreted as a bit *aggressive* (which is not the case at all). Now that I had the chance to get to know you better, I know that it is about passion. Your passion about science and your capacity to transmit it to the people around you is something absolutely amazing. I consider that this is especially important for students like me, during the PhD period, the training that most probably will determine our future in science and when we face many up and down moments. Therefore, I would like to thank you for the motivation. To be more specific, I thank you for asking me to do the pump probe experiments on PSII RC. I had really enjoyed doing the experiments as well as our discussions about the results. Well, I do not want to be too long with this nawoord but there is something I need to say. Rienk, I feel honoured for the wonderful opportunity you have offered me in the form of a post doc position. In the moment you told me about it I was socked, I could not react, that is why I want to express you here my sincere gratitude and excitement about this opportunity. The complex nature of our project is a real challenge. It will involve a lot of hard work, but I am positive we will succeed!

My next THANK YOU ALL is for the INTRO2 family. First of all, I would like to thank Jacques for considering me a colleague even before we had meet, for your mastery in the lab, your explanations and your guidance. I also remember the meeting in France when I had to give a talk but we had realized that there was something wrong with the samples. You encouraged me not to drop the talk (which would have been the easiest) but to change the focus of it and still be able to present the preliminary results of our project. This was a great lesson (not only applicable to science but, most important, to life in general). I would also like to thank Roberta for asking me to do the experiments which led to my first publication. It was nice to collaborate with you (and to do the experiments with Milena) and I hope we will collaborate even more in the future. Alison, it was fun to work with you in the lab, thanks for that. Well, I would also like to thank all the INTRO2 group leaders: Claudia, Gyozo, Alexander, Egbert, Herbert, Alfred, Stefan, Diana, Imre and Peter for the great atmosphere during our meetings and training courses.

I have great memories from the times I have spent with the INTRO2 PhDs and post docs, many crazy parties and many scientific discussions.

For all this experiences and for your friendship I would like to thank: Milena, Anett, Sabah, Ruth, Sofia, Cristian, Dario, Sami, Alessandro, Jakob, Matt, Petar, Radek, Chavdar, José, Julia, Malwina, Andy, Ana, Fernando, Sonia, Marisa, ... well, we were so many that maybe I forget someone . . . .

And back in Amsterdam . . . . I would like to thank all my colleagues and friends in the Biophysics group. Especially the students and post docs: Mariangela, Sofia, Kinga, Kate, Natalia, Elena, Magda, Lucy, Anjali, Jingyi, Tjaart, Alessandro, Cristian, Hande, Miroslav, Janneke, Andy, Thomas, Joris, Bart, Danielis, Manolis, Cosimo, Maxime, Luke and my office mates: Rudi and Wahado. I also would like to welcome our newest group member, Marco. Again we are so many that I may forget someone. Thanks to Henny, Marloes, John and Silvia and specially to Raoul for being part of the reading committee and tribunal of my Thesis. I would like to thank Ivo for his help with the analysis of the data. Your suggestion of applying Target analysis to my PSII RC pump-probe data was a great one, it was not an easy task but the outcome was worth the effort. Ivo, is not only that I have learned to analyze the Stark and pump-probe data (here also Kate was a great help), it was also about the questions you asked me about the data which helped me to understand it better. Thanks for that and for your advices.

Vladimir, thank for your explanations about our model, energy dynamics and quantum coherence. It is great to collaborate with you!

Peter, thanks for your fantastic samples. The newly isolated *Synechocystis* antennas gave us more information than we expected. It was really nice to collaborate with you and with Marko. Thanks for that. Our collaboration has been very productive, hopefully we will get two publications (one is already in press). I hope we will collaborate in the future, I really like your mutants!

I would also like to thank the members of the reading committee of my Thesis: Roberta, Alfred, Hans, Peter and Raoul.

And now it is time for my wonderful Paranimfen.

Jos, you are the best. You are the kind of person that leaves his problems in a waiting list and first of all helps the others. If a technical problem appears in the lab, it is extraordinary to see how you get involved and look for a solution. And you do find the solution. We have faced many different problems in the lab, and in all this time I have learned so much from you, you cannot imagine. Now, exciting times are in front of us, I am sure we are going to have a lot of fun building the 2D setup!

Sandrine, my crazy friend. We have spent so many hours in the darkness of the lab . . . . it was sometimes hard, and always fun! And we will spend much more, great! We have also lived many other experiences together outside the lab and your energy and optimistic view of everything was always there, keep on going!!

Giuliano, Mister Brush, thanks for your help and artistic touch for the design of the cover of this book.

I also would like to thank all the good friends I have found in Amsterdam.

First of all, the Spanish people. Javi, cuando llegué aquí tu ya llevabas un año y conocías a un montón de peña, gente de p. madre. Me acuerdo de las fiestas Trance, vaya tela, no voy a entrar en más detalles. Sólo decirte que siempre me he sentido arropada contigo y que espero bajar a verte pronto. La peñita, la spanish people, por los momentos que hemos vivido, gracias. Entre ellos: Kandasu, te quiero un montón, Cristina, Alma, la Alma del Kandasu, la Nena, el Veterano, el Bruno, Aida, ..., sólo espero tener más tiempo para poder disfrutarlo con vosotros.

Now, my Guardian Angels, Maria and Sindey. Maria, the passion woman. Syndey, always true, honest and fun. We have shared wonderful moments and difficult ones. And you always helped me. It is amazing how much support, in all senses, I got from you when I needed. All the time you spend with me working on my new apartment, this was fantastic. Many thanks for your friendship.

Ray, I also would like to thank you for the wonderful time we spent together, and for your family. The Da Graça family has been my second family in The Netherlands. Jack and Louise, you have considered me as a daughter, thank you so much for that.

Monika, my sista. When I met you a new world opened in front of me: the trapeze, the clowns, ..., and the most important, many great and true friends. Monika, you have a beautiful light.

Agustin, mi hermano del barrio. Tu filosofía de vida es muy bonita. Me encanta conversar y beber cervecita contigo. Suzanne, you are a great woman.

Christina, mi mama clown. Gracias por tus enseñanzas y tu energía.

Giorgia, mi buena amiga. Gracias por lo que hemos vivido juntas y lo que nos queda! Nacho, espero que todo vaya bien por Roma y que nos veamos pronto.

RebelAct, clowns fighting for a better world!! You are fantastic. Thanks for the energy and inspiration, and for the craziest moments!

Después de este repaso a la gente que he conocido en Amsterdam, no podía olvidar a mis amigos de siempre, de la Koope, de Sant Boi y alrededores. Gracias por vuestro apoyo y por vuestras visitas. No voy a decir nombres porque la lista sería largísima. Sólo nombrar a una persona, mi Robotino, Jose Mari. Gracias por quererme tanto y por estar orgulloso de mi, y por nuestras papas!!

También quiero recordar a todos mis profesores, especialmente Fina Miret y Antonio Lara. Vuestras enseñanzas han sido muy importantes para mi. També recordar als profes del Insti y de la universitat de Barcelona. També vull agrair molt especialment Luís Julià i als companys de laboratori (Marc, Maria i Aurora) pel temps del màster i tot el que vaig apendre allà. També vull agrair a totes les amiges i amics de la facultat de Química.

Por último quiero mencionar a toda mi familia, tios y tias, primos y primas.

Gracias a mis padres por su apoyo incondicional, por saber comprenderme (aunque no siempre ha sido fácil) y darme libertad para encontrar mi camino.

Gracias a mi hermano Daniel por apoyarme en todo (incluso cuando sabías que no estaba haciendo lo correcto, y además tenías razón). Mabel, gracias por estar ahí. Y gracias a los dos por darme la alegría más grande, el Biel y la Iara.